# 15

# Geology of Europa

**Ronald Greeley**
*Dept. of Geological Sciences, Arizona State University*

**Christopher F. Chyba**
*SETI Institute and Dept. of Geological & Environmental Sciences, Stanford University*

**James W. Head III**
*Dept. of Geological Sciences, Brown University*

**Thomas B. McCord**
*Hawaii Institute of Geophysics & Planetology*

**William B. McKinnon**
*Dept. of Earth & Planetary Sciences and McConnell Center, Washington University*

**Robert T. Pappalardo**
*LASP and Dept. of Astrophysical & Planetary Sciences, University of Colorado*

**Patricio H. Figueredo**
*Dept. of Geological Sciences, Arizona State University*

## 15.1 INTRODUCTION

### 15.1.1 Overview

Europa is a rocky object of radius 1565 km (slightly smaller than Earth's moon) and has an outer shell of water composition estimated to be of order 100 km thick, the surface of which is frozen (Figure 15.1). The total volume of water is about $3 \times 10^9$ km$^3$, or twice the amount of water on Earth. Moreover, like its neighbor Io, Europa experiences internal heating generated from tidal flexing during its eccentric orbit around Jupiter. This raises the possibility that some of the water beneath the icy crust is liquid.

The proportion of rock to ice, the generation of internal heat, and the possibility of liquid water make Europa unique in the solar system. In this chapter, we outline the sources of data available for Europa (with a focus on the *Galileo* mission), review previous and ongoing research on its surface geology, discuss the astrobiological potential of Europa, and consider plans for future exploration.

### 15.1.2 Background

Europa has been viewed from Earth since its discovery through a simple telescope in the early 17th century by *Galileo* Galilei (Coyne 1997). Modern observations include those of Kuiper (1957) and Moroz (1965) who showed that Europa is probably covered with water frost. Reviews of these and more recent telescopic observations are given in relevant chapters in Burns (1977), Morrison (1982), Burns and Matthews (1986), and Barbieri *et al.* (1997).

The first close-up observations of the Jupiter system were from the *Pioneer 10* spacecraft in December, 1973 (Fimmel *et al.* 1974), followed by *Pioneer 11* one year later. These spacecraft flybys enabled new estimates of the masses and densities of the jovian moons and refinement of the concept that Europa is a rocky object with a surface of water ice. Although the flyby distances to Europa were too great to enable the *Pioneer* camera systems to obtain anything but cursory images, it was possible to discern a mottled dark and bright surface, indicating that materials other than water frost are present. Coupled with Earth-based determinations of Europa's general properties, these new data led Cameron (1977) and Consolmagno and Lewis (1977) to derive models of Europa's interior and its thermal evolution.

In 1979, *Voyager 1* and *2* flew past Jupiter in March and July, respectively, and returned about 70 useful images of Europa. However, the best images (from *Voyager 2*) are only ~2 km/pixel (Smith *et al.* 1979a,b). Nonetheless, these were adequate to identify many of Europa's unique characteristics, including the presence of lineaments longer than 1000 km and a marked paucity of large impact craters. Color data (McEwen 1986a) suggested the presence of non-ice materials on the surface. These and other geological characteristics are described by Lucchitta and Soderblom (1982) and

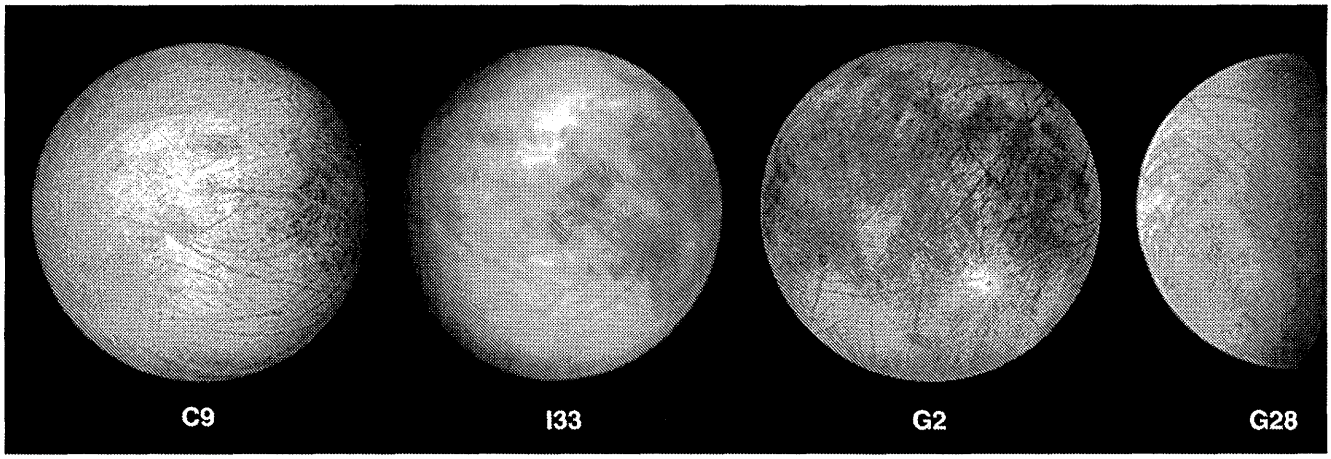


**Figure 15.1.** These four false-color views of Europa were taken by the *Galileo* spacecraft to cover approximately the *leading hemisphere* (observation C9, centered at 0, 40° W), *subjovian hemisphere* (observation I33, centered 0, 9° W), *trailing hemisphere* (observation G2, centered at +1, 292° W), and *antijovian hemisphere* (G28, centered at –1, 147° W). At the time of going to press a colour version of this figure was available for download from http://www.cambridge.org/9780521035453.

Malin and Pieri (1986). The relative lack of impact scars led to the idea that Europa's surface is remarkably young, thought to be a result of extensive "resurfacing" by floods of liquid water erupted from the interior, a process referred to as cryovolcanism. *Voyager* results also enabled refinement of the interior models for Europa, as reviewed by Cassen *et al.* (1982), and Schubert *et al.* (1986), and consideration of the exobiological potential of Europa (Reynolds *et al.* 1983).

After a 6-year journey from Earth, the *Galileo* spacecraft began orbiting Jupiter in December 1995 and over the next 6 years made 18 flybys of Europa. This enabled the return of substantial remote sensing data, including images with scales as good as 6 m/pixel. *Galileo* image resolution and coverage are non-uniform, but most of the satellite has been imaged at better than 13 km per pixel, and most longitudes from 140° westward to 50° have been imaged at better than 1.6 km per pixel.

Although most of the geological considerations are based on the results from the Solid State Imaging (SSI) system (Belton *et al.* 1996, Carr *et al.* 1998) (see eTable 1 in accompanying CD) and the Near Infrared Mapping Spectrometer (NIMS) (Carlson *et al.* 1996), other instruments and data from the spacecraft also provide critical data. Particularly important for interpretations of the interior are data from the magnetometer (Kivelson *et al.* 1999) and the gravitational characteristics of the flybys from which the moment of inertia is determined (Anderson *et al.* 1998). Despite some significant hardware problems, the mission was incredibly successful (Chapter 1). Reviews of the general geology of Europa include Greeley (1997), Greeley *et al.* (1998a, 2000), and Pappalardo *et al.* (1999a,b). The results from the *Galileo* mission include proposed identifications of non-ice compositions on the surface, including various salts (e.g., McCord *et al.* 1999), the discovery of numerous surface features, only some of which can be explained readily, and elucidation of the interior and its evolution (Anderson *et al.* 1998). Particularly noteworthy is the debate concerning the presence or absence of liquid water beneath the ice crust. As reviewed previously by Pappalardo *et al.* (1999a,b), while the evidence for liquid water in the past is favorable, there is no unambiguous indication from spacecraft imaging that such conditions exist today. Interest in Europa for future exploration is high because the satellite could contain environments conducive for prebiotic and exobiological evolution. These and other issues are discussed in the following sections.

### 15.1.3 Sources of Spacecraft Data

Most of the information relevant for the geology and geophysics of Europa is derived from the *Voyager* and *Galileo* missions as archived in the Planetary Data System (McMahon 1996). On the accompanying CD, eTable 1 and eFigure 1 list and show the SSI image foot prints for Europa from the *Galileo* mission, while eFigure 2 shows the *Galileo* NIMS data. eTable 2 lists the *Voyager* images obtained for Europa.

## 15.2 SURFACE PROPERTIES

The surface of an object is a window to its interior. For example, evidence of the interior evolution is seen in the type and distribution of surface features, composition, and mineralogy. The surface is also an interface between the interior and the atmosphere and the space above it. Consequently, it is a rich zone for chemical and physical processes, which are often sensitive to temperature, pressure, and other environmental factors. Although considerable information about the bulk surface properties of Europa has been determined over the last 50 years using Earth-based telescopes, the knowledge has been vastly expanded recently by the *Voyager* and *Galileo* missions (cf. McCord 2000). Earth orbital telescopes have also made valuable contributions recently, even with the limited spatial resolution possible.

Before spacecraft visited Europa, the surface was known from ground-based spectrophotometry to be mostly water ice (Kuiper 1957, Harris 1961, Moroz, 1965, Johnson and McCord 1971, Pilcher *et al.* 1972, see reviews by Morrison and Morrison 1977, Calvin *et al.* 1995, McCord *et al.* 1998a, 1999, McCord 2000). An unidentified non-water ice component was suspected, especially on the trailing side, but was reported to be present in minor amounts (e.g., Clark 1980). The daytime surface temperature was found to range from

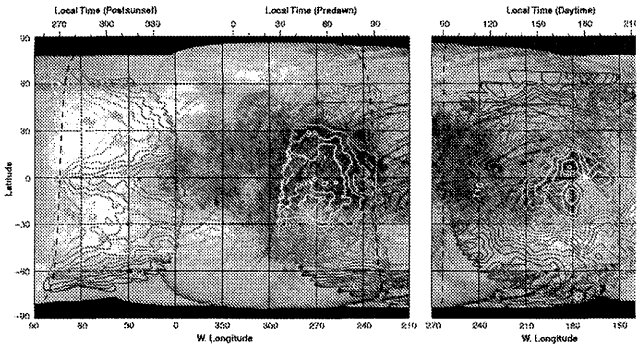


**Figure 15.2.** Contours of brightness–temperature distributions on Europa obtained from the *Galileo* Photopolarimeter-Radiometer (from Spencer *et al.* 1999). At the time of going to press a colour version of this figure was available for download from http://www.cambridge.org/9780521035453.

120 to 135 K and eclipse-cooling thermal and photometric observations indicated a particulate, possibly multi-layered surface (reviewed by Morrison 1977). Spencer (1987a,b) proposed a checkerboard surface segregation model, while Matson and Brown (1989) proposed a solid-state greenhouse model (hotter temperature just below a colder surface) to explain the eclipse observations (Tamppari *et al.* 1995).

The *Voyager* mission returned some additional data on surface temperatures, but the data were noisy and consisted of hard-to-interpret non-blackbody spectra (Spencer 1987a).

Many images from the *Voyager* cameras showed complex surface features, including geologic/compositional units with sharp boundaries, but little information on specific surface composition. The *Galileo* NIMS has provided the most detailed and extensive information about the surface composition so far available, augmented by the Ultraviolet Spectrometer (UVS) and Earth-orbital spectroscopy using the International Ultraviolet Explorer (IUE) and the Hubble Space Telescope (HST). They have generally confirmed the earlier findings, except that there appear to be more extensive non-water-ice materials than originally thought.

The *Galileo* Photopolarimeter-Radiometer (PPR) showed low-latitude diurnal brightness temperatures in the range of 86 to 132 K (Figure 15.2) (Spencer *et al.* 1999). These are thought to be near the kinetic temperatures because of the high emissivity ($\geq$0.9) of water ice in the IR. Daytime temperatures are inversely correlated with surface albedo, as expected. On a global scale, this is true for nighttime temperatures as well. Significant local variations in temperature below the spatial resolution of the PPR are likely due to local distributions of darker and lighter materials (Spencer 1987b). There are deviations at night from the darker-is-hotter trend, such as the bright but warm ejecta blanket near the crater Pwyll, perhaps due to crater ejecta and surface boulders. Most difficult to explain are systematic variations with latitude, with higher post-sunset temperatures at northern latitudes than at corresponding southern latitudes and with a temperature minimum along the equator. These are most likely due to variations in thermal inertia related to thermal conductivity, perhaps due to grain-to-grain contact variations.

In addition to water ice with a range of particle sizes, the surface of Europa contains considerable amounts of a hydrated mineral(s). This is evident from the highly distorted water absorption bands present in the NIMS spectra (Figure 15.3). McCord *et al.* (1998b, 1999) reported on the nature and distribution of these spectral features and interpreted them to indicate the presence of hydrated salt minerals, sulfates, and perhaps carbonates. They and Fanale *et al.* (2000) showed these hydrated deposits to be associated closely with the lineaments and mottled/chaos terrain, regions of most recent disruption (Figure 15.4). Thus, the hydrates were interpreted to be due to endogenic processes, probably related to a briny ocean below the surface. However, it was suggested by Carlson *et al.* (1999b) that sulfuric acid ($H_2SO_4$) hydrate, created by radiolysis of sulfur from Io, processing of endogenic $SO_2$, or from the previously suggested sulfate salts, also or instead could be present in these deposits (Chapter 20).

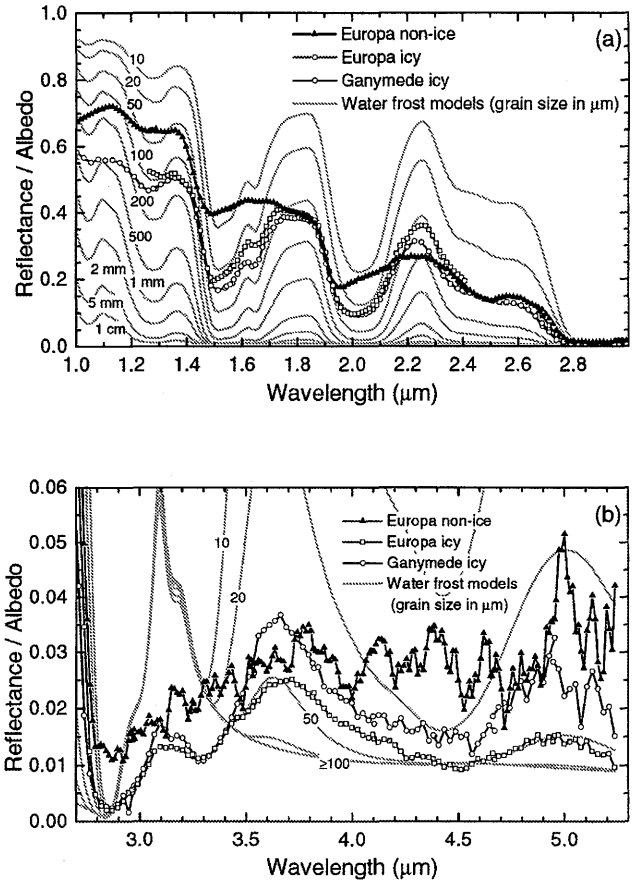


**Figure 15.3.** Reflectance spectra for the Europa hydrated mineral deposits compared with those for a variety of water ice grain sizes (from McCord *et al.* 1999).

Several investigators expressed concern that hydrated salt minerals might readily undergo dehydration and/or dissociation on Europa's surface. McCord *et al.* (2001b) showed experimentally that at least some of the hydrated salts, especially doubly-bonded materials such as magnesium sulfate hydrate, are more stable than water ice to dehydration and could exist over the age of the solar system on the surface of Europa. This result was in agreement with theoretical calculations (Zolotov and Shock 2001). Thus, lag deposits with increasing concentrations over time might be expected and could explain the apparently high concentrations of salts in

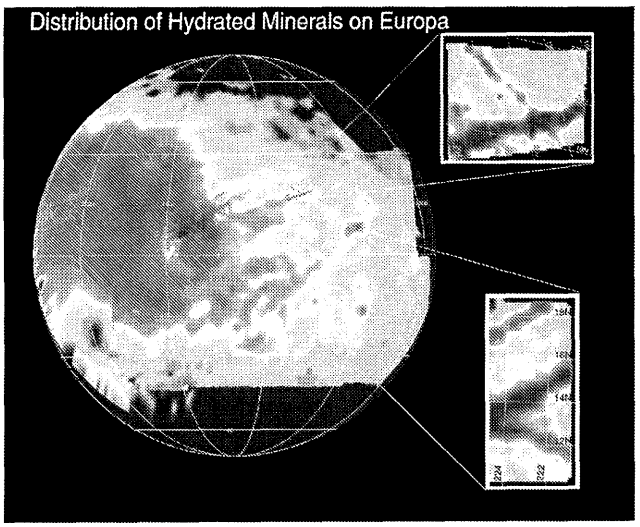


**Figure 15.4.** Distribution of hydrated mineral spectral signatures on Europa from the NIMS observations (from McCord *et al.* 1998b, 1999). At the time of going to press a colour version of this figure was available for download from http://www.cambridge.org/9780521035453.

some areas. Moreover, it was found that magnesium sulfate brines rapidly quenched on cold surfaces under vacuum produce poorly-crystalline and heavily hydrated materials with reflectance spectra even more like those for Europa than for crystalline samples produced at room temperature (McCord *et al.* 2002).

Magnesium sulfate hydrate is expected in large quantities from the thermal evolution and aqueous differentiation of an Europa-like body composed initially of carbonaceous chondrite material (Fanale *et al.* 1977, 2001, Kargel 1991, 1999, Kargel *et al.* 2000, Zolotov and Shock 2001, McKinnon 2002). From spectral evidence, geochemical modeling, meteorite leaching experiments (Fanale *et al.* 1998) and geological associations, McCord *et al.* (2001b) postulated that a mixture of mostly $MgSO_4 \bullet nH_2O$, with some $Na_2SO_4 \bullet nH_2O$, is the most likely hydrate present on Europa. Nevertheless, from the reflectance spectrum alone, it is not possible to rule out sulfuric acid and perhaps other materials being present. In fact, if $Na_2SO_4$ were present, some singly bonded Na is likely to be radiolyzed, $H^+$ taking its place, producing sulfuric acid (see Chapter 20). Thus, both salt minerals (mostly $MgSO_4$) and some sulfuric acid ($H_2SO_4$), derived from $Na_2SO_4 \bullet nH_2O$, could be present as hydrates. The hydrated salt minerals seem to exhibit a grain size in the 300–500 μm range (Van Keulen *et al.* 2000).

Various minor molecular constituents have also been discovered in the surface materials of all three icy Galilean satellites. They are apparently both indigenous and due to radiation processing. $CO_2$ has been reported (Carlson *et al.* 1996, McCord *et al.* 1997, 1998b, Smythe *et al.* 1998, Hibbitts *et al.* 2000) and has been found escaping from at least Callisto (Carlson 1999). Other constituents ($SO_2$, S–H, C≡N, C–H) were also reported for Ganymede and Callisto from absorptions in the 3–5 μm region (McCord *et al.* 1997, 1998a), but the near-complete coverage of Europa's surface by $H_2O$-bearing minerals, which absorb strongly in this spectral region, allows little radiation to be reflected, and thus signatures of minority materials are easily hidden. Nevertheless, Carlson *et al.* (1999a) reported $H_2O_2$ from a 3.50-μm absorption visible in regions containing finer-grained water ice (approximately the leading side). The UVS detected spectral evidence of $H_2O_2$ on all three icy satellites (Hendrix *et al.* 1999), which is probably a product of radiolysis of water ice (Moore and Hudson 2000). The UVS team also reported a UV absorber concentrated on the trailing side of Europa (Hendrix *et al.* 1998), consistent with the UV-absorbing surface stain on the trailing side mapped using the *Voyager* multispectral images (Johnson *et al.* 1983, Johnson *et al.* 1988, McEwen 1986a, Nelson *et al.* 1986) and attributed to sulfur delivered to the surface from Io by the Jupiter magnetosphere.

The processes affecting Europa's surface materials are generally related to thermal processing and radiation bombardment. Over a longer timescale, meteorite impact would be expected to influence the nature of the surface, but the rapid resurfacing of Europa, probably due to interaction with a warm ocean below, might dominate. The temperature range for Europa's surface (~90 to 130 K) is in the critical range in which the properties of water ice and the chemistry induced by low-energy electrons change rapidly with temperature. Thus, the surface processes are likely to be complex and interactive, making Europa a rich laboratory for studying material properties.

Perhaps the most important environmental factor is the intense, high-energy (up to 10 MeV) radiation flux impacting the surface due to trapped particles in Jupiter's magnetosphere (Cooper *et al.* 2001). This includes electrons and protons as well as heavy ions such as O and S. A major process, especially due to the heavy ions, is sputtering, i.e., physical disruption of the surface molecules tending to blast fragments from the surface (Chapter 20). One consequence is the creation of an exosphere of sputtered products such as Na (Brown and Hill 1996, Johnson 2000), possibly from $Na_2SO_4$ hydrate, that could be used as a probe of the surface constituents using mass spectrometers on or near the surface (Johnson *et al.* 1998).

Low-energy electrons are also produced as secondaries by sputtering as well as induced directly. These are the most important for causing reactions that change the chemical (rather than the physical) nature of the materials. Extensive research on this surface chemistry is developing, and is elaborated on in Chapter 20. For example, Moore and Hudson (2000) and studied $H^+$ irradiation of ices to produce $H_2O_2$ and McCord *et al.* (2001b) and Zolotov and Shock (2001) investigated the chemistry and stability of hydrated salt minerals under Europan conditions.

The physical nature of the surface is important for studies of thermal and optical radiation transport and other processes. Water ice on the surface of Europa exhibits a variety of grain sizes. The ice between ±60° latitude is generally abundant and fine-grained (radius <50 μm) on the leading side (Hansen *et al.* 1998, Shirley and Carlson 2000) but less abundant, well segregated, and large grained (radius >200 μm) on the trailing side (e.g., McCord *et al.* 1999). The polar caps have an unusual water-ice spectrum, which is likely the result of mixtures or layering of frost particles with a large range of grain sizes. The top micrometer of surface ice is amorphous over all of Europa (Hansen and McCord 2000). This is probably an indication of the relatively high radiolytic disruption of the ice crystalline structure compared to the other icy satellites, where there is much more

crystalline surface ice. Thermal annealing and recrystallation of the ice can counteract the radiolytic disruption, but this is less operative on Europa because of its cold temperatures.

Water molecules from water ice and to a lesser extent from hydrated minerals are removed by sputtering and by thermal desorption, but probably mostly re-condense elsewhere. The redistribution of water molecules probably creates an underdense, frosty surface that slowly sinters with time. This effect will vary with temperature, i.e., with latitude and albedo, producing polar frost deposits for example. Further, it appears that the dark lineaments brighten with age (Greeley *et al.* 1998b, Geissler *et al.* 1998a), which could be due to water frost slowly covering the older surfaces. One consequence might be to produce free $H_2O$ molecules that create a "humid" layer just above the surface and induce re-hydration, slowing the overall dehydration process.

Therefore, study of Europa's surface has revealed a rich set of processes that are important for the other icy Galilean satellites as well as for other cold surfaces in the solar system. In comparison with Europa, Ganymede's surface (see Chapter 16) seems to be mostly water ice but with some hydrated minerals, probably salts, also present in the darker regions (McCord *et al.* 2001a). Ganymede has prominent polar frost caps, possibly indicating transport of water as a vapor. Callisto (see Chapter 17) is much less icy, with over 50% of the surface covered with dark material having a strong O–H absorption near 3 μm but no detectable $H_2O$ features, suggesting hydroxide minerals such as clays. Both Ganymede and Callisto are reported to have various minority constituents, including $H_2O_2$, $CO_2$, $SO_2$, CH, CN, and oxygen (see summary in McCord 2000); these could be on Europa as well, but their detection is difficult.

## 15.3 GEOLOGY

### 15.3.1 Surface Features

*Global Perspective*

The highest resolution *Voyager* images of Europa revealed a variety of colors (McEwen 1986a) and morphological features. Lucchitta and Soderblom (1982) divided the surface into plains (generally bright areas transected by linear features) and mottled terrain (darker speckled units which generally seemed to be superimposed on older plains). Lineaments were subdivided by their albedo, planform, and apparent topography (Pieri 1981, Lucchitta and Soderblom 1982, Schenk and McKinnon 1989). Categories included dark bands (dark stripes up to ~10 km wide and as long as hundreds of kilometers, generally oriented along great circles and intersecting at low angles), triple bands (paired dark stripes separated by a medial bright stripe), wedge-shaped bands (short dark polygonal features up to 30 km wide), gray bands (intermediate albedo zones up to ~25 km wide), bright bands, and ridges (several kilometers wide and up to ~200 m high). Cycloid ridges, or "flexūs," consist of connected arcuate segments of similar length, convex in the same direction. Most dark bands were generally thought to be tensile in origin, created by global expansion and/or tidal flexing. Ridges were considered to result from compression or intrusion of ice into fractures.

It was considered that Europa's lineaments and terrain types might have distinctive distributions (Pieri 1981, Lucchitta *et al.* 1981, Lucchitta and Soderblom 1982, Schenk and McKinnon 1989, Schenk and Pappalardo 1996). For example, the polar regions appeared to consist of bright plains, dark wedge-shaped bands were seen to be concentrated in the region (0–180° longitude), and ridges (including the flexus) were generally observed roughly concentric to the antijovian point. However, it was recognized that the limited image coverage and sensitivity of landform detection to lighting and viewing geometry made such correlation uncertain. For example, some dark and triple bands were observed to be ridges near the terminator, suggesting that many dark bands and bright cores of triple bands might be ridges. Ridges turned out to be the satellite's most ubiquitous landform; *Galileo* images confirm that ridges form the bright cores of triple bands, which show diffuse dark margins (Greeley 1997), and in general, *Galileo* data now allow structural and albedo-based classifications to be disentangled.

As shown in Figures 15.1 and 15.5, dark mottled terrain dominates the trailing hemisphere and is concentrated in other locations as well. The high latitude bright plains are especially apparent in color images that include the near-infrared (968 nm) filter, in which they are relatively dark due to impurities and/or larger grain size (Clark *et al.* 1998, Geissler *et al.* 1998a). The distribution of bright plains and dark mottled terrain must be viewed cautiously, however, because high resolution images show that albedo does not always correlate to morphology (Greenberg *et al.* 1999).

*Galileo* images show that the wedge-shaped bands known from *Voyager* images are part of a ~2000 km by 600 km zone of disrupted terrain stretching southwest from the antijovian point (Belton *et al.* 1996, Sullivan *et al.* 1998). IR-bright bands are the oldest stratigraphic lineaments in *Galileo* color images (Geissler *et al.* 1998a). They are relatively bright in near-infrared filters, but are dark at short wavelengths and colorimetrically indiscernible in broadband clear filter images.

*Troughs*

The simplest of Europa's landforms are linear to curvilinear troughs (Figure 15.6). They are generally V-shaped in cross section, 100–300 m wide, and can be >100 km long. Their rims are level or raised with respect to the surrounding terrain. These characteristics suggest an origin as tension fractures. The width of most troughs implies that they became wider after the initial fracturing, perhaps from mass wasting and/or movement along the trough axis. In some areas, en echelon troughs curve inward toward one another in the region of their overlap, as the troughs taper in width and intersect, presumably reflecting interaction of the stress fields of simultaneously propagating tension fractures. The elevated flanks of some troughs appear to be transitional to the formation of some double ridges (Head *et al.* 1999, Geissler *et al.* 1998a).

*Ridges*

Ridges are Europa's most ubiquitous landform (Figure 15.6) but are not well understood. They most commonly take

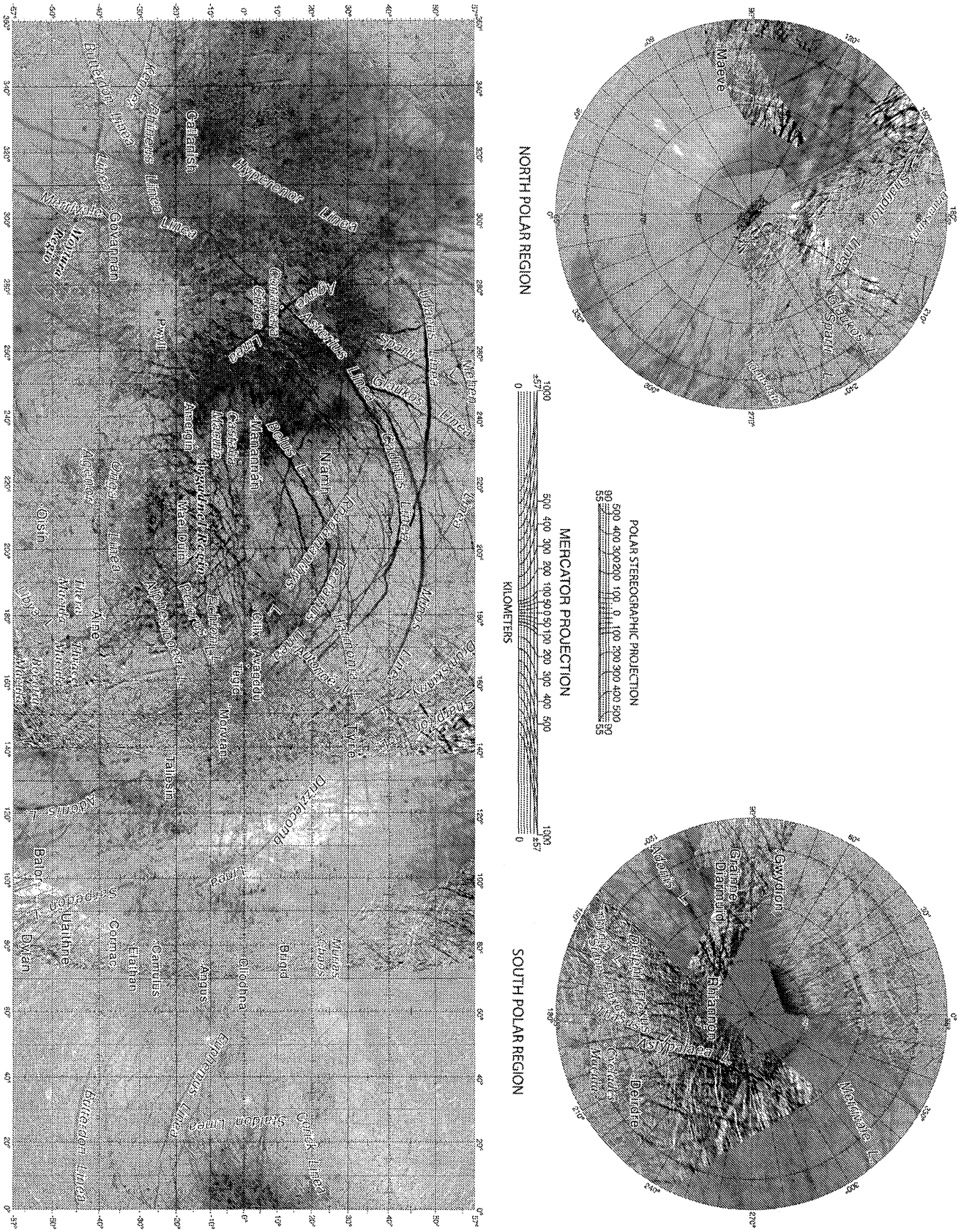


**Figure 15.5.** (a) Polar and (b) mercator maps of Europa showing key place names (from U.S. Geological Survey).

the form of double ridges, i.e., a ridge pair with a medial trough (Figure 15.6a). Some classifications (Pappalardo *et al.* 1998b, Greenberg *et al.* 1998) suggest an evolutionary transition from isolated troughs, to double ridges (including "triple" bands), to complex ridges which generally show a series of subparallel features. Ridges can be short or can have lengths of >1000 km. Their great along-trend uniformity poses a challenge to ridge formation models.

Double ridges are ~500 m to ~2 km wide, have flank slopes near the angle of repose for loose, blocky material, and are characterized by a continuous axial trough. In cross section, some double ridges are slightly convex to trapezoidal, with a central depression. Pre-existing topography has been identified on some ridge flanks (Head *et al.* 1999), though this interpretation has been disputed (Sullivan *et al.* 1999). Mass wasting is prevalent along the ridges, with the debris apparently draping over pre-existing terrain (Sullivan *et al.* 1999). In some cases the trend of the pre-existing topography appears to be deflected as the ridge flank is encountered (Figure 15.6b, full arrow). Many ridges show evidence for strike-slip motion (e.g., Figure 15.6b, half arrows), a characteristic not seen in isolated troughs (Hoppa *et al.* 1999a). Extension is clearly indicated by pre-existing structures offset by some wide ridges that show complex, lineated morphology (Pappalardo *et al.* 1998b, Tufts *et al.* 2000).

Apparent ridge morphology is sensitive to lighting geometry. At low solar incidence angle, some complex ridges appear as triple bands (Figure 15.6c) with diffuse dark material flanking the ridge and infilling topographic lows (Greeley 1997). In high resolution stereo images, it is apparent that dark material is situated in local topographic lows, such as the floors of axial troughs and on wall terraces (Figure 15.6d). The ridge of Figure 15.6e appears to change morphology where it changes direction at a cusp; the apparent change could be due to the orientation with respect to the illumination. The cycloidal pattern of some ridges (e.g., Figure 15.6e) suggests they originated as cycloidal fractures influenced by Europa's diurnally rotating stress field (see Section 15.3.4), while straight ridges probably evolved from relatively straight cracks, perhaps formed with initially greater propagation velocity (Hoppa *et al.* 1999b). Some ridges are flanked by topographic depressions and/or fine-scale fractures (Figure 15.6f), suggesting loading of the lithosphere either from above (due to the weight of the ridge material) or from below (e.g., due to withdrawal of subsurface material) during ridge formation.

We emphasize that cracking patterns and ridge formation could be related, but are inherently different issues. As discussed below, quantitative investigations of stress models and implied cracking patterns indicate that Europa's lineaments probably originated as tensile or extensional tectonic features formed and opened by diurnal and nonsynchronous stresses (Helfenstein and Parmentier 1980, 1983, 1985, McEwen 1986b, Leith and McKinnon 1996, Greenberg *et al.* 1998, 2002a, Hoppa *et al.* 1999a,b). The inference that ridges have evolved from isolated troughs suggests that ridge patterns reflect the major crack patterns within Europa's ice shell. Cracking models are broadly consistent with a range of possible ridge formation models and do not demonstrate any specific ridge formation model. Successful formation models must take into account the observed ridge morphologies, inferred transitions among ridges and other structures, geologic setting and associations, and geophysical constraints.

At least six models have been proposed for the origin of Europa's double ridges (a topic reviewed by Pappalardo *et al.* 1999a). Each model has different implications for the presence and distribution of liquid water at the time of ridge formation. Some models invoke a shallow subsurface ocean, some rely on the action of warm mobile ice with perhaps an ocean at depth, and some imply that liquid water exists in the shallow subsurface.

**Tidal squeezing.** Greenberg *et al.* (1998) suggest that fractures penetrate through an ice shell and open and close by ~1 m in response to diurnal stresses, allowing water and icey to be pumped toward the surface with each cycle to build ridges. Because this model explicitly assumes that the ice shell of Europa is penetrated by dry cracks, the model necessitates a thin ice shell, because cracks can penetrate at most ~6 to 10 km (Golombek and Banerdt 1990, Leith and McKinnon 1996). Crawford and Stevenson (1988) demonstrated the difficulty of cracks penetrating the ice shell, notably in cracking through warm ductile ice near the ocean interface. They found that liquid-filled cracks could ascend to the surface, but the cracks cannot be held open through the entire ice shell. Other difficulties with the model are that diurnal tidal stresses appear insufficient to crack the shell to more than ~150 m depth – although stresses resulting from nonsynchronous rotation may open surface tension cracks to significantly greater depth (see Section 15.4.2), and water in narrow cracks is expected to freeze faster than the tidal cycle (Gaidos and Nimmo 2000).

**Linear volcanism.** Kadel *et al.* (1998) propose that double ridges are linear volcanic constructs, built of debris associated with gas-driven fissure eruptions. Volcanic models suggest that volatiles such as $CO_2$ or $SO_2$ are capable of driving eruptions, despite the negative buoyancy of water relative to ice (Fagents *et al.* 2000). Like the tidal pumping model, the volcanic model has difficulty in cracking the ice if it is presumed that open conduits extend from a subsurface ocean to the surface. It is conceivable that shallow melt chambers feed conduits instead, or that volatiles have driven pinched off water-filled cracks toward the surface (Crawford and Stevenson 1988). However, this model has difficulty accounting for the great length of some ridge complexes across Europa's surface.

**Dike intrusion.** Turtle *et al.* (1998) consider ridges to form by intrusion of melt into a shallow vertical crack to build a double ridge. In this model, a subsurface dike intrudes a shallow subsurface crack that is constricted at its bottom, causing outward and upward plastic deformation to build a ridge.

**Compression.** Sullivan *et al.* (1998) propose that ridges are compressional structures. Compression is a viable model for some ridges, based on reconstruction of preexisting features (Patterson and Pappalardo 2002) and kinematic arguments (Sarid *et al.* 2002).

**Linear diapirism.** Head *et al.* (1999) propose that double ridges form in response to cracking and diapiric rise of warm ice, which intrudes and lifts the surface to form ridges. This model suggests that cracks penetrate to a subsurface ductile ice layer, rather than through the ice shell. Warm subsurface ice moves buoyantly into the fracture, aided by tidal heating. The process is envisioned as anal-

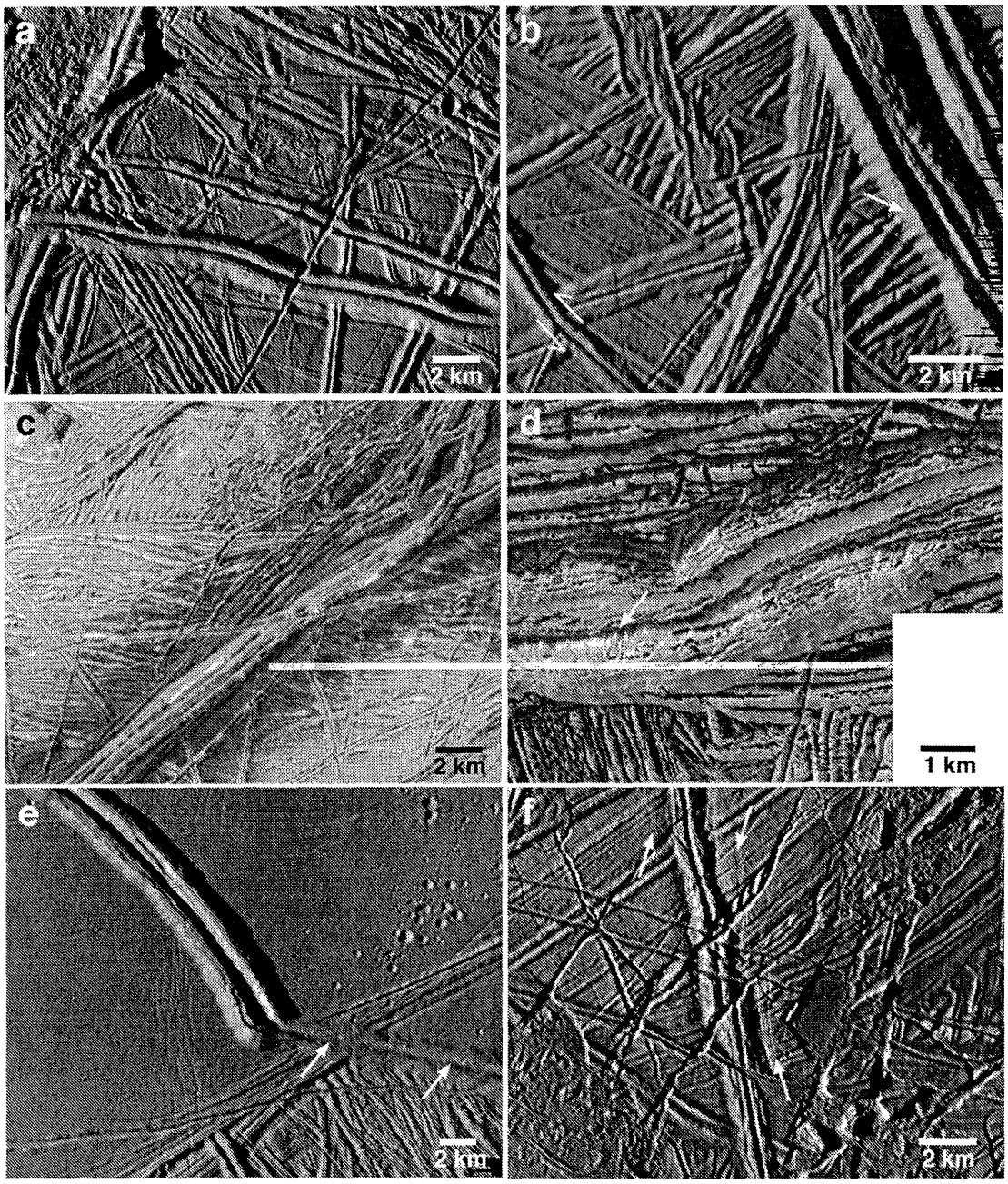


**Figure 15.6.** Examples of ridge and trough morphologies and characteristics seen on *Galileo* images: (a) typical double ridges observed near the terminator (11ESMORPHY01; 33 m/pixel); (b) a complex ridge with possible uplift of pre-existing ridge structures along its flanks (full arrow), and a ridge showing evidence for strike-slip displacement (half arrows) of pre-existing structures (17ESSOUTHP01; 40 m/pixel); (c) a triple band seen at high resolution and low solar incidence angle (14ESTRPBND01; 70 m/pixel); (d) a double ridge seen at low solar incidence angle, revealing dark mass wasted material (arrow) within its crestal trough (12ESWEDGE-02; 25 m/pixel); (e) the cusp of a cycloidal ridge that crosses Astypalaea Linea, with arrows indicating the ridge axis where topography is less prominent (17ESSTRSLP01; 40 m/pixel); (f) a ridge with flanking cuspate troughs and associated fractures (arrows), suggesting flexural downwarp of the brittle surface layer (E6ESBRTPLN01; 53 m/pixel). Some images have been rotated with respect to north, so that illumination is from the left.

ogous to the rise of tabular-shaped "salt walls" which rise along extensional fractures on Earth (e.g., Jenyon 1986) and can cause intrusive uplift. This model has been criticized on the grounds that inner ridges would not be expected of upwelling diapirs (Greenberg *et al.* 2002a).

**Shear heating.** Gaidos and Nimmo (2000) and Nimmo and Gaidos (2002) modify the diapirism model in suggesting that diurnal motion along tidally deformed fractures induces shear heating sufficient to trigger upwelling of warm ice to form a ridge, and perhaps induce partial melting. Frictional heating along a discrete fracture will reduce the ice viscosity within a corresponding shear zone of finite width. The warm,

low-viscosity ice can rise buoyantly to create a ridge, potentially building a few-hundred-meter high ridge in 10 years. Shear heating could enable the intrusion, uplift, and extrusion proposed in the linear diapirism model (Pappalardo *et al.* 1998b, Head *et al.* 1999).

**Triple bands.** *Galileo* observations provide insight into the nature and origin of Europa's triple bands. Their dark margins are seen to be diffuse, and their specific morphologies diverse (Greeley *et al.* 1997, 1998a,b). Although a ridge load might depress a thin ice lithosphere below a water line to cause surface flooding (Greenberg *et al.* 1998), Pappalardo and Coon (1996) argue that this is possible only if the lithosphere is $\leq$2 km thick. Fagents *et al.* (2000) considered the possibility that the dark flanks of triple bands were created by ballistic emplacement of dark materials entrained in gas-driven cryovolcanic eruptions, or that they are thin dark lag deposits formed adjacent to a water or solid-state ice intrusion due to sublimation of surface frosts and local concentration of refractory materials. Along the lines of a model suggested by Head and Pappalardo (1999), ridge-related heating might trigger partial melt generation, perhaps mobilizing brines that contribute to formation of dark flanks.

### *Bands*

The geometries of dark wedge-shaped and gray bands on Europa enable reconstruction of their original configuration, restoring structures that were apparently displaced as the bands opened along fractures (Schenk and McKinnon 1989, Pappalardo and Sullivan 1996, Sullivan *et al.* 1998). These features have been termed "pull-aparts" (Greeley *et al.* 1998a,b) or simply "bands" (Prockter *et al.* 2000). The morphological relationships of pull-apart bands are most clearly seen southwest of Europa's antijovian point, where small plates separate darker material (Schenk and McKinnon 1989, Belton *et al.* 1996, Sullivan *et al.* 1998, Tufts *et al.* 2000). Reconstructions of pull-apart bands imply that the surface layer has behaved brittlely, separating and translating ice slabs underlain by a low-viscosity subsurface material, with the region of separation being infilled with relatively dark, mobile material. Thus, pull-apart bands offer compelling evidence for warm, mobile material in the shallow subsurface at the time of their formation. Stratigraphic evidence indicates that dark bands brighten with time (Pappalardo and Sullivan, 1996, Greeley *et al.* 1998a,b, Geissler *et al.* 1998b), perhaps related to chemical changes and/or sputtering processes that redistribute surface frost (Geissler *et al.* 1998a, Pappalardo *et al.* 1999a).

Analogies have been made between pull-apart formation on Europa and the formation of leads in terrestrial sea ice (Pappalardo and Coon 1996, Greeley *et al.* 1998a,b). Greenberg *et al.* (1998) and Tufts *et al.* (2000) consider that cyclical tension and compression due to Europa's diurnal tidal flexing might create bands through a ratcheting process. In this view, cracks open during the tensile phase of the diurnal cycle, allowing water to rise and freeze. The cracks are unable to close completely during the compressional phase due to the addition of new material; hence, the band widens with time as new material is added. However, as described above, models which rely on cracking through the ice shell to the depth of liquid water face a number of objections.

Arguing from morphological analyses of *Galileo* images, Sullivan *et al.* (1998) and Prockter *et al.* (2002) suggest that band formation could be analogous to terrestrial spreading centers. In terrestrial plate tectonics, "spreading" occurs where the lithosphere has separated and new material is intruded and extruded as the opposing original lithospheric plates are pulled apart. Regional *Galileo* images of pull-apart bands show an internal structure of ridges and troughs trending subparallel to each other and the boundaries of the band (Figure 15.7a). An overall bilateral symmetry suggests that the spreading analog may be appropriate in some cases.

Pull-apart band margins are generally sharp, and some show rounded bounding ridges (Figures 15.7a,e). A narrow central trough is common and is remarkably linear and uniform in width (Figures 15.7b,c, arrows). A hummocky textured zone commonly occurs on either side of the trough (braces on Figures 15.7b,c), or sometimes throughout much of a band (Figure 15.7d). Outside of the hummocky zone (Figures 15.7b,c,d) are subparallel ridges and troughs 300 to 400 m wide, which are regularly spaced and generally triangular in cross section. In the band of Figure 15.7d, the ridges and troughs have been interpreted as south-facing domino-style fault blocks (Figueredo and Greeley 2000, Prockter *et al.* 2000). Some bands, notably Astypalaea Linea (Figure 15.7e), show a significant strike-slip component, suggesting oblique opening (Tufts *et al.* 1999).

Reconstruction of bands suggests that at least some have opened along pre-existing ridges (Prockter *et al.* 2002). *Galileo* stereo images of several dark pull-apart bands (Figures 15.7a and 15.7b) show that bands commonly stand higher than the surrounding ridged plains (Giese *et al.* 1999, Prockter *et al.* 2000, Tufts *et al.* 2000). This is consistent with emplacement of buoyant material, such as ice that is warm and/or clean relative to the cold and/or saltier surrounding lithospheric material (Prockter *et al.* 2000). These bands can cause significant tectono-volcanic resurfacing of Europa (Pappalardo and Sullivan, 1996, Greeley *et al.* 2000). The bright ridged plains of Europa contain many bands and band fragments; however, ridge morphologies in the ridged plains are diverse, suggesting a complex origin through multiple processes.

Agenor Linea is a rare bright band on Europa's surface, considered from *Voyager* analyses to be possibly of compressional origin (Schenk and McKinnon 1989). It has unusual photometric properties suggesting that it might have been active recently (Geissler *et al.* 1998c). However, high-resolution observations during *Galileo* orbit E17 show that it is cross-cut by small fractures and mottled terrain, reducing the likelihood that it is currently active (Prockter *et al.* 1999). Structural relationships within the band suggest that it formed by right-lateral strike-slip motion of ice slabs (Prockter *et al.* 2000), whereas Sarid *et al.* (2002) present evidence for a component of convergence.

### *Folds*

Extensional tectonics was identified on Europa beginning with the *Voyager* mission (e.g., Schenk and McKinnon 1989). However, only tentative examples of compressional structures have been identified. Morphological evidence for folds with ~25 km wavelength is found in the Astypalaea Linea region (Prockter and Pappalardo 2000) (Figure 15.8).

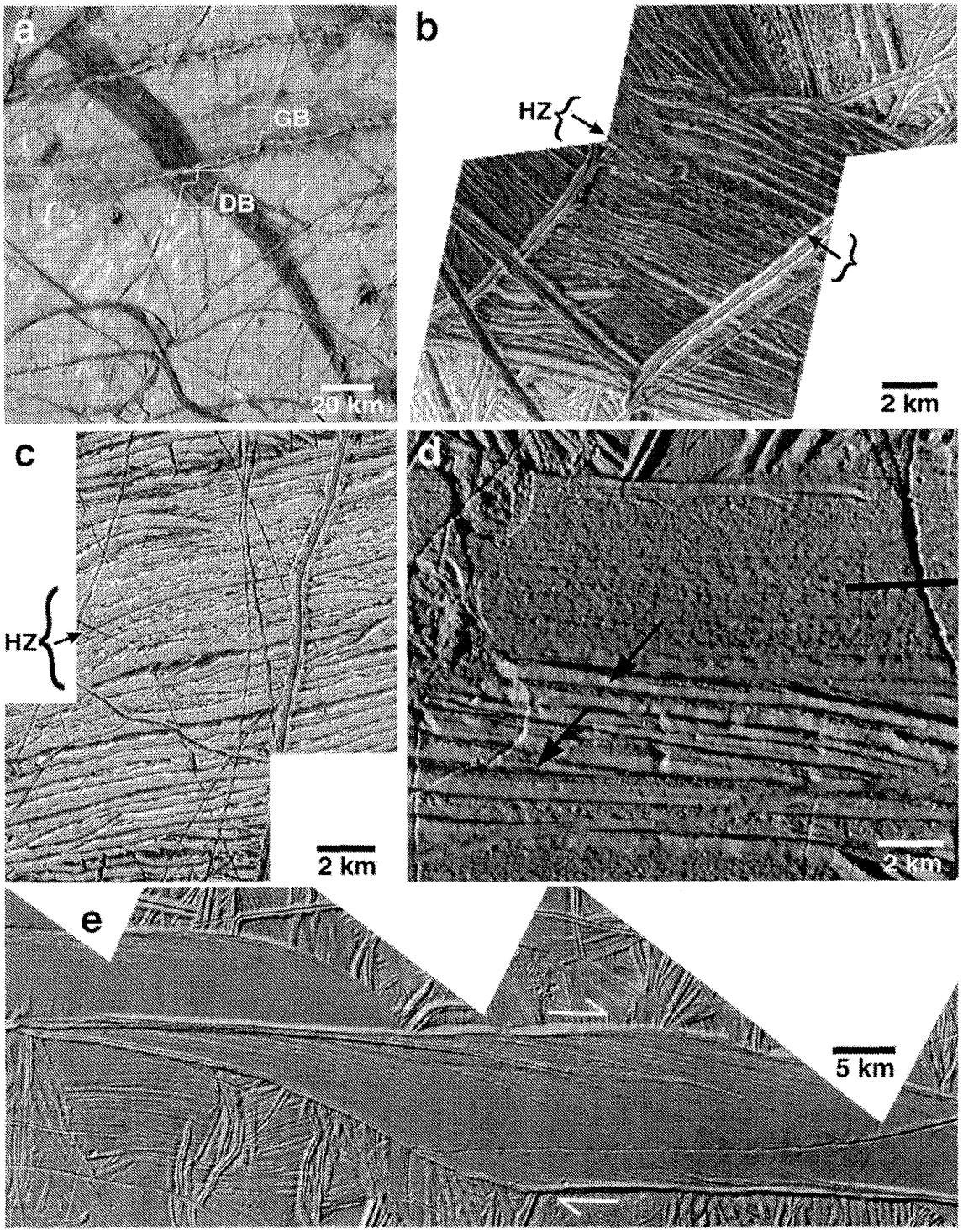


**Figure 15.7.** Examples of band morphologies and characteristics seen on *Galileo* images: (a) a wedge-shaped dark band (DB) cross-cuts a brighter gray band (GB); outlines mark locations of the two subsequent views (C3ESWEDGES01; 420 m/pixel); (b) at high resolution, the dark band shows multiple subparallel ridges and troughs that flank a central trough (arrows) and hummocky zone (braces, HZ) (12ESWEDGE-02; 25 m/pixel); (c) at high resolution the gray band shows similar characteristics of a central trough (arrow) and hummocky zone (braces, HZ) (12ESWEDGE-02; 25 m/pixel); (d) a band seen at high resolution and low solar incidence angle displays subparallel ridges and troughs with characteristics of normal fault blocks (11ESMORPHY01; 33 m/pixel); (e) Astypalaea Linea has probably opened by strike-slip motion (arrows) along a pre-existing double ridge (17ESSTRSLP01; 40 m/pixel).

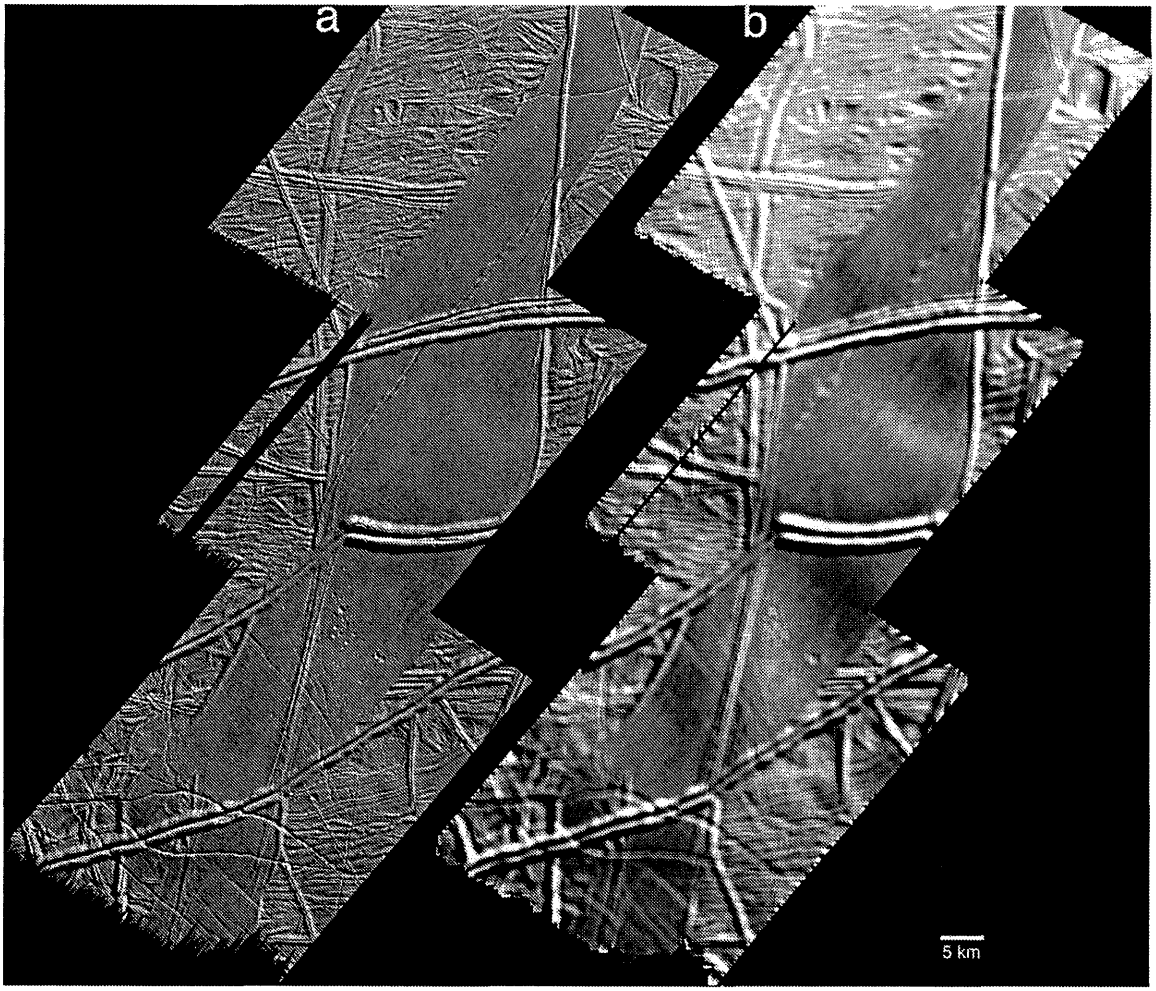


**Figure 15.8.** Possible folds on Europa: (a) subtle shading variations across Astypalaea Linea are inferred to be folds of ~25 km wavelength (17ESSTRSLP01; 40 m/pixel); (b) a low-pass filter highlights the long-wavelength anticlinal swells and synclinal valleys (after Prockter and Pappalardo 2000).

*Galileo* images show subtle shading variations suggestive of folds, including anticlines and synclines. Relaxation of fold topography could cycle material back into Europa's deeper interior, of relevance to astrobiological models (see Section 15.5).

Other folds could exist (Figueredo and Greeley 2000, Prockter *et al.* 2002) but subtle long-wavelength topography makes them generally difficult to recognize. Some rounded ridges in the plains could be small folds. Overall, these folds can accommodate only small amounts of strain. Possible convergent bands have also been identified by Greenberg *et al.* (2002b) and Sarid *et al.* (2002), and may help alleviate the overall strain problem.

### *Pits, Domes, and Spots*

*Galileo* images show that Europa's domes, pits, and spots (commonly referred to as "lenticulae"), along with larger chaos regions and smooth dark plains, comprise the satellite's mottled terrain (Figure 15.9, Carr *et al.* 1998, Pappalardo *et al.* 1998a, Greeley *et al.* 2000). Pappalardo *et al.* (1998a) argue that most lenticulae have diameters of ~10 km (see also Spaun *et al.* 1999a,b, 2001), and that this size similarity and morphological gradation among pits, domes, and spots suggests that they are genetically related (Carr *et al.* 1998, Greeley *et al.* 1998b, Pappalardo *et al.* 1998a), which would be consistent with an origin through diapirism as the manifestation of solid-state convection of Europa's icy shell (Rathbun *et al.* 1998). However, Greenberg *et al.* (1999) argue that pits and spots are only small members of a continuous size distribution of chaos areas.

The domes have been subdivided into two endmember types based on their relationship to the pre-existing surface (Carr *et al.* 1998). Type 1 domes consist of material different from the ridged plains. Typically this material is darker than the ridged plains. Pre-existing terrain has been destroyed in situ and/or obscured by newer material. Proposed models of formation include: (1) ice volcanism (Fagents *et al.* 2000), (2) diapirism (Pappalardo *et al.* 1998a, Rathbun *et al.* 1998) possibly accompanied by partial melting of a salt-rich icy lithosphere (Head and Pappalardo 1999), and (3) melt-through of the ice shell (Carr *et al.* 1998, Greenberg *et al.* 1999). The claim (Pappalardo *et al.* 1998a) for regular size and spacing suggests diapiric origin, a mechanism predicted by models of tidally heated ice above liquid water (Reynolds and Cassen 1979, Squyres and Croft 1986,

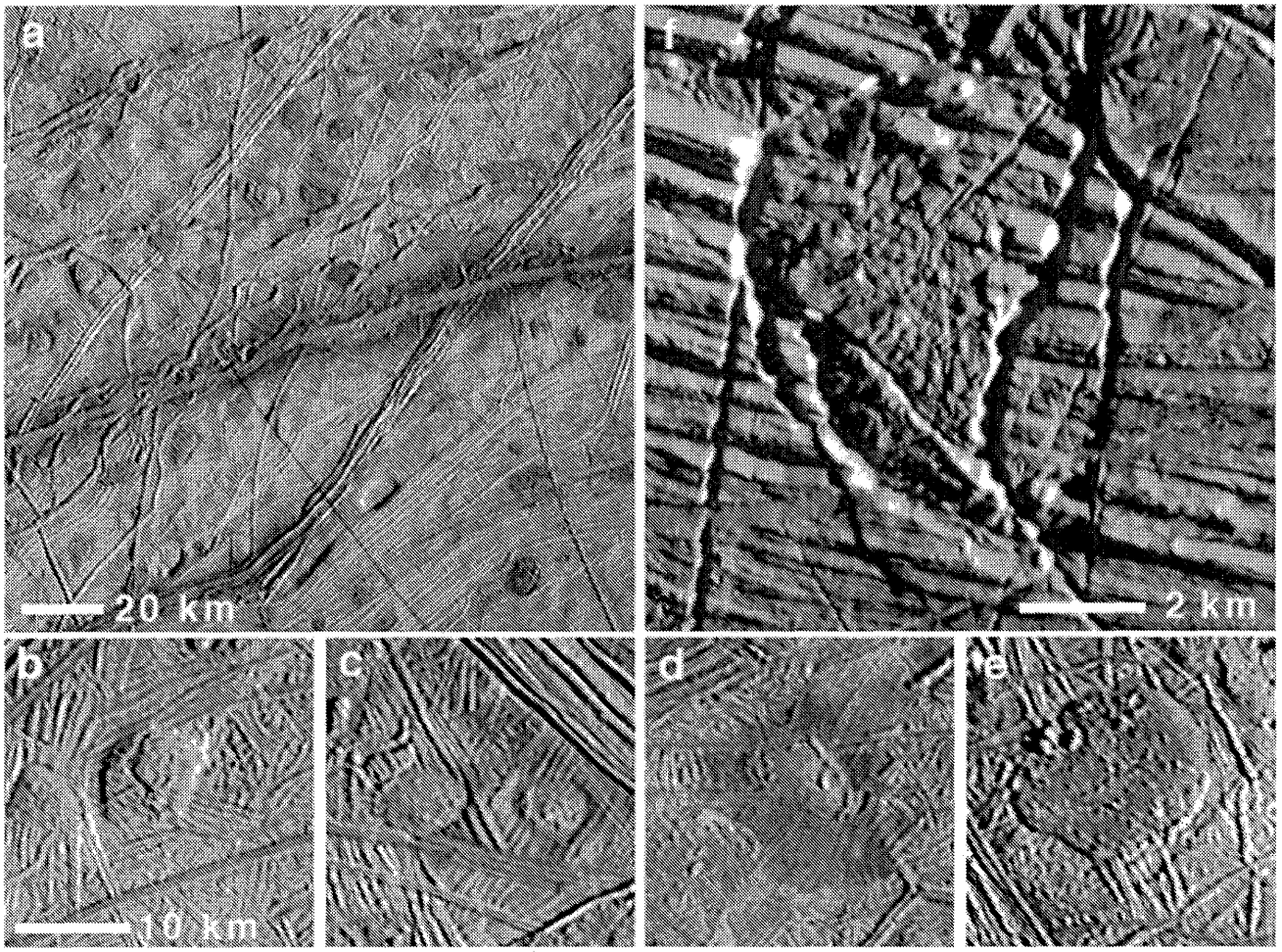


**Figure 15.9.** *Galileo* views of lenticulae: (a) regional view of an area dense with lenticulae, illustrating their common ~10 km diameters and morphological variety as pits, domes, and spots (15ESREGMAP01; 230 m/pxl). (b) a dome showing evidence for localized uplift of the pre-existing ridged plains; (c) pits showing surface disruption and/or extrusion to create hummocky material; (d) lenticula with an annulus of smooth, relatively low albedo material, suggesting thermal alteration of the surface or localized extrusion of melt; (e) lenticula with convex margins that stand slightly above the surrounding terrain, suggesting extrusion of viscous material; (f) high-resolution view of a lenticula illustrating in situ disruption of pre-existing ridged plains and replacement by hummocky material, in a manner similar to the formation of larger chaos regions (11ESMORPHY01; 33 m/pxl). Illumination is from the right in all images; north is toward the top in all images except (f), which is south toward the top.

Pappalardo *et al.* 1998a, Rathbun *et al.* 1998, McKinnon 1999, Wang and Stevenson 2000).

Pre-existing terrain is preserved on the surfaces of many domes, suggesting that the surface was upwarped but not destroyed (Carr *et al.* 1998, Greeley *et al.* 1998b, Pappalardo *et al.* 1998a, Pappalardo 2000). These Type 2 (Carr *et al.* 1998) or "upwarped" (Pappalardo 2000) domes are subcircular to elliptical, locally high features on which continuous pre-existing structure is preserved. Fractures can occur along their crests. Dome boundaries can be continuous with respect to the surrounding terrain with no discrete scarp, producing a gentle convex dome, or a relatively flat-topped surface. These morphologies suggest upwarp and flexure of an elastic surface layer. Domes are commonly bounded by abrupt scarps of apparent tectonic origin. Associated dome tops are tilted or relatively flat, suggesting brittle failure and punching upward of the dome along bounding fractures, consistent with laccolith-like intrusions (Pappalardo 2000).

Chaos regions are typically composed of polygonal blocks of pre-existing ridged plains that have shifted within a matrix of hummocky material (Carr *et al.* 1998). Chaos matrix material can be either low-lying or high-standing relative to the surrounding plains (Collins *et al.* 2000, Greeley *et al.* 2000). In Conamara Chaos (Figure 15.10), ~60% of the pre-existing terrain was replaced or converted into matrix material, and many of the surviving blocks can be restored to their original positions (Spaun *et al.* 1998).

Morphological transition to larger chaos areas suggests related formational processes for lenticulae and chaos (Spaun *et al.* 1999a, Riley *et al.* 2000). Chaos regions have been interpreted as areas of amplified heat flow and perhaps local melting (Carr *et al.* 1998, Williams and Greeley 1998, Greenberg *et al.* 1999). In a melting model, blocks are analogous to buoyant icebergs. Alternately, solid-state ice

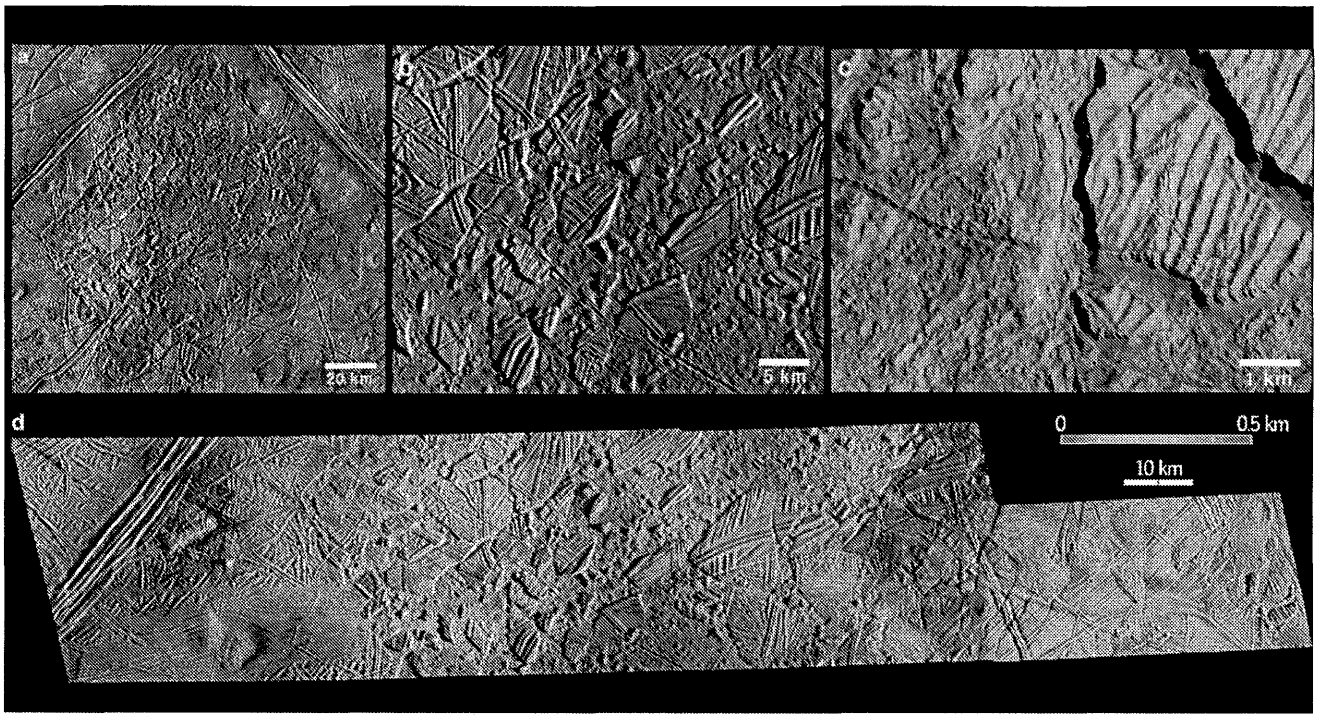


**Figure 15.10.** Conamara Chaos imaged at three scales, and corresponding topographic model: (a) regional-scale (180 m/pixel) view of Conamara shows its overall low albedo, angular boundaries, and location south of the intersection of two prominent ridges (E6ESDRKLIN01); (b) at high resolution (54 m/pixel), it is apparent that polygonal blocks have translated and rotated in a mobile matrix (E6ESBRTPLN01); (c) at very high resolution (11 m/pixel), mass wasting is apparent along steep slopes, and craters and fractures in the matrix material indicate that it is brittle and immobile today (12ESCHAOS01); (d) topographic model across Conamara derived from stereo and photoclinometric techniques, showing that Conamara Chaos stands generally higher than its surroundings; color bar shows relative elevation (courtesy Paul Schenk). At the time of going to press a colour version of this figure was available for download from http://www.cambridge.org/9780521035453.

might have risen diapirically to the surface, disrupting the relatively cold and rigid lithosphere similar to the means proposed for lenticulae (Pappalardo *et al.* 1998a) and translating fragmented slabs of colder lithospheric material. The conversion of pre-existing ridged terrain to chaos appears to involve separate disruptions that merge (Spaun *et al.* 1999a).

Complete melt-through of Europa's ice shell would require a weakly stratified ocean to permit transfer of heat from the silicate mantle to the base of the ice shell, and a large plume of concentrated heat that is stable for at least hundreds of years (Collins *et al.* 2000, Thompson and Delaney 2001, O'Brien *et al.* 2002, Buck *et al.* 2002). If the ice shell is thick, flow of the warm base of the ice shell would be so rapid as to preclude melting (Stevenson 2000b). However, this mechanism does not preclude melt-through in a thin $\leq$6 km ice shell (O'Brien *et al.* 2002).

The fact that small blocks were mobilized and tilted within the chaos challenges the notion that the matrix was emplaced as solid-state ice, because the timescale of block movement in warm ductile ice is expected to be longer than the timescale of thermal diffusion causing blocks to cool in place (Collins *et al.* 2000). In models without melt-through, it is more likely that chaos formed in response to local melting within the ice shell, triggered by rising warm diapiric masses. This could be partial melting as the diapir impinges on relatively salt-rich ice (Head and Pappalardo 1999, Collins *et al.* 2000). Melting due to concentrated tidal heating within warm ice diapirs was suggested (McKinnon 1999, Wang and Stevenson 2000, Sotin *et al.* 2002), but the small size of diapirs could mean that their tidal heating is negligible (Moore 2001).

Topographic data across Conamara (Figure 15.10d) provide evidence that much of the chaos is ~300 m higher than the surrounding plains (Schenk and Pappalardo 2002). Similar results are found for a mitten-shaped chaos region in the leading hemisphere (Figueredo *et al.* 2002). High-standing topography is hard to understand if chaos formed by melt through of an ice shell and then allowed to cool to thermal steady state, but can occur if warm diapiric ice rises from the base of ice shell and is extruded.

### 15.3.2 Age Relationships

The existence, stability, and evolution of a subsurface ocean through time are intricately tied to Europa's surface age and geologic activity. Most chaotic and dark plains materials are among Europa's youngest units, cross-cutting older bands and ridged plains, while ridged plains materials are commonly inferred to be the oldest units (Figure 15.11) (Head *et al.* 1999, Sullivan *et al.* 1999, Prockter *et al.* 2000, Figueredo and Greeley 2000, Kadel *et al.* 2000, Greeley *et al.* 2000). Greenberg *et al.* (1999, 2002a) and Riley *et al.* (2000) argue that this impression is an artifact of the difficulty of recognizing older terrains that have been cut up by cracks, ridges and bands.

If the former interpretation is correct, Europa would appear to have changed in geological style over time, from

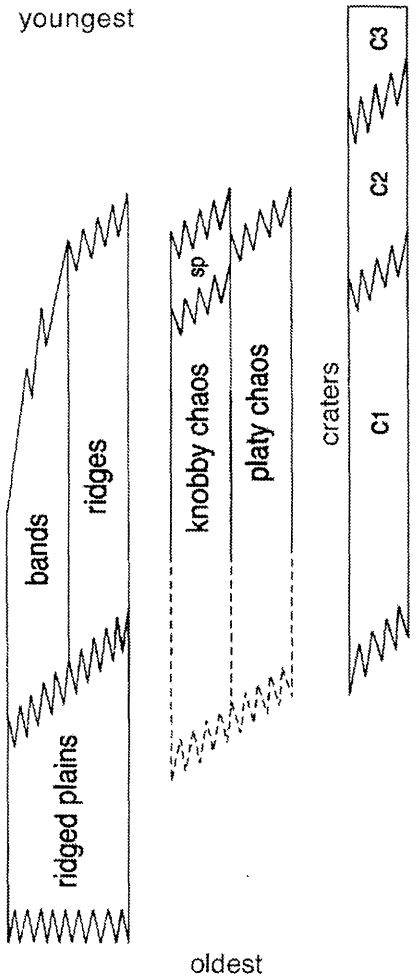


**Figure 15.11.** Generalized stratigraphic column of Europa (from Greeley *et al.* 2000).

ridged plains formation to mottled terrain formation. Perhaps mottled terrain units formed by diapirism that was triggered as an ice shell cooled and thickened to the point at which it reached a critical thickness and solid-state convection was initiated (Pappalardo *et al.* 1998a, McKinnon 1999, Figueredo and Greeley 2004).

If Europa's average surface age is only ~60 Myr old (Section 15.3.3), it seems unlikely that a fundamental change in style occurred only during the last ~1% of the satellite's total history. Four possible evolutionary scenarios can be envisioned (Pappalardo *et al.* 1999a): (1) the satellite is in steady state and resurfaces in a patchy style; (2) the satellite is now at a very special time in its history; (3) the global resurfacing is episodic or sporadic; or (4) the surface is instead very old. Models of Europa's tidal evolution suggest scenarios in which episodic or sporadic resurfacing are plausible (see Section 15.4.3).

### 15.3.3 Craters and the Cratering Record

*Voyager* images of Europa showed features interpreted to be of impact origin (Smith *et al.* 1979a,b, Lucchitta and Soderblom 1982, Malin and Pieri 1986). The relatively low image resolution, however, led investigators to postulate that either the surface was very young, or that many of the mottled albedo features could be craters that had undergone viscous relaxation. For example, Lucchitta and Soderblom (1982) classified features observed in *Voyager* data into two catagories: (1) craters several tens of km in diameter characterized by rims, central peaks and ejecta deposits, and (2) large, dark, flat circular spots ≥100 km in diameter (e.g., Tyre) on which lineaments appear to converge. Features in this latter catagory were interpreted to be relic, relaxed impact craters (Lucchitta and Soderblom 1982, Malin and Pieri 1986). Uncertainties about the identification and number of craters led to differences in the interpretation of surface ages (e.g., Lucchitta and Soderblom 1982).

*Galileo* targeting was designed to address many of the issues raised by the *Voyager* observations (Carr *et al.* 1995), including the nature of impact craters (e.g., Moore *et al.* 1998, 2001), implications for surface ages (e.g., Neukum 1997, Chapman *et al.* 1998, Zahnle *et al.* 1998), and insight into the outer layers of Europa (Turtle and Pierazzo 2002, Schenk 2002). These topics are reviewed here and in Chapter 18.

#### *Morphology and Structure*

*Galileo* data show that impact craters on Europa have the full range of features typical of craters on silicate bodies (Figure 15.12), such as bowl shapes in smaller examples (e.g., Govannan, ~10 km in diameter), and flat floors, central peaks and massifs, terraces and extensive bright ray systems in larger examples (e.g., Manannán and Pywll, both in the 20–25 km diameter range). The larger features suspected to be of impact origin, such as Tyre, exhibit extensive secondary crater fields, excavated dark material, and an unusual interior structure.

Although there are similarities to craters on silicate bodies, fundamental differences are seen. For smaller craters, the transition from bowl-shaped to complex features occurs at about 5–6 km, with larger craters exhibiting central peak structures (Schenk 2002). Cilix (18 km diameter) is a good example of a complex crater; it has an elongate central peak complex, a flat floor, and terraced walls. The rim is polygonal and there is a reddish brown continuous ejecta deposit, suggesting that material different than that of the surface was excavated. A digital terrain model (Giese *et al.* 1999) shows that the floor is relatively flat and is at the same elevation as the surrounding terrain; the central peaks rise about 300 m above the floor, comparable to the elevation of the crater rim crest.

As crater diameter increases, some changes are observed. The 24 km diameter crater Pwyll (Figure 15.12; Moore *et al.* 1998) has an extensive bright ray system extending >1000 km and a central circular dark spot that is a pedestal-like continuous ejecta deposit. The crater floor is relatively flat and extremely shallow (Geise *et al.* 1999). The proximal edge of the ejecta gives way to a bright braided pattern and radial rays of secondaries. A large peak complex ~100–300 m high is offset from the center.

Secondary impact craters from Pwyll range in diameters from ~1 km to the limit of resolution (~10 m). High-resolution images in Conamara Chaos, some 1000 km from Pwyll, show secondary craters from Pwyll up to ~500 m in

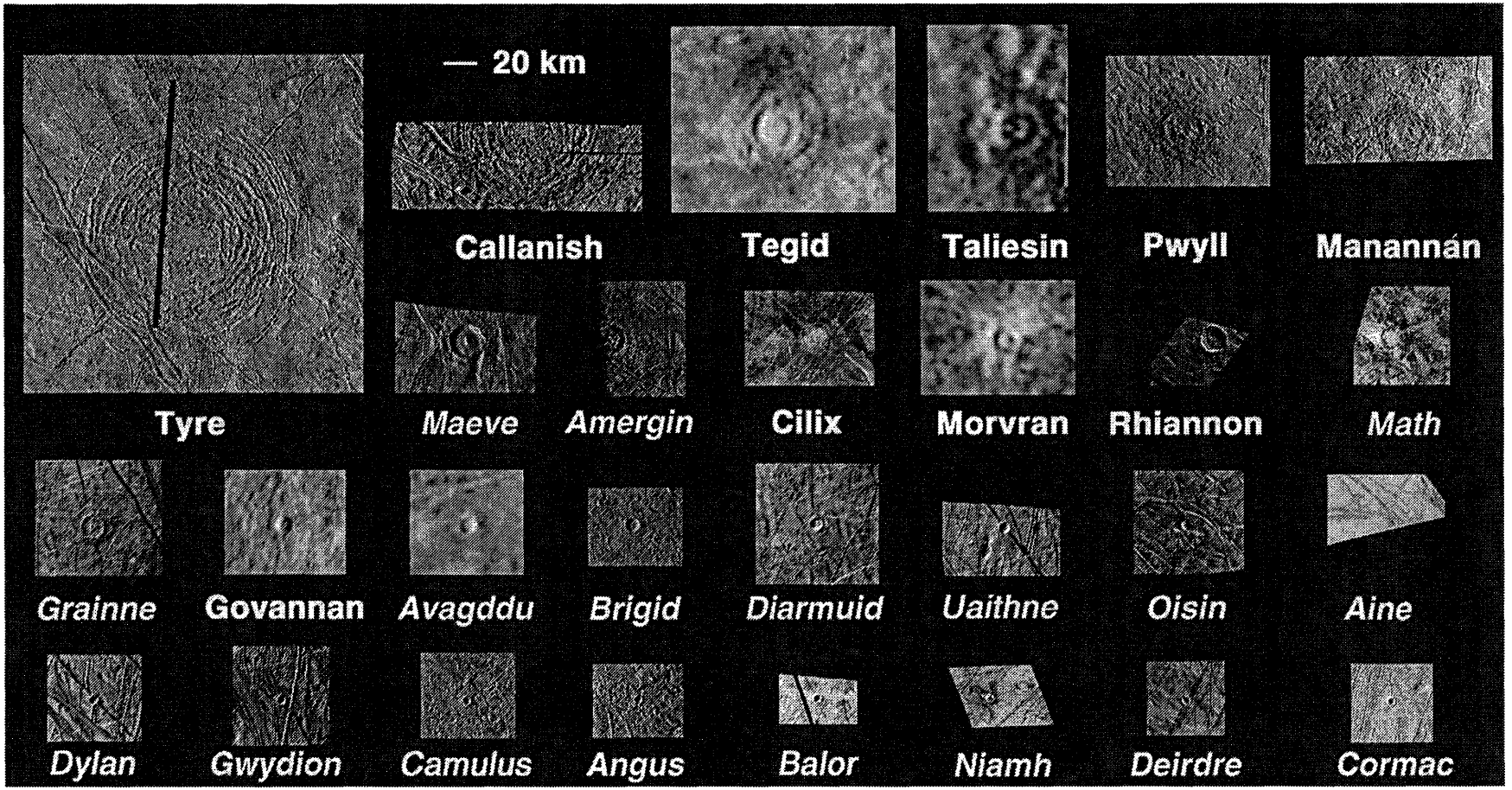


**Figure 15.12.** Impact craters >4 km in diameter on Europa, arranged in order of decreasing size. Italicized names are provisional (from Moore *et al.* 2001).

diameter. The fact that the surface of Europa is nearly "pristine" provides an opportunity to assess the characteristics of Pwyll rays and the nature of secondary craters (Bierhaus *et al.* 2001). For example, Moore *et al.* (1998) found that the number and distribution of Pwyll secondaries was more consistent with an impact into solid ice than into a solid ice layer overlying liquid water at shallow (~5 km) depths (based on comparison to Callanish). Further analyses show that the secondary ejecta fragments are smaller than those formed on silicate bodies at equivalent ejecta velocities, and that there is an azimuthal variation within rays, with ejecta fragment sizes being larger near the center of the ray. The Pwyll secondary crater size–frequency distribution suggests that most of the small craters on Europa are secondaries, rather than an abundance of small primaries (Moore *et al.* 2001, Beirhaus *et al.* 2001, Chapter 18).

Tyre and Callanish provide examples of the morphology and structure of larger craters (43–44 and 29–47 km diameter, respectively)(Moore *et al.* 1998, 2001, Kadel *et al.* 2000). Both show complex interiors and concentric troughs but rim crests are not obvious. The center of Tyre has a smooth, high-albedo patch interpreted to be impact melt, or possibly material that was derived as a fluid emplaced from below. A rough inner unit surrounds the smooth inner unit and is interpreted to be impact melt and fragmented target material. This zone is surrounded by a smoother surface characterized by darker, redder material interpreted to be part of the continuous ejecta, the texture of which suggests that it was emplaced as a fluid. Concentric troughs and fractures are interpreted as tectonic features. Examination of Callanish shows that the formation of the concentric troughs mostly predated the emplacement or solidification of the continuous ejecta. The rapid formation of the troughs suggests that the substrate behaved as a low-viscosity material on the timescales of basin formation (Turtle *et al.* 1999). Numerous small pits, some with raised rims, form radially oriented pit chains beyond the continuous ejecta unit, and are interpreted to be secondary craters.

The distal zones of craters such as Pwyll show a pedestal-like ejecta facies (Figure 15.12). High-resolution images fail to show definitive evidence of liquid associated with the facies emplacement. Moore *et al.* (1998) concluded that the pedestal is due to a convex upward scarp, possibly formed by outward creep of across warm, plastically deforming ice.

In summary, Europan craters show the influence of target characteristics on crater morphology, including: (1) the transition from simple to complex occurs at a lower diameter than on silicate bodies of comparable gravity; (2) craters are anomalously shallow, relative to those on silicate bodies of comparable gravity, interpreted to be due to post-impact isostatic adjustment; and (3) concentric rings surrounding the two largest craters (Callanish and Tyre) suggesting that ductile flow at relatively shallow depths occurred.

*Implications for Crustal Structure and Surface Ages*

The onset diameter of central peaks and crater structure can be used to probe the nature of the outer layer(s) of Europa. Simple craters are interpreted to be too small to undergo significant collapse. Using the onset diameter for central peaks (>5 km) and estimates of transient crater depths, Moore *et al.* (2001) concluded that craters ~10–18 km in diameter (3–6 km deep transient craters) did not penetrate to a liquid layer and, thus, that the ice must be at least several km thick at the time of crater formation. Moore *et al.* (1998) and Schenk (2002) argue that the unusual morpohology of impact structures ≥30 km in diameter, such as Callanish and Tyre, suggests that there was excavation to liquid water or possibly very warm ice at depth. Overall, the impact crater data appear to place the base of a solid ice layer at ≥20 km (Schenk 2002). The young age of the surface, as well as wide separation of Tyre and Callanish, suggest that this could represent a typical value for Europa for geologically recent times.

*Galileo* data show that the number of primary impact craters on Europa is small (e.g., Moore *et al.* 1998, 2001), suggesting a relatively young age, but there is debate about the absolute age of the surface. On the one hand, Chapman *et al.* (1998) suggested a mean age of $\sim 10^7$ to $10^8$ years, while Neukum (1997) suggested that some surfaces on Europa are as old as $3.0–3.3 \times 10^9$, but could be as young as 10 million years. The differences are due to several factors, including assumptions about the age of Ganymede's oldest large basin (Gilgamesh), and uncertainties in the present-day comet impact rate in the jovian system. These issues are reviewed and discussed by Zahnle *et al.* (1998) and in Chapter 18, where it is argued, based on the dynamics of small body populations, that Europa's average surface age is nominally $\sim 6 \times 10^7$yr.

### 15.3.4 Global Tectonic Patterns and Stress Mechanisms

*Diurnal Stressing*

Europa's orbit has a forced eccentricity of 0.01, maintained by the 3-body Laplace resonance with its neighboring satellites Io and Ganymede. The resultant tidal flexing of Europa occurs on the 3.55 day period of its orbital revolution, producing "diurnal" stresses. The magnitude of tidal flexing is a function of the satellite's interior structure. Total vertical deflection is expected to be only 1 m if the interior is solid, or 30 m if an icy shell is able to flex above a subsurface water layer, with only very weak dependence on the depth to the ocean (Moore and Schubert 2000). Consequently, stresses due to diurnal orbital flexing are expected to decrease markedly if there is no liquid layer at depth. Moore and Schubert (2000) show that an interior rigidity as low as $10^6$ Pa could produce a significant tidal amplitude (18 m) without a subsurface ocean, but rigidity is so low that it would require the rock mantle to be substantially partially molten. The magnitude of the stresses for a floating ice shell is ~100 kPa = 1 bar (Helfenstein and Parmentier 1980, Cassen *et al.* 1982, Greenberg *et al.* 1998, Hoppa *et al.* 1999a).

Greenberg *et al.* (1998) modeled the diurnal stress surface pattern as it changes continuously, and recognized that the direction to Jupiter changes in Europa's reference frame as the satellite orbits. As a result, surface stresses at any given location change in magnitude and rotate during an orbital cycle, resulting in clockwise stress rotation in the southern hemisphere and counterclockwise in the northern hemisphere. This could account for some of the observed sur-

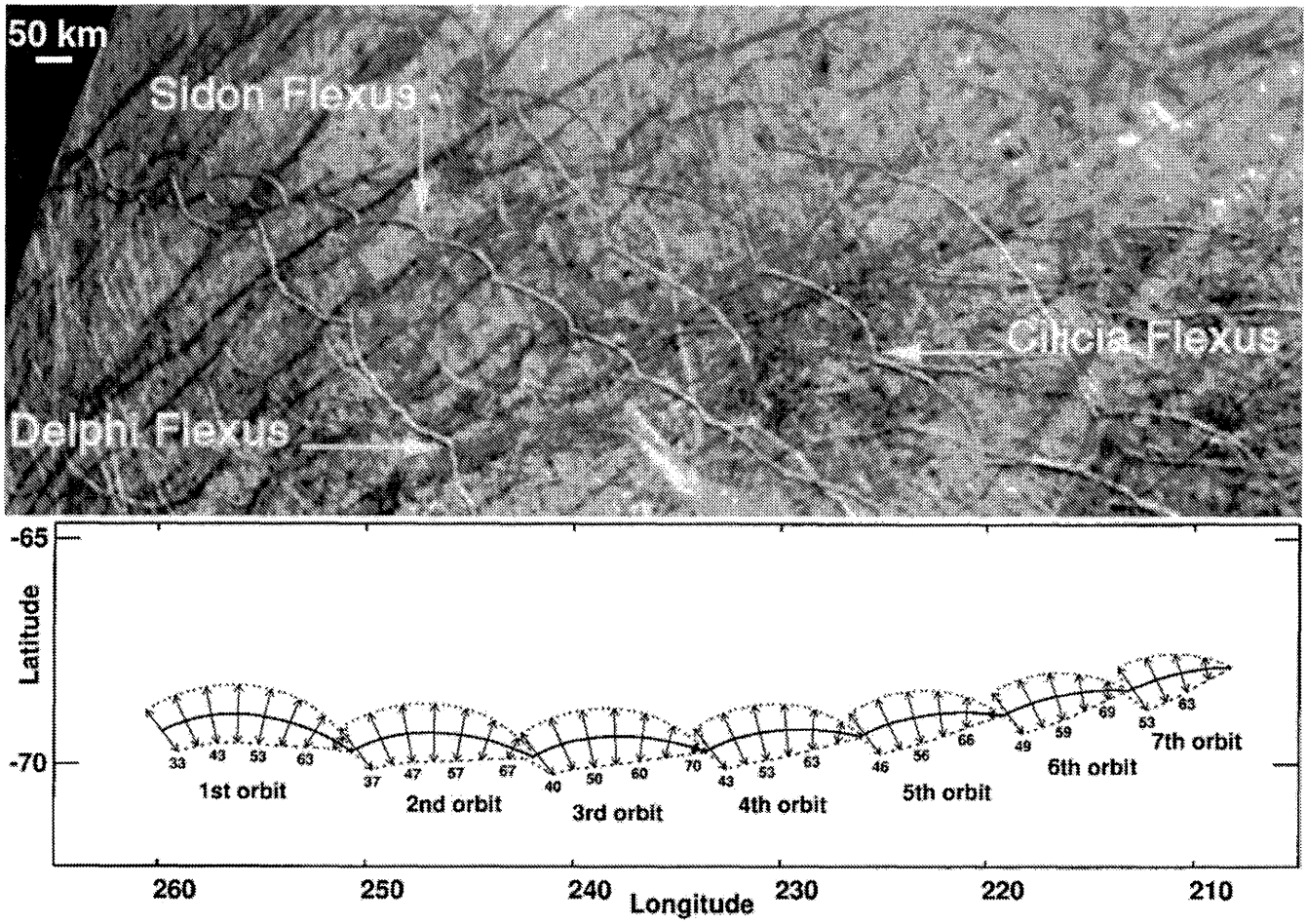


**Figure 15.13.** (upper) Cycloidal ridges (flexūs), as imaged by *Voyager 2*; (lower) model trajectory of a fracture propagating eastward across Europa. Arrows (within each segment) indicate the direction of least compressive (maximum tensile) stress. The magnitude and direction of diurnal stress vary to allow the fracture to trace a cycloidal path, with one arc traced each Europan orbit. At cusps, stress magnitude diminishes and crack propagation wanes, until sufficient stress builds during the next orbit to permit further propagation (after Hoppa *et al.* 1999b).

face features. For example, *Galileo* images show many cases of strike-slip offsets on Europa. Hoppa *et al.* (1999a) and Sarid *et al.* (2002) show a preferred direction of strike-slip offset in each hemisphere, with propensity for right-lateral strike-slip in the southern hemisphere, and left-lateral in the northern hemisphere. This could be explained by the rotation of diurnal stresses, with faults effectively "walking" in a right-lateral sense in the southern hemisphere, and in a left-lateral sense in the northern hemisphere (Hoppa *et al.* 1999a). Hoppa *et al.* (1999a) suggest that the observed strike-slip features formed at different longitudes with respect to Jupiter than currently occupied, and were shifted by nonsynchronous rotation (discussed below and in Section 15.4.2).

Diurnal stresses can explain the patterns of cycloid ridges (Figure 15.13) and other cycloidal structures, such as some gray and dark band boundaries (Hoppa *et al.* 1999a, Greenberg *et al.* 2002a). If a fracture propagates across Europa's surface at an appropriate speed (about 3 km $h^{-1}$), the stress orientation rotates during a fraction of the Europan day and the propagating fracture traces out the curvature of a single cycloidal arc. The diurnal stress then decreases below the critical value for fracture until the following orbit, when tensile stress again increases, and fracture propagation reinitiates, generating the next cycloidal arc. This model produces an excellent match to the shapes of cycloidal features if tensile failure occurs at a stress of ~25 kPa and propagation halts when stress is below ~15 kPa (all quite low values).

The Hoppa *et al.* (1999b) model explains several aspects of cycloidal structures shown in Figure 15.13. For example, the arcs of an individual cycloidal chain always show a consistent direction of convexity, while different chains can have opposite convexity directions. In the Hoppa *et al.* model, convexity direction simply depends on the fracture propagation direction relative to the sense of stress rotation. Similarly, the overall curvature of a cycloidal chain reflects the regional change in stress orientations from the latitude and longitude regime in which the fracture initiated, and into which it propagates. As with the strike-slip "walking" model for strike-slip tectonism, longitudinal shifts must be invoked to account for present locations of cycloid ridges relative to the local stress fields, suggesting nonsynchronous rotation of the surface since the formation of the visible cycloidal features (Hoppa *et al.* 2001).

*Nonsynchronous Rotation*

Europa's eccentric orbit causes its oscillating tidal bulge to lag behind the Jupiter-facing direction at perijove, creating a torque that acts to accelerate the satellite's rotation to slightly faster than synchronous (Goldreich 1966, Greenberg and Weidenschilling 1984, Ojakangas and Stevenson 1989b). We expect the rocky interior of Europa to maintain a permanent mass asymmetry sufficient to counter this torque, so it should be synchronously locked. However, Europa's icy near-surface layer could rotate nonsynchronously if it is decoupled from the rocky interior, as by a subsurface ocean.

Mechanisms and timescales of nonsynchronous rotation of Europa were considered by Greenberg and Weidenschilling (1984) and Ojakangas and Stevenson (1989b). With a permanent mass asymmetry, Greenberg and Weidenschilling (1984) envision a satellite locked in synchronous rotation with its "permanent" tidal bulge offset ahead of the Jupiter-facing direction at perijove, so that the average torque over an orbital period is zero. The permanent bulge could attempt to creep toward hydrostatic equilibrium (i.e., toward the Jupiter-facing direction), with the result that the satellite's surface will rotate nonsynchronously. Ojakangas and Stevenson (1989b) consider that nonsynchronous rotation could result from thermal adjustment of a floating ice shell. Predicted longitudinal variations in ice thickness (due to variations in tidal strain rate) will drive the ice shell slightly out of hydrostatic equilibrium. In attempting to move back toward hydrostatic equilibrium, the shell will rotate nonsynchronously (see Section 4.2).

The Greenberg and Weidenschilling (1984) model in its original form might operate if the subsurface is warm ice as opposed to an ocean, but viscous coupling with the presumably tidally locked rocky interior would certainly act to retard nonsynchronous rotation. In the Ojakangas and Stevenson (1989b) model, liquid water beneath the ice shell assures decoupling. However, nonsynchronous rotation is not a given in this model, because warm ice might flow rapidly at the base of the floating ice shell, eliminating the longitudinal shell thickness variations envisioned to drive the rotation (Stevenson 2000b). Alternatively, it is possible that nonsynchronous rotation is a permanent condition of the ice shell, and perhaps relatively rapid (Ojakangas and Stevenson 1989b). A lower limit of $10^4$ years was derived for the period of any ongoing nonsynchronous rotation, based on comparison of terminator views of the same features in *Voyager 2* and *Galileo* images obtained 17 years apart (Hoppa *et al.* 1999c).

Helfenstein and Parmentier (1985) and McEwen (1986b) predicted the stress pattern which should result from nonsynchronous rotation (Figure 15.14), based on a small eastward shift of Europa's surface relative to its fixed tidal axes (the pattern is independent of the amount). In the equatorial region, alternating zones of biaxial tensile and compressive stresses are predicted as the surface is stretched over, and falls off, the tidal bulge, respectively. Principal stresses are of opposite sign elsewhere across the satellite, with maximum differential stress occurring near the poles, and minima at the subjovian and antijovian points. *Voyager* global-scale lineaments were compared to this pattern by McEwen (1986b) and Leith and McKinnon (1996), who concluded that the best match of the nonsynchronous

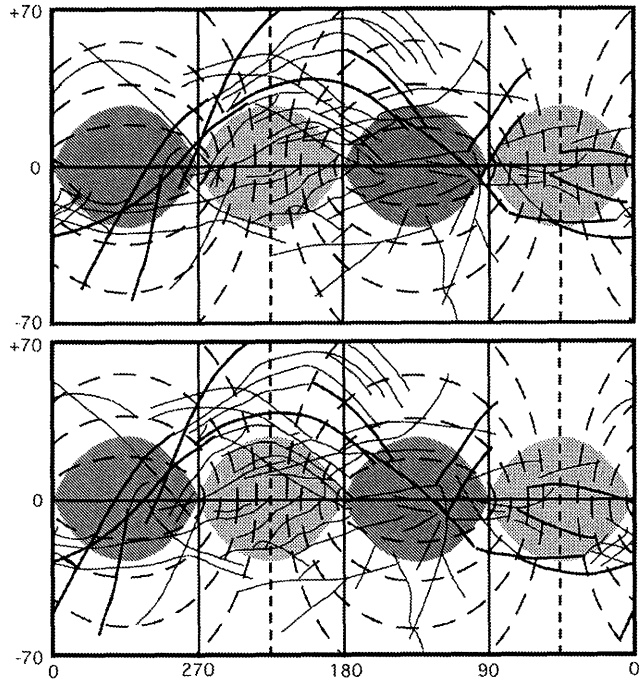


**Figure 15.14.** Global-scale lineaments (solid) compared to the trajectories of least compressive stress (dashed) as predicted from nonsynchronous rotation (Helfenstein and Parameter 1985): (upper) the present-day position of surface features relative to the tidal axes, and (lower) surface features rotated "backward" (westward) in position by 25° of longitude. The shifted pattern offers a good overall fit in that the stress trajectories tend to be perpendicular to the observed lineaments. This suggests that Europa's prominent global-scale lineaments have formed over ~50° of nonsynchronous rotation. Light gray indicates zones in which both horizontal principal stresses are tensile, and dark gray indicates zones in which both principal stresses are compressive. Longitude is labeled in the tidal reference frame (after McEwen 1986b).

stress pattern occurred by considering a westward longitudinal shift in the locations of surface features relative to the fixed tidal axes (Figure 15.14). If the longitude of surface features is shifted westward (or equivalently, the tidal axes shifted eastward) to "back up" nonsynchronous rotation by ~25°, then lineament orientation is approximately perpendicular to the least compressive (greatest tensile) stress direction, as expected if the lineaments originated as tension or extension fractures. The implication is that Europa's major lineaments formed over a range of ~25–50° of nonsynchronous rotation (because the stress pattern moves at half the nonsynchronous rotation rate), giving the observed best fit. Stresses generated by nonsynchronous rotation can be significant. Maximum stresses of ~0.14 MPa can be achieved per degree of rotation; thus, accumulated tensile stress can exceed the tensile strength of cold, solid ice upon ~12° of nonsynchronous rotation (Leith and McKinnon 1996).

*Galileo* color images of the northern high-latitude region of Europa's trailing hemisphere support and strengthen this argument. Imaging at near-infrared wavelengths discriminates older lineaments that were invisible to *Voyager* (Clark *et al.* 1998, Geissler *et al.* 1998a,b). Geissler *et al.* (1998b) categorized lineament age based on color characteristics, and found that lineament orientations have pro-

gressively rotated clockwise over time, implying that stress orientation rotated similarly. This rotation sense is just as predicted by eastward migration of the surface relative to fixed tidal axes due to nonsynchronous rotation. Nonsynchronous rotation is not necessarily the formational stress mechanism, however, because the orientations of the most recent lineaments mapped by Geissler *et al.* (1998b, 1999) are better fit by diurnal stresses. It is plausible that diurnal stresses create some cracks, while nonsynchronous rotation opens those cracks into wider ridges and bands. The total amount of rotation inferred from the oldest global-scale lineaments is ~60° (Greenberg *et al.* 1998), slightly more than inferred from *Voyager* visible-wavelength imaging.

*Galileo* images show that Europa's ridged plains are overprinted by ridges and ridge sets of various orientations. Cross-cutting relationships throughout the visible geologic record suggest evidence for at least one full rotation of Europa's ice shell (Figueredo and Greeley 2000, Kattenhorn 2002). Considering Europa's apparently young surface age of ~60 Myr (Chapter 18), the ice shell is usually assumed to rotate nonsynchronously at the same rate today as during the formation of its surface features (Hoppa *et al.* 1999c, 2001). However, it is also possible that Europa's internal activity, including nonsynchronous rotation, has slowed, halted, or is episodic.

The equatorial region of isotropic tension west of the antijovian point, predicted by nonsynchronous rotation (Figure 15.14), correlates generally well with the zone of pull-apart bands originally recognized in *Voyager* images (Helfenstein and Parmentier 1980, Pieri 1981, Lucchitta *et al.* 1981, Lucchitta and Soderblom 1982, Schenk and McKinnon 1989), and recognized in *Galileo* images to extend westward to ~250° longitude (Belton *et al.* 1996, Sullivan *et al.* 1998). More complex (but uncertain) stress sources are implied by the findings that this extensional zone is centered ~15° south of the equator, and that dark and wedge-shaped band opening directions have preferred orientations (Schenk and McKinnon 1989, Sullivan *et al.* 1998). Minor polar wander of Europa's ice shell (Ojakangas and Stevenson 1989a) might influence patterns of band opening. Although this process is not indicated by global-scale lineament orientation as imaged by *Voyager* (Leith and McKinnon 1996), and would not be expected if the warm base of Europa's ice shell can flow rapidly (Stevenson 2000b, cf. O'Brien *et al.* 2002), evidence for this process is suggested by the sense and distribution of strike-slip faults in Europa's leading and trailing hemispheres (Sarid *et al.* 2002). A similar extensional region is predicted west of the subjovian point, but is not observed in *Galileo* images, perhaps because cracks formed in this region did not dilate (Hoppa *et al.* 2000). Zones of compressional stress are also predicted, centered 90° in longitude away from the tensional zones (Figure 15.14), and these could be regions where the ice shell fails in shear rather than in tension (Spaun *et al.* 2003, Stempel and Pappalardo 2002).

Greenberg *et al.* (1998, 2002a) recognized that the rapidly changing pattern of diurnal stresses could add to the longer-term pattern of nonsynchronous stress to affect the overall surface fracture pattern. This additive stress pattern changes throughout the Europan day, with tensile stresses peaking at different locations at different positions along the orbit. Tensile failure is expected to occur when the additive effects of nonsynchronous stress and diurnally varying stress overcome the lithosphere's tensile strength. In some regions analyzed, the net effect on the expected fracture pattern is a 10° westward shift of the nonsynchronous pattern relative to the tidal axes, apparently explaining why some surface features would better fit the nonsynchronous stress pattern if the lineaments are shifted 10° eastward of their present locations (Greenberg *et al.* 1998).

**Table 15.1.** Properties of Europa.[a]

| | |
|---|---|
| Radius, $R$ | 1560.7 (± 0.65) km |
| Mass, $M$ | 4.799 82 (± 0.000 62) × $10^{22}$ kg |
| $GM$ | 3202.72 (± 0.05) km$^3$ s$^{-2}$ |
| Surface gravity | 1.315 (± 0.001) m s$^{-2}$ |
| Mean density | 3014 (± 4) kg m$^{-3}$ |
| $C_{22}$ | 132.2 (± 2.1) × $10^{-6}$ |
| $C/MR^2$ | 0.348 ± 0.003 |
| Distance from Jupiter | 6.709 × $10^5$ km |
| | 9.397 $R_J$ |
| Orbit period | 3.551 day |
| Forced eccentricity | 0.0093 (variable) |
| Inclination | 0.464° |

[a] Based on Anderson *et al.* (1998), Davies *et al.* (1998), Burns and Matthews (1986), Yoder (1995).

## 15.4 THE INTERIOR

The interior of Europa exerts a primary control on the satellite's geological evolution and astrobiological potential. Results from the *Galileo* mission and theoretical studies have greatly enhanced our understanding of the interior with respect to that of the immediate post-*Voyager* era (Malin and Pieri 1986).

### 15.4.1 Gravity and Magnetic Data

Europa's density and icy surface suggest that it is primarily a silicate body that is partly differentiated. Early models ranged from an anhydrous rock and metal core covered with ~100-km-thick layer of ice (Consolmagno and Lewis 1976, Fanale *et al.* 1977, Cassen *et al.* 1982), to a partly hydrated silicate interior (serpentine rich) with only a thin carapace of ice (Ransford *et al.* 1981). *Galileo* encounters enabled refined determinations of Europa's mass, radius, and density (Table 15.1), and measurements of its second-degree gravitational harmonic coefficient $C_{22}$ to determine a normalized moment of inertia of 0.346 ± 0.005 (Anderson *et al.* 1998) (the slightly different values in Table 15.1 are normalized to the radius in Davies *et al.* 1998). This result is based on a combined analysis of passes E4, E9, E11, and E12, and assumes that the second-degree gravity field is due entirely to hydrostatic distortion of Europa's figure by rotation and jovian tides. Because independent confirmations of close-to-hydrostatic conditions exist for Io (Anderson *et al.* 2002) and Ganymede (Anderson *et al.* 1996) from equatorial and polar passes, the same is assumed for Europa.

Europa's relatively low moment of inertia implies a differentiated interior; for comparison, the values for the Earth and Mars are 0.334 and 0.366, respectively (Folkner *et al.* 1997). More importantly, the thin-ice layer model of Ransford *et al.* (1981) can be rejected. Although an interior model

with a thin (<25 km thick) ice shell can be proposed in order to fit both the density and moment-of-inertia constraints, the non-ice interior would have to consist of a metallic core and an underdense (<3000 kg $m^{-3}$) mantle. Cosmochemically, such underdense compositions are only possible through hydration, but this is not consistent with the high temperatures, melting, and differentiation that are involved in the formation of a metallic core (Anderson *et al.* 1998).

Constraints on the internal structure can be determined from gravity data through models. Figure 15.15 shows the ice layer, mantle, and core size in a three-layer model as a function of two representative core densities (Fe and Fe–FeS composition). The ice shell density is assumed to be 1050 kg $m^{-3}$, which is plausible for an ice or water shell that contains some salts or sulfates (e.g., the density of cold polar seawater is 1028 kg $m^{-3}$). From such models, Anderson *et al.* (1998) conclude that the ice shell is 80 to 170 km thick. Although they do not favor two layer models that lack metallic cores, because these require a rock interior density (≈3800 kg $m^{-3}$) greater than that of bulk Io (3530 kg $m^{-3}$), such interior densities are cosmochemically possible (Consolmagno *et al.* 1998, Mueller and McKinnon 1988). Variations in shell density, from pure ice to sulfate rich (e.g., Kargel *et al.* 2000), also broaden the range of ice shell thicknesses. Of the models in Figure 15.15, the Fe–FeS model is likely closer to reality, based on thermal evolution considerations. Consequently, the metallic core is probably about half the rock interior in radius (Anderson *et al.* 1998). For mantle densities similar to Earth's upper mantle (~3400 kg $m^{-3}$), the ice shell is probably >100 km thick (Chapter 13). Note that the gravity models are not sensitive to the physical state of the "ice" layer, i.e., whether it is solid or liquid beneath the surface.

*Galileo* magnetometer data provide additional constraints on models of the interior (Khurana *et al.* 1998, Kivelson *et al.* 1999, 2000, Zimmer *et al.* 2000). These data show evidence of an induced dipole magnetic field consistent with the presence of a salty ocean (Chapter 21). Jupiter's magnetic field is inclined to its rotation axis, and the Galilean satellites (in Jupiter's equatorial plane) experience a time-varying magnetic field with a synodic period of 11.23 hr at Europa. Europa responds to this field as a nearly perfectly conducting sphere, generating electrical currents that create a magnetic field that opposes and cancels the time-varying component in its interior, but exterior to Europa this induced field is manifested as a time-varying dipole.

On the timescale of a given spacecraft pass, this time variation is not seen, but multiple flybys show the proper dipole signature, oriented principally in the equatorial plane and in the appropriately different directions for each encounter (Kivelson *et al.* 2000). There is little doubt that this observed behavior indicates a conducting layer within Europa (cf. Stevenson 2000a). Because the ionosphere of Europa is insufficiently conductive to carry the required currents, the conductive layer must be within the body of Europa (Zimmer *et al.* 2000).

Figure 15.16 illustrates the characteristics of a conducting shell model. The normalized amplitude $A$ and phase lag of the induced response are plotted as a function of shell thickness and conductivity. A perfect conductor will have an $A \equiv 1$ and zero phase lag. A real conductor will have

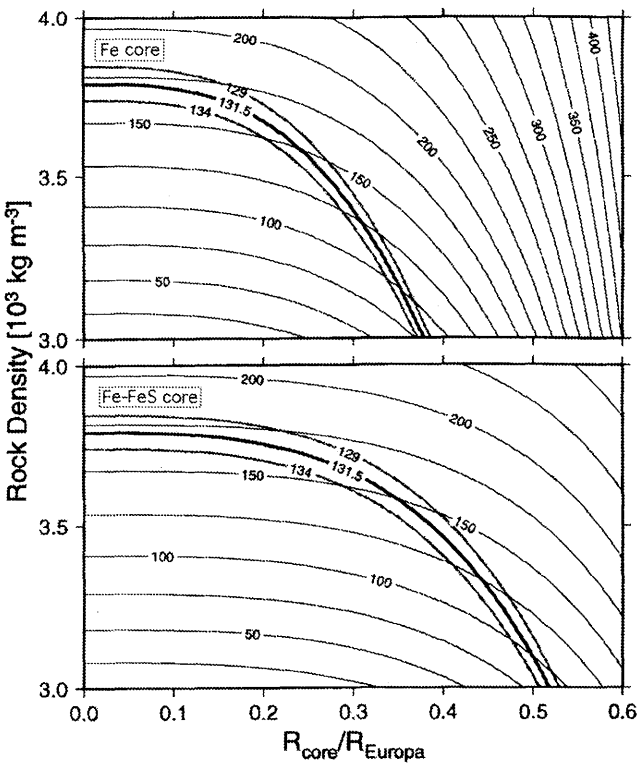


**Figure 15.15.** Representative Europa three-layer models having an ice shell density of 1050 kg $m^{-3}$ for a pure Fe core (density 8000 kg $m^{-3}$) and an Fe–FeS core (density 5150 kg $m^{-3}$). Ice shell thicknesses (in km) are given as a function of core size and mantle density, but only those models that fall near the solid curve labeled 131.5 ± 2.5 (x $10^{-6}$) have the proper $C_{22}$ and moment of inertia (after Anderson *et al.* 1998).

$A < 1$ and a finite phase lag. The magnetometer data indicate that Europa responds with an $A \geq 0.7$ (Zimmer *et al.* 2000), which sets constraints on the conducting layer. This minimum $A$, given the $r^{-3}$ dependence of dipole fields, implies that the conducting layer can be no deeper than 175 km below the surface. This rules out a metallic core (e.g., Figure 15.15) as the conductivity source because it would be too deep.

On the other hand, the conducting layer could lie at the top of the rock mantle if the ice layer is thin, but the rock conductivity would have to exceed ~0.2 S $m^{-1}$ (Zimmer *et al.* 2000). These conductivities are unrealistically high for ordinary rock and would require a hot, saline pore fluid at volume fractions in excess of ~10% (or something exotic, such as an interconnected network of graphite or pyrrhotite; Grant and West 1965, p. 398, Stevenson 2000a). This amount of hot, reactive fluid is not stable at the pressures characteristic of the putative conducting layer (>0.1 GPa), and should be largely expelled to the ice layer. In contrast, very hot (>800° C), electrolyte-bearing (for normal porosities) or even partially molten rock could have the required conductivity (Hermance 1995, p. 201), but such high temperatures in the outer 100 km of the rock mantle would imply high heat flows and, as Zimmer *et al.* (2000) argue, would probably melt the ice layer above.

The source of high conductivity is thus most plausibly within the ice layer. The inferred 80 to 170 km thickness for the ice layer requires that its average conductivity ex-

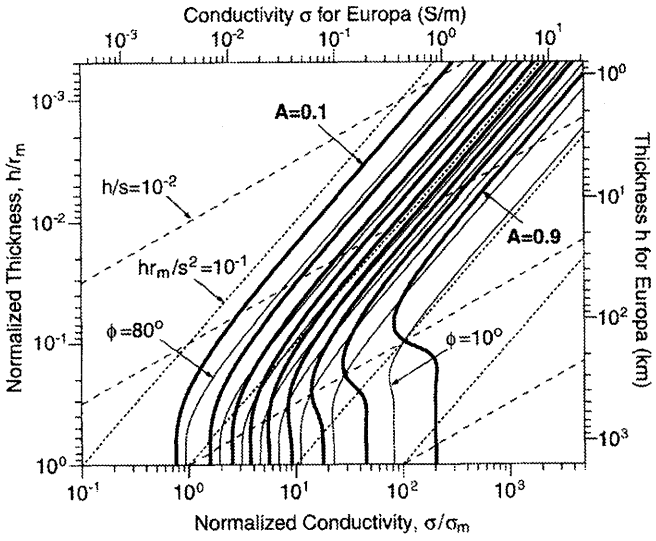


**Figure 15.16.** Normalized amplitude $A$ and phase lag $\phi$ as a function of shell thickness $h$ and shell conductivity $\sigma$. The thickness $h$ is given in non-dimensional units normalized to Europa's radius $R$, and in km for $R = 1560$ km; the conductivity $\sigma$ is given in non-dimensional units normalized to a reference conductivity $\sigma_m = 2/(\mu_0 \omega R^2) = 4.2$ mS m$^{-1}$, where $\mu_0$ is the vacuum permeability ($4\pi \times 10^{-7}$ in SI units) and $\omega$ is Europa's angular rotation rate, and (on top) in siemens per meter on a scale appropriate for Europa. The thick solid lines are isocontours of $A$, and the thin solid lines are isocontours of $\phi$; the dotted lines show where $hR/s^2$ equals 0.1, 1, 10, and 100, from left to right, and the dashed lines show where $h/s = 0.01$, 0.1, 1, and 10, from left to right, where $s$ is the electromagnetic skin depth ($\equiv [2/\mu_0 \sigma \omega]^{1/2}$). By choosing a different normalizing radius, this graph can be used to evaluate conducting layers that do not extend to Europa's surface (after Zimmer *et al.* 2000).

ceed 0.14 to 0.08 S m$^{-1}$ respectively (Figure 15.16). This conductivity exceeds that of ice or pure water, but is less than terrestrial seawater (2.7 S m$^{-1}$ at the freezing point; Montgomery 1963) or an $H_2O$–$MgSO_4$ eutectic brine (~2.5 S m$^{-1}$; Kargel and Consolmagno 1996). As a complementary limit, the minimum thickness $h$ of a near-surface liquid layer that can account for the magnetometer observations is 3.5 km (Zimmer *et al.* 2000), if the layer has the conductivity of freezing, terrestrial seawater. Such liquid could be distributed throughout a much thicker ice layer as a partial melt, but there would have to be much more of it, and distributed at porosities >10%, as discussed by Zimmer *et al.* (2000).

In summary, *Galileo* gravity and magnetometer data suggest that Europa has an ocean at least several kilometers thick beneath its ice shell and that the ocean contains an electrolyte (e.g., sulfates, alkali salts); this ocean does not need to be as conductive (or salty) as Earth's ocean.

### 15.4.2 Tides and Tectonics

Europa's complex geology reflects substantial processes originating in the interior. Europa is in a mean-motion resonance with both Io and Ganymede (the Laplace resonance), which currently forces Europa's eccentricity $e$ of 0.01 (Greenberg 1982, Peale 1986). This eccentricity creates variations in the tidal potential and associated deformation of ~3% on an orbital period of 85.2 hr, and the dissipation of the resulting strain energy heats the interior.

Tidal dissipation in planetary bodies can occur by many mechanisms and on several scales, e.g., from viscoelastic heating on the grain scale, to solid friction along faults, to turbulence at liquid–solid boundaries. Viscoelastic heating depends on the rheology of the material and peaks when the period of forcing equals the Maxwell time $\tau_M = \eta/\mu = \sigma/3\dot{\epsilon}\mu$, where $\eta$ is viscosity, $\mu$ is the shear modulus (3.52 GPa for solid ice; Gammon *et al.* 1983), $\sigma$ is stress, and $\dot{\epsilon}$ is strain rate. For water ice, the dominant low-stress deformation mechanism should be dislocation-accommodated grain-boundary sliding (GBS, or superplastic creep), unless the grain sizes are large (Goldsby and Kohlstedt 1997, 2001). Durham *et al.* (2001) and Durham and Stern (2001) refer to this more generically as grain-size-sensitive, or GSS, creep. Moreover, with this mechanism, there does not appear to be any observed interval of transient creep (Durham *et al.* 2001), so it should be applicable to modeling the response to tidal strains on Europa, which are small.

Using the rheological parameters of Goldsby and Kohlstedt (2001) the Maxwell time of ice on Europa is

$$\tau_M = 77 \text{ hr} \left(\frac{d}{5 \text{ mm}}\right)^{1.4} \left(\frac{\sigma}{0.1 \text{ MPa}}\right)^{-0.8} \exp\left(\frac{270}{T} - 1\right) \quad (15.1)$$

For an average stress level $\sigma$ of 0.1 MPa (see below) and a grain size d of 5 mm (comparable to polar glacier ice), the Maxwell time at the melting temperature ($T \approx 270$ K) is close to the tidal forcing period. This estimate is sensitive to grain size and stress level, but the most important variable is the rheology. Near the melting temperature (>258 K), the viscosity of ice (and thus the Maxwell time) decreases with respect to GBS or GSS creep by an order of magnitude or more due to premelting on grain boundaries (De La Chappelle *et al.* 1999, Goldsby and Kohlstedt 2001). Consequently, Europa's ice layer is probably mostly heated near its base (Ojakangas and Stevenson 1989b), which maximizes the influence of tidal heating on the layer as a whole; indeed in conducting ice tidal heating models, the resulting temperature gradient is exponential in the subsurface with tidal heating, peaking just above the ice–water interface (Chyba *et al.* 1998). Moreover, it implies that warm ice elsewhere could be similarly tidally heated (McKinnon 1999, Sotin *et al.* 2002). In contrast, the Maxwell times in Europa's much more viscous rock mantle cannot approach the tidal period unless the rock is partially molten.

Diurnal tides also affect the outer, brittle part of the ice shell and are responsible for tectonic processes. Europa's equilibrium tide and rotation combine to yield a hydrostatic triaxial figure with $a$, $b$, and $c$ axes whose lengths differ from Europa's average radius by 1.87, −0.53, and −1.33 km, respectively, where $a$ is the tidal axis (oriented toward Jupiter), $c$ is the rotational axis (perpendicular to the orbital plane), and $b$ is the intermediate axis (orthogonal to the other two).

As Europa's distance from Jupiter varies during its orbit, the tidal potential rises and falls by $3e$, whereas the rotation of Europa's mass is close to invariant (the forced libration is $\pm 8 \times 10^{-5}$; Peale (1977), Eq. 22). Thus, the tidal distortion alone fluctuates, reaching its maximum and minimum at perijove and apojove, respectively, and the $a$ axis of

a hydrostatic (fluid) Europa rises and falls, respectively, by 48 m. The rigidity of the body of Europa offers resistance to this relatively high-frequency deformation, however, and Yoder and Sjogren (1996) and Moore and Schubert (2000) calculate that the $a$-axis change is reduced to ±30 m. A floating, thin ice shell (up to a few tens of km) will conform to this shape change (e.g., Ojakangas and Stevenson 1989b). The resultant elastic stresses in the shell are given by the solution to the biaxial distortion of a thin shell (Melosh 1977)

$$\sigma_{\theta\theta} = \frac{1}{3}(f - f_0)\mu\left(\frac{1+\nu}{5+\nu}\right)(5 + 3\cos 2\theta) \quad (15.2)$$

$$\sigma_{\phi\phi} = -\frac{1}{3}(f - f_0)\mu\left(\frac{1+\nu}{5+\nu}\right)(1 - 9\cos 2\theta) \quad (15.3)$$

where $\sigma_{\theta\theta}$ and $\sigma_{\phi\phi}$ are the meridional and azimuthal stresses referenced to the $a$-axis. The parameter $\theta$ is the colatitude, $f - f_0$ is the difference between initial and final flattenings, $\mu$ and $\nu$ are the shear modulus and Poisson's ratio, respectively, of the shell ($\nu = 0.325$ for solid ice; Gammon *et al.* 1983), and compression is defined as positive. The change in flattening can be written $3e\gamma_t$, where $\gamma$ is a factor that accounts for the flattening reduction due to rigidity (≈0.62), and $f_t$ is the tidal flattening (negative for elongation; see Leith and McKinnon 1996, p. 394). Evaluation of these parameters indicate that at perijove and apojove maximum stresses do not exceed ≈0.08 MPa.

Between perijove and apojove, the tidal potential passes through its average value, but because Europa's instantaneous orbital angular velocity and spin rate are not exactly equal, the tidal potential and $a$ axis are offset by $2e$ radians (Greenberg *et al.* 1998). The resulting elastic stresses in the shell are determined by the partial relaxation of the tidal bulge and its reimposition with a $2e$ offset, equivalent to nonsynchronous rotation of the shell by the same amount (Greenberg *et al.* 1998). The stress generated in this case (Leith and McKinnon 1996) is

$$\sigma_{\max,\min} = \pm 6\gamma f_t\left(\frac{1+\nu}{5+\nu}\right)\sin\Omega \quad (15.4)$$

where $\Omega$ is the nonsynchronous rotation angle ($2e$), or 0.10 MPa.

Thus, diurnal eccentricity stresses are small (≤1 bar), but they have been invoked to explain ridge-building (Greenberg *et al.* 1998, 2002a, Gaidos and Nimmo 2000, Nimmo and Gaidos 2002), incremental strike-slip motion (Hoppa *et al.* 1999a), wedge-shaped band dilation (Tufts *et al.* 2000), cycloid ridge propagation (Hoppa *et al.* 1999b), and even eruption of ocean water (Greenberg *et al.* 1998, 2002a). With regard to the latter, 0.1 MPa of tension can open a single crevasse no deeper than $\pi\sigma/2\rho g \sim 150$ m, where $\rho$ is the ice density and $g$ is surface gravity (e.g., Weertman 1971). Fluid-filled crevasses can propagate upward from the base of the shell to much greater heights if sharp cracks can be initiated in the soft basal ice (Crawford and Stevenson 1988), as can be seen by replacing $\rho$ in formula above with $\Delta\rho$, the density difference between the ice and ocean water. For the minimum $\Delta\rho$ given by Kargel *et al.* (2000) of ≈64 kg m$^{-3}$, for a eutectic sulfate ocean and shell, basal crevasses may reach heights of ~2 km driven by diurnal stresses alone.

The diurnal tides and stresses are much reduced if Europa's shell is mostly or completely frozen. The tidal variation in the $a$-axis in this case would be <1 m (Yoder and Sjogren 1996, Moore and Schubert 2000), which implies a >30-fold reduction in stresses and a $>(30)^2 \approx 10^3$ reduction in tidal heating. Most important, if the kinematic requirements for diurnally varying stress in generating cycloid cracks (Hoppa *et al.* 1999b) are accepted, in which each cycloid arc is generated within one Europan day, then it is inconceivable that these could be met by <3 kPa tidal stresses driving the propagation of <5-m-deep surface cracks across hundreds of km of uneven terrain. The suggestion that cycloid ridges evolve from cycloid cracks, and the stress cycle needed to generate them, are powerful arguments for the presence of an ocean decoupling the shell from the interior.

Diurnal tidal stresses in a floating ice shell can propagate tension cracks, but if such cracks are to reach the surface from the base of the shell or penetrate from the surface to ductile ice below, one or more of the following are required: (1) a more sophisticated crack mechanics (e.g., the gas exsolution model of Crawford and Stevenson (1988); (2) a relatively thin (<3–4 km thick) ice shell, now or in the past; and (3) additional sources of stress to fracture the shell.

One additional stress source is nonsynchronous rotation. With internal dissipation, the diurnal tidal response is retarded in time or delayed in phase. The phase lag, expressed as an angle, is usually small and depends on the magnitude of the dissipation (i.e., the tidal $Q$). The average torque on Europa is weighted towards perijove, however, where the tidal response trails the tidal potential and is positive (i.e., acts to spin up the satellite). Normally, for solid satellites in 1:1 spin–orbit resonance, this average torque is balanced by an opposite torque on the permanent tidal bulge, which is slightly offset in the other direction at perijove, ahead of the tidal potential (e.g., Yoder 1979). The position of the permanent bulge with respect to the body of Europa in the long term is determined by the non-hydrostatic mass distribution within the satellite, such that the $a$-axis and $c$-axis are also the minimum and maximum moment-of-inertia axes, respectively, of the undistorted satellite. As long as the non-hydrostatic contribution of the rock interior to $C_{22}$ is $>10^{-6}$, the interior should stay tidally locked in the 1:1 spin–orbit resonance, and for so-called Darwin tides, the minimum non-hydrostatic $C_{22}$ for tidal locking is 10–100 times less (Greenberg and Weidenschilling 1984, Schenk and McKinnon 1989, Ojakangas and Stevenson 1989b). The non-hydrostatic stresses necessary to support these interior mass anomalies are ~10% of those supported in the lunar lithosphere (Solomon 1986), or ~10 MPa. Unfortunately, there is no independent measure of the non-hydrostatic mass distribution within Europa, but if it is insufficient, then the permanent bulge will seek to relax viscously to the position of the potential minimum at perijove (Greenberg and Weidenschilling 1984). Because it can never catch up, the permanent bulge slowly creeps westward through the body of Europa, and Europa effectively rotates slightly faster than synchronously (Greenberg and Weidenschilling 1984).

Even if the rock interior is tidally locked, a floating ice shell is subject to the same subtle interplay of torques (e.g, for shell thicknesses <30 km, the tidal lag angle is <0.5°; Moore and Schubert 2000), and the shell can undergo independent nonsynchronous rotation. It is unlikely that a non-hydrostatic distribution of ice phases could permanently stabilize a floating ice shell with respect to the tidal axis given viscous creep at its base (cf. Stevenson 2000b). In the tidally heated shell model of Ojakangas and Stevenson

(1989b), however, variations in tidal heating with latitude and longitude imply maximum shell thicknesses and, thus, the minimum moment of inertia of the shell along the $a$ axis, appropriate for stability. Even in this case, the maximum thickness will be offset dynamically from the potential that ultimately creates it, leading to nonsynchronous rotation on a timescale governed by the continuous thermal reequilibration of the shell.

For their estimated shell thickness $b$ of ~15–25 km, Ojakangas and Stevenson (1989b) predicted a nonsynchronous rotation time of ~10 Myr, consistent with the lower limit of Hoppa *et al.* (1999c) but inconsistent with the upper limit of Hoppa *et al.* (2001). This timescale goes as $\sqrt{b}$; thus, a 10-km-thick shell could rotate in 2.5 Myr. The shell could rotate at an even faster rate (governed by viscous processes), and the tidal heating would be zonally averaged, leading to a maximum and uniform shell thickness on the equator. Regardless of the nonsynchronous rotation rate, the possible stresses in Europa's lithosphere are large. For a full 90° of rotation and $\gamma = 0.62$, the maximum tensile stresses from Eq. (15.3) reach 8.1 MPa, adequate in principle to open surface tension cracks to a depth of >10 km (Leith and McKinnon 1996). More likely, small amounts of nonsynchronous rotation stress could enhance the rise of fluid-filled cracks from the base of the shell (Greenberg *et al.* 1998), and such stresses would not necessarily overwhelm the diurnal stress pattern variations suggested for some of the tectonics.

Ojakangas and Stevenson (1989a,b) noted that in their nominal (triaxial) tidal heating model the polar regions of the shell were sufficiently thick due to low surface temperature, that the polar axis was actually the intermediate moment-of-inertia axis, rather than the minimum as required by stability. Thus, a dynamic driver could exist for true polar wander, attempting an interchange of the $b$ and $c$ axes by means of rotation about the $a$ axis. Whether this polar wander actually occurs depends on the dissipative properties of the shell; it may be episodic, occur continuously as the shell thickness adjusts to the evolving position-dependent tidal heating, or not occur at all. The shell stresses it creates are identical in form to nonsynchronous stresses, except that the $a$ axis rather than the $c$ axis is invariant, and the stress levels are reduced by a factor of 3 for a given rotation angle (Leith and McKinnon 1996).

In summary, the tides and torques raised on the ice shell lead to several stress sources for tectonic activity. These operate on various timescales and stress levels, which could explain the variety of tectonic surface features. In detail, however, much remains to be understood, especially in regard to how much nonsynchronous rotation has occurred through time and whether polar wander has occurred.

### 15.4.3 Tidal Evolution

The Laplace resonance supplies the orbital eccentricity that drives Europa's tectonics and heats its interior. A leading model for its initiation (Yoder, 1979, Yoder and Peale 1981) postulates that differential tidal expansion first caused Io to move into the 2:1 mean-motion resonance with Europa, after which the pair was tidally driven outward until Ganymede was captured into the 2:1 resonance with Europa as well. In this model, Europa's eccentricity was much smaller (0.0014) when it was solely in the 2:1 resonance with Io, and it is only when the Laplace resonance formed that modern values of Europa's eccentricity $e \sim 0.01$ were achieved.

The Laplace resonance can be illustrated through the pair-wise relationship between satellite mean motions, $n_i$, and the drift rate between conjunctions,

$$2n_2 - n_1 = \omega_1 \quad (15.5)$$

$$2n_3 - n_2 = \omega_2 \quad (15.6)$$

where $n_1$, $n_2$, and $n_3$ refer to the mean motions of Io, Europa, and Ganymede, respectively. Currently, $\omega_1$ and $\omega_2$ are small and equal (time averaged), and equal to the orbital precession rate of either Io or Europa. Malhotra (1991) and Showman and Malhotra (1997) show that before Io and Europa entered the 2:1 mean-motion commensurability, all three satellites may have been temporarily captured into low order Laplace-like resonances characterized by $\omega_1/\omega_2 = 1/2$, 3/2, or 2, after which the satellites evolved into the present $\omega_1/\omega_2 = 1$ (Figure 15.17). Eccentricities are enhanced in these temporary resonances for both Europa and Ganymede, with Europa attaining $e$ values that varied but which could have averaged up to ~0.01 (somewhat greater as the $\omega_1/\omega_2 = 3/2$ and 2 resonances were exited). Thus, Europa's modern eccentricity and level of tidal heating could date from this era in solar system history.

Alternatively, Greenberg (1982, 1987) argued that the Laplace resonance is primordial, and that the satellites were originally "deeper" in the resonance, meaning that their primordial forced eccentricities and heating rates were higher. Peale (1999) criticized this scenario as *ad hoc*, in that it was unlikely that the satellites simply formed in the resonance. In the model of Canup and Ward (2002), however, satellite–disk torques can cause substantial inward satellite migration. Because more massive Ganymede would drift faster, they speculate and Peale and Lee (2002) demonstrate that the Laplace resonance might have been assembled from the outside-in during this earliest epoch. Furthermore, Peale and Lee (2002) show that after satellite migration ceases, tidal dissipation causes the system to evolve to the current orbital configuration.

Unfortunately, Europa's early history is not preserved in the geological record. Moreover, tidal heating rates could vary through time, even during the modern epoch. Fundamentally, there is a strong nonlinear feedback between tidal heating and orbital eccentricity: high dissipation (high $T$ and low $Q$) lowers $e$, which lowers dissipation, causing $T$ to decrease and $Q$ to increase, which allows $e$ to be tidally pumped back up, causing $T$ to increase and $Q$ to decrease, and the cycle repeats. This argument, first articulated by Greenberg (1982) for Io and modeled in detail by Ojakangas and Stevenson (1986), suggests that Io's eccentricity could vary up to ~0.01 from its present 0.0041 on a ~100 Myr timescale. In the resonance, the variation in Io's $e$ is accompanied by a variation in $n_1$. The variation in $n_1$ must also drive variations in $n_2$ and $n_3$ to maintain the overall Laplace resonance lock, which can be expressed as $n_1 - 3n_2 + 2n_3 = 0$ (subtracting Equation 15.6 from 15.5). If the Ojakangas and Stevenson (1986) model is correct, the implications for Europa could be significant. From Yoder and Peale (1981), a doubling in Io's eccentricity could similarly result in a doubling of Europa's $e$ to ~0.02, which would increase the present tidal heating rate by a factor of 4. We note that

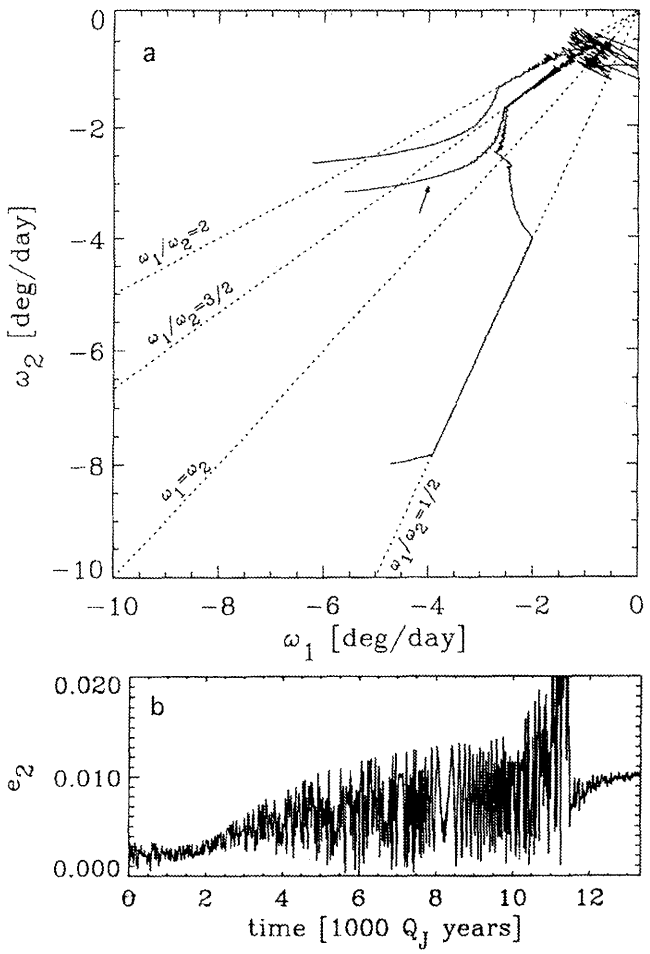


**Figure 15.17.** (a) Example of tidal evolutionary paths for Io, Europa, and Ganymede displayed in a $\omega_1$–$\omega_2$ diagram. The initial slopes are flatter because Io's outward evolution is initially the greatest of the three; (b) time evolution of Europa's eccentricity for the example of temporary capture into the $\omega_1/\omega_2 = 3/2$ resonance (arrowed path in (a)); $Q_J$ is Jupiter's dissipation factor, ($\sim 10^5$; Peale 1999). In this numerical calculation Io and Europa were relatively dissipative, while Ganymede was not, and the system "jumped" into the Laplace resonance ($\omega_1 = \omega_2$) when Io's dissipation was lowered by a factor of 3. The state of the system at the end of the integration is close to that presently observed. After Showman and Malhotra (1997).

the preserved geological history of Europa overlaps the last eccentricity tidal heating maximum for Io, as modeled by Ojakangas and Stevenson (1986). This could be of relevance to arguments for secular changes in Europa's geological expression.

### 15.4.4 Thermal Evolution

Europa presumably formed within a flattened, rotating gaseous subnebula about Jupiter as Jupiter formed (e.g., Pollack and Fanale 1982, Stevenson *et al.* 1986, Peale 1999). The details of formation are under study (Canup and Ward 2002, Mosqueira and Estrada 2003a,b, Chapter 13), but because Europa is rock+metal-rich, its differentiation in terms of ice from rock+metal was assured. The melting and separation of water in a hypothetical primordial Europa of mixed ice and rock+metal is a given even if only long-term radiogenic heating is assumed. Based on gravity data, the ice/water volume within Europa is 15–30%, much less than the critical 40% or more needed for convective regulation to maintain internal temperatures below the ice melting point (Friedson and Stevenson 1983).

Much of the rock might have been initially hydrated, either in the jovian subnebula (Prinn and Fegley 1981) or by aqueous alteration within Europa, but hydration has not survived in bulk, given the gravitational evidence for metallic core formation or (in the absence of a metallic core) a dense, metal-bearing interior composition. It is not completely clear if radiogenic heating was sufficient to drive the water out of the hydrated minerals (Ransford *et al* 1981). Europa, however, could have been more strongly heated during accretion (Lunine and Stevenson 1982, Stevenson *et al.* 1986) or by tidal activity.

Once the rock+metal interior separates, its internal temperature is no longer buffered by the presence of the ice, and temperatures can rise by radiogenic heating alone to approach the silicate solidus. Approaching the solidus from below means that iron can melt and drain downward before silicate melting occurs, provided that the presence of sulfur lowers the melting point of the resulting metallic alloy (McKinnon 1996). Otherwise, solid-state convection of the dominant rock fraction will regulate the internal temperatures to remain below the relatively high melting point of pure iron, and a metallic core will never form (e.g., Stevenson *et al.* 1983). The only alternative is for Europa's internal temperatures to have been so overdriven by tidal heating that sufficient rock melting occurs, such that metal-rich solids segregate to the center of the satellite. This is unlikely for present rates of tidal heating, but the effects of excursions to high eccentricity and tidal heating discussed earlier have yet to be evaluated.

Figure 15.18 illustrates models by McKinnon (1996), updated for internal structures that satisfy both density and moment-of-inertia constraints. The models assume early formation of a rock+metal interior and radiogenic heating based on the U/Si, Th/Si, and K/Si abundance ratios in carbonaceous chondrites (Mueller and McKinnon 1988). The interior heats during the first Gyr and reaches temperatures comparable to the Fe–FeS eutectic melting temperature, but still below temperatures characteristic of solid-state convection in rock. Once sufficient heat is released to supply the latent heat of melting of an Fe–FeS core, at ~1.5 Gyr, the core is considered formed, and the gravitational potential energy released compensates for the latent heat consumed. As the temperature continues to rise, solid-state convection in the rock mantle sets in (based on an olivine rheology), indicated by the flattened temperature profiles in the lower mantle. The flattened profiles in the core are simply due to the high thermal conductivity of molten Fe–FeS. Later, radiogenic heating decreases and the mantle cools and becomes conductive (Figure 15.18a). As core temperatures approach the Fe–FeS eutectic curve, refreezing might occur, but the details depend on the precise core composition and are not addressed.

The potential effect of tidal heating on thermal evolution is shown in Figure 15.18b, in which tidal heating is proportional to the ratio $k/Q$, where $k$ is the second-degree potential Love number. A substantial liquid core and the

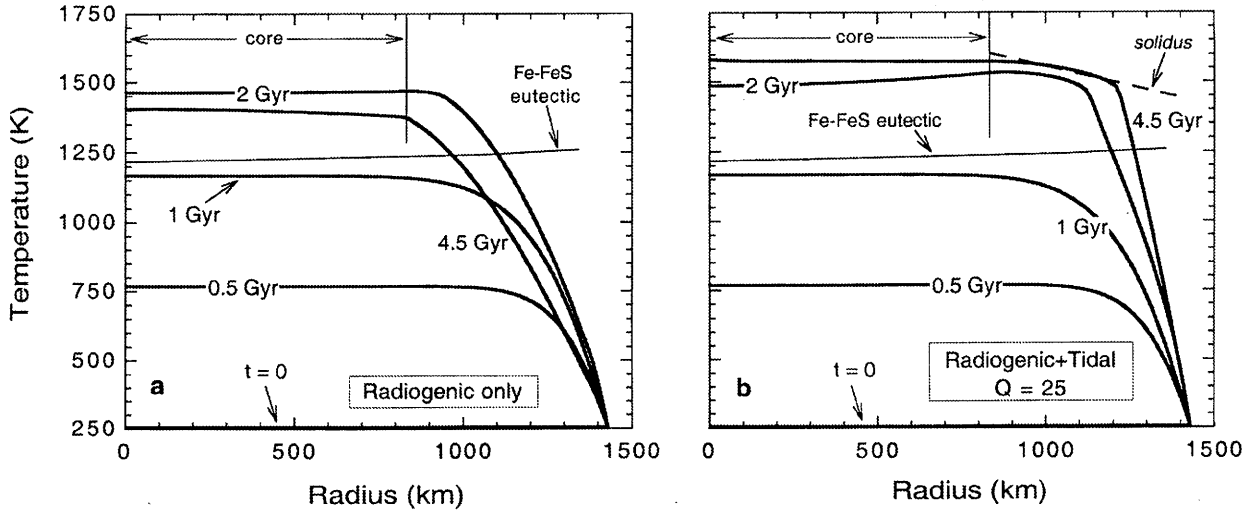


**Figure 15.18.** Thermal evolution models of Europa's interior, starting from a uniform temperature of 250 K at $t = 0$, for the cases of (a) radiogenic heating and (b) radiogenic and tidal heating for $Q = 25$. Structural and heat budget effects of metallic core formation are incorporated, but silicate dehydration is ignored. Characteristic material parameters are used (e.g., rock conductivity and heat capacity are 4 W $m^{-1}$ $K^{-1}$ and 1 kJ $kg^{-1}$ $K^{-1}$, respectively), and enhanced rock conductivity for $T > 1450$ K mimics the effects of solid-state convection in the rock mantle (stagnant-lid regime). For radiogenic heating only, Europa's rock mantle is conductive for most of its history, whereas for $Q = 25$, mantle convection lasts until the present, with temperatures comparable to the Allende meteorite solidus (iron-rich silicates). Fe–FeS eutectic melting temperature is from Fei *et al.* (1997).

oceanic layer raise and lower $k$, respectively, relative to that of a solid, uniform elastic sphere (cf. Cassen *et al.* 1979, Ross and Schubert, 1987), but the combined effect is an increase in $k$ for the rock+metal interior. In contrast, estimating the tidal dissipation factor $Q$ is difficult. It is generally supposed that $Q \sim 100$ is a good measure of solid body dissipation, although the lunar $Q$ at the monthly libration period is ~25, a fact exploited by Squyres *et al.* (1983) in their early study of Europa's possible shell thickness (cf. Williams *et al.* 2001). $Q = 25$ is used in Figure 15.18b, where the tidal heating begins with core formation. The long-term decline in radiogenic heating is more than compensated by this level of tidal heating. The metallic core remains at temperatures well above the Fe–FeS eutectic and is heated from above, factors not conducive to operation of a magnetic dynamo. Moreover, the lower rock mantle remains convective and the model temperature profile intersects the silicate solidus of the Allende carbonaceous chondrite (Agee *et al.* 1995). If partial melting occurs, then basaltic volcanism is possible.

Tidal dissipation in this calculation is evenly distributed in the mantle, and the heating rate is constant. Although these assumptions are simplistic, the calculations demonstrate that for plausible choices of physical parameters, Europa could have a thermally and volcanically active rock mantle at the present time. A corollary is that simple extrapolation of the tidal heating equations from Io to Europa (assuming that $k/Q$ is similar for both bodies; e.g., O'Brien *et al.* 2002) is problematic without an explicit model for $k/Q$.

### 15.4.5 Thickness and Thermal State of the Ice Shell

Ojakangas and Stevenson (1989b) established that a floating, conductive ice shell 15 to 25 km thick could be maintained by basal tidal heating, with or without heat flow from the interior. For their models based on Newtonian rheologies, it was assumed that maximum heating was at the very bottom of the shell. Based on the discussion of Maxwell times, it is plausible that the maximum heating occurs within the shell, which makes shell thicknesses $\leq$15 km more likely for present-day conditions. On the other hand, frictional dissipation along faults or locally in the shell (e.g., Nimmo and Gaidos 2002) will tend to concentrate heat, which might lead to a warmer, thinner crust locally, but also reduce the strain energy available elsewhere, allowing the shell elsewhere to thicken (Stevenson 1996).

McKinnon (1999) considered the initiation of convection in the ice shell, based on scaling of convection in temperature-dependent fluids, low-stress ice rheologies, and the current tidal strain field, and found that convection could start in shells <20 km thick if the ice grain size were ~1 mm or less. Convective overturn in shells as thin as 5–10 km is conceivable as well, but the grain size and basal viscosity would have to be very low (~100 μm and a few $10^{12}$ Pa s). Even if convection initiates, there might be no steady state because convective ice should be relatively hot and dissipative at tidal frequencies (McKinnon 1999). Hussman *et al.* (2002) propose, based on a different rheological model, equilibrium solutions for thick (~35–40 km) shells, with convecting sublayers if the melting-point viscosity is sufficiently low. As discussed in Section 15.3.1, the sizes, spacings, and morphologies of pits, spots, and domes suggests some form of convective upwelling.

Unfortunately, the thickness and thermal state for Europa's shell cannot be specified from theoretical arguments alone, because there is a lack of information on parameters such as grain size and the roles of viscous and frictional dissipation, and because the history of the shell and interior strongly determines the shell's present behavior. Nonetheless, models suggest shell thicknesses that vary with location and time, and which are consistent with the tectonic, volcanic, and other morphologies observed. Uncertainties in our knowledge of shell and ocean properties have a direct bearing on the prospects for life on Europa, discussed next.

## 15.5 ASTROBIOLOGY

Life as we know it depends on liquid water, a suite of "biogenic" elements (e.g., carbon, but others discussed below), and a source of energy (on Earth, either sunlight or chemical disequilibrium, which may or may not be traceable to sunlight). The suggestion for a subsurface liquid water ocean on Europa, coupled with discoveries of an extensive subsurface biosphere on Earth (Gold 1992, Whitman *et al.* 1998) combine to make Europa's putative subsurface ocean one of the most promising sites for exobiology in the solar system.

We note that if the origin of life requires direct access to the enormous free energy available from the Sun, then life on Europa would not exist unless it arose in a possibly brief, early intense greenhouse stage, and quickly adapted to life beneath an ice cover, or if it reached Europa through the successful interplanetary transfer of microorganisms from elsewhere. Although such a transfer is feasible between Earth and Mars (Mileikowsky *et al.* 2000), it is far more difficult with Europa. Objects will strike Europa at velocities unimpeded by any significant atmosphere, making high temperature shock heating much harder to avoid (Pierazzo and Chyba 2002).

Certain prebiotic chemical processes under hydrothermal conditions might have been important in the origin of terrestrial life (Wächtershäuser 1988, Cody *et al.* 2000), but it is possible that other required compounds included molecules such as sugars (Weber 2000) which could have required a surface origin. The terrestrial origin of life remains too poorly understood (Chyba and McDonald 1995) for firm conclusions to be drawn. The investigation of Europa could provide insight into the importance of different environments to the origin of life.

### 15.5.1 Biogenic Elements

Besides liquid water, life requires a suite of biogenic elements, including carbon, hydrogen, oxygen, nitrogen, phosphorus, sulfur, and others. Spectroscopic observations provide some data on the composition of the upper surface of Europa, as reviewed in Section 15.2. Various organic groups, such as C≡N and C–H, have been detected on Callisto and Ganymede, and there are suggestions of these compounds on Europa.

However, estimates of abundances of biogenic elements rely on Europa formation models, some of which suggest that Europa should be volatile-rich. But even if Europa formed extremely volatile-poor, comet impacts should have delivered substantial quantities of biogenic elements (e.g., $\sim 10^{12}$ kg C) over the age of the solar system (Pierazzo and Chyba 2002). Thus, the availability of biogenic elements seems unlikely to be an impediment to the existence of life on Europa.

### 15.5.2 Sources of Free Energy

We already know of one planetary environment in solar system history, suggested in meteorites, where liquid water and organics were present but in which little progress seems to have been made toward the origin of life (Chyba and McDonald 1995). Carbonaceous chondrite meteorites derive from parent bodies that may have seen liquid water for between $\sim 10^4$ and $10^8$ yr, yet prebiotic chemistry in these meteorites seems not to have progressed very far beyond monomers such as individual amino acids and low concentrations of diglycine (Cronin 1976, Shimoyama and Ogasawara 2002). It is tempting to conclude that meteorite parent bodies simply lacked sufficient sources of free energy to drive substantial chemical disequilibria. This emphasizes the importance of assessing possible sources of free energy on Europa as a prelude to speculation about life on that world, however water- and organic-rich it might prove to be.

Discussion of energy sources for life on Europa began with Reynolds *et al.* (1983), who emphasized the difficulty of powering a substantial ecosystem by photosynthesis through Europa's ice layer. Gaidos *et al.* (1999) extended this line of reasoning to argue that it is difficult to identify any sources of chemical disequilibrium on an ice-covered world lacking photosynthesis, with grim consequences for the prospects of life on Europa.

But if hydrothermal vents exist at the base of Europa's ocean (Section 15.4.4), an ecosystem could be powered through methanogenesis or other reactions, for example, combining $CO_2$ with $H_2$ derived from fluid–rock reactions (McCollom 1999). Whether or not such hydrothermal activity is expected on Europa remains a matter of debate (Moore and Schubert 2000, McKinnon and Shock 2001).

A second possibility is that life could take advantage of the disequilibrium production of $O_2$ and $H_2$ in the putative ocean due to the decay of $^{40}K$ (Chyba and Hand 2001). Recombination of these molecules by microorganisms could produce $\sim 10^7$ to $10^9$ kg yr$^{-1}$ of biomass today. Steady-state biomasses are difficult to calculate, because appropriate maintenance energies are difficult to estimate (Chyba and Phillips 2001). If we use a biological turnover time of $\sim 10^3$ yr, appropriate for Earth's deep biosphere (Whitman *et al.* 1998), the above calculation suggests a potential biomass of $\sim 10^{10}$ to $10^{12}$ kg, which could be compared with the terrestrial oceanic microbial biomass of nearly $10^{15}$ kg. This potential energy source would be largely independent of the thickness or heat loss mechanisms of Europa's ice cover.

Two other sources of chemical disequilibrium for a europan biosphere depend on the behavior of Europa's ice shell. One is decay of $^{40}K$ in the ice shell; this mechanism is likely less important in the shell than in the ocean because K will be excluded from ice as water freezes (Chyba and Hand 2001). However, a second source is potentially important: the production of oxidants such as $O_2$ and hydrogen peroxide (Delitsky and Lane 1997, 1998, Gaidos *et al.* 1999, Chyba 2000a,b, Cooper *et al.* 2001) and organics such as formaldehyde (Chyba 2000a,b) in the uppermost meter of Europa's

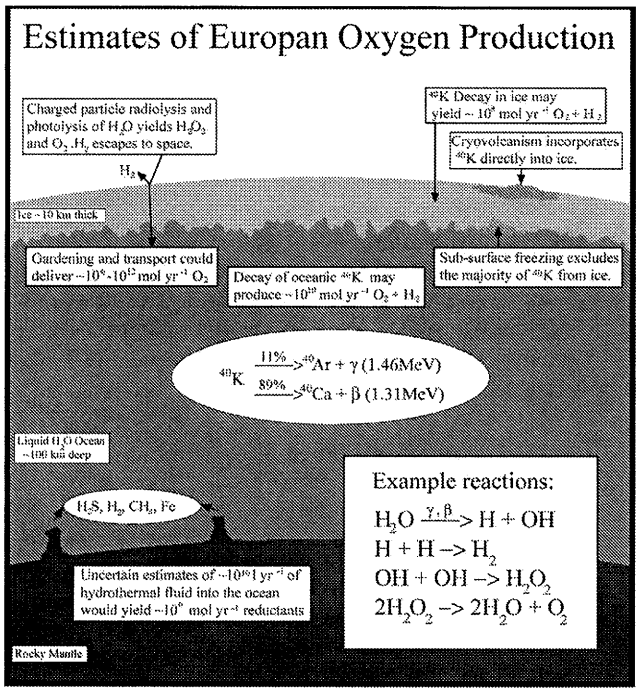


**Figure 15.19.** Potential sources of chemical disequilibrium on Europa (after Chyba and Hand 2001).

ice due to charged-particle bombardment followed by impact gardening to meter depths (Cooper *et al.* 2001, Chyba and Phillips 2001). This effect would be important for life on Europa only if the uppermost meters of Europa communicate with the putative ocean. If the timescale for this communication is 50 Myr – i.e., if Europa's surface is mixed into the ocean once every 50 Myr on average – then $\sim 10^7$ to $10^{11}$ kg $yr^{-1}$ of biomass could be produced on Europa, depending on $O_2$ production and microbial growth efficiencies (Chyba and Hand 2001). These various potential sources of chemical disequilibrium on Europa are summarized in Figure 15.19.

It has also been suggested that regions or niches might exist within Europa's ice cover where photosynthesis may be possible within liquid-water environments (Reynolds *et al.* 1983). Some of these models rely on a cracks or melt-through events in a relatively thin ice layer (Greenberg *et al.* 2000, 2002a). Dissipative heating in Europa's cracks may provide a different route to this end (Gaidos and Nimmo 2000). Were photosynthesis possible in limited environments on Europa, the energy available for life in these regions would swamp other sources. If life exists on Europa, and were it to have access to near-surface liquid-water environments, there would be strong selection pressure for it to colonize these environments because of this huge energy advantage.

### 15.5.3 Broadening the Definition of Habitability

The notion of "habitability" of a world once referred to those conditions suitable for human life (Dole 1964). The word has since come to refer to conditions less stringent: those necessary for stability of liquid water at a world's surface (Kasting *et al.* 1993). The elucidation of Earth's subsurface biosphere, and the discovery of a likely ocean on Europa, suggest that the universe may provide a much more expansive arena for life than the "classical" definition suggested (Sagan 1996, Chyba 1997, Chyba *et al.* 2000). But the only way to know whether life exists on Europa is to go and search.

## 15.6 SUMMARY AND CONCLUSIONS

Each of the Galilean satellites exhibits unique characteristics in terms of its surface evolution. Io (Chapter 14) is distinguished as a rocky moon and is the most volcanically active object in the solar system. Europa is primarily a rocky object but has an outer shell of water and a "lithosphere" of ice. Its surface history is characterized by tectonic deformation of the ice and local resurfacing by melted and/or ductile ice. The relative paucity of preserved impact craters on Europa suggests a rapid rate of resurfacing (Figueredo and Greeley 2004). Ganymede (Chapter 16), composed of about half water and half rocky material, shares some attributes with Europa by having extensive tectono-volcanic resurfacing of its ice-rich surface, but also has substantial terrains that preserve the record of cratering. Thus, the rate and intensity of internal activity is less than that of Europa. Finally, Callisto's surface (Chapter 17) is dominated by impact craters of all sizes; yet, it also might contain a deep-seated "ocean" of liquid water. However, the high depth and low amount of internal energy have apparently precluded processes leading to endogenic resurfacing.

A key question for Europa remains unanswered. Does this moon currently have liquid water beneath its icy outer shell? Most investigators agree that many of the surface features described in the previous sections reflect the presence of liquid water (or at least warm, ductile ice) at the time of their formation, but the features do not necessarily reflect today's conditions. However, given the relative youth of the features, it would seem unlikely that liquid water/warm ice would have frozen in the last ~60 million years, after a period of several billion years of its existence. This consideration, coupled with the results from the *Galileo* magnetometer suggesting the presence of a brine-rich ocean, leads most researchers to conclude that liquid water/warm ice is present today.

The question of Europa's putative ocean is unlikely to be resolved definitively with currently available data. The experiments for the *Galileo* mission were conceived in the early 1970s (prior to the *Voyager* spacecraft flybys) and were not designed to address this question. Because of the high interest in Europa for astrobiological exploration, numerous formal (e.g., Space Studies Board 1999, 2003) and other studies (e. g., Chyba 1998) have considered the types of space flight projects that might be implemented. One sequence involves an orbiter around Europa that would (1) measure the degree of daily tidal flexing (which would enable the presence of an ocean to be detected and the thickness of the brittle ice to be constrained), (2) obtain global imaging at uniform resolutions and illumination conditions, and (3) map surface compositions. Should liquid water be detected, the next step would involve a landed system to make in situ measurements of compositions and conduct biologically relevant experiments. Subsequently, subsurface probes might be deployed to make observations and measurements below the radiation-intense zone on and near the surface.

The implementation of this sequence of missions was

initiated with plans for the Europa Orbiter. Unfortunately, the escalating costs of this project led to its cancellation in 2002. Currently, various missions options are being reconsidered, including the Jupiter Icy Moons Orbiter, which would derive both power and propulsion from nuclear sources. The fundamental issue is whether to conduct the projects serially, as outlined above, or whether to combine elements into a larger project(s). For example, most groups agree that a lander of some type is required to address the key astrobiology questions for Europa. Thus, rather than fly an orbiter and lander separately, the two components might be combined.

In summary, the outstanding questions that need to be addressed for Europa include:

- Is there liquid water on Europa and, if so, what is its spatial distribution? If there is a globally distributed "ocean" of water, how thick is the layer of ice that covers it, and what are the properties of the liquid? If there is not liquid water today, was there any in the past, and what is the time dependence of its occurrence?
- Are the kilometer-scale ice rafts seen on Europa's surface a product of the movement of ice on an underlying liquid-water sea or through a warm, soft (but not necessarily melted) ice? What is the overall relationship between the surficial geologic units and the history of liquid water?
- What is the composition of the deep interior of Europa, including both the presumed silicate mantle and the iron or FeS-rich core? Is the core solid or liquid? Was there ever a global magnetic field produced by motions within the core? What are the dynamics of the interior, especially regarding the possible physical decoupling of the rotation of the surface ice from the deep interior and the possible non-synchronous rotation of the surface or of the entire satellite? What is the magnitude of tidal heating of the interior, and how is the heating distributed within the interior? Is the rock mantle convecting and is there active volcanism?
- What are the "absolute" ages of the features seen on Europa and what is the timescale for the key events in the evolution of the surface?
- What is the composition of the non-ice component (such as salts) of the surface materials that are seen in imaging and spectroscopic investigations? How do they vary over the surface? What are the source and history of these materials, and how do they relate to the geologic history of the surface and the potential for the at-least-intermittent presence of liquid water?
- What is the nature of the ice-tectonic processes that have affected the surface, and how are they reflected in the features that are seen (such as triple bands and spots)? Is there active or ongoing cryovolcanism?
- What is the composition of the neutral atmosphere and of the ionosphere? What are the sources and sinks of these species? What are the spatial and temporal variations in the atmosphere, and how do they relate to the physical processes that might control them? What is the composition of the magnetospheric ions that can sputter the surface, and of the sputtering products?
- What are the characteristics of the radiation environment at the surface of Europa (currently and in the past), and what are the implications for organic/biotic chemistry and the survival of life on the surface?
- What is the abundance of geochemical sources of energy that could support an origin of life on Europa or its continued existence? Is there extant life, or has there been life in the past? If there has been liquid water, access to biogenic elements, and a source of energy but there is no life present, what factors might explain the lack of occurrence of life, and does the potential exist for an independent origin of life in the future?

**Acknowledgements.** We thank three anonymous reviewers for thoughtful comments that resulted in substantial improvements to this chapter. This work was supported by the NASA Jupiter System Data Analysis, Planetary Geology and Geophysics, and Exobiology programs and the NASA Astrobiology Institute.

## REFERENCES

Agee, C. B., J. Li, M. C. Shannon, and S. Circone, Pressure–temperature phase diagram for the Allende meteorite, *J. Geophys. Res.* **100**, 17 725–17 740, 1995.

Anderson, J. D., E. L. Lau, W. L. Sjogren, G. Schubert, and W. B. Moore, Gravitational constraints on the internal structure of Ganymede, *Nature* **384**, 541–543, 1996.

Anderson, J. D., G. Schubert, R. A. Jacobson, E. L. Lau, W. B. Moore, and W. L. Sjogren, Europa's differential internal structure: Inferences from four *Galileo* encounters, *Science* **281**, 2019–2022, 1998.

Anderson, J. D., G. Schubert, A. Anabtawi, R. Jacobson, C. Lau, and W. B. Moore, Recent results on Io's gravity field and internal structure, *Eos* p. S212, 2002.

Barbieri, C., J. Rahe, T. V. Johnson, and A. M. Sohus, eds, *The Three Galileos: The Man, The Spacecraft, The Telescope*, Kluwer, 1997.

Belton, M. J. S., J. W. Head, A. P. Ingersoll, R. Greeley, A. S. McEwen, K. P. Klaasen, D. Senske, R. T. Pappalardo, G. Collins, A. R. Vasavada, R. Sullivan, D. Simonelli, P. Geissler, M. H. Carr, M. E. Davies, J. Veverka, P. J. Gierasch, D. Banfield, M. Bell, C. R. Chapman, C. Anger, R. Greenberg, G. Neukum, C. B. Pilcher, R. F. Beebe, J. A. Burns, F. Fanale, W. Ip, T. V. Johnson, D. Morrison, J. Moore, G. S. Orton, P. Thomas, and R. A. West, *Galileo*'s first images of Jupiter and the Galilean satellites, *Science* **274**, 377–385, 1996.

Bierhaus, E., C. Chapman, W. Merline, S. Brooks, and E. Asphaug, Pwyll secondaries and other small craters on Europa, *Icarus* **153**, 264–276, 2001.

Brown, M. E. and R. E. Hill, Discovery of an extended sodium atmosphere around Europa, *Nature* **380**, 229–231, 1996.

Buck, L., C. F. Chyba, M. Goulet, A. Smith, and P. Thomas, Persistence of thin ice regions in Europa's ice crust, *Geophys. Res. Lett.* **29**, 12–1, 2002.

Burns, J. A., ed., *Planetary Satellites*, University of Arizona Press, 1977.

Burns, J. A. and M. S. Matthews, eds, *Satellites*, University of Arizona Press 1986.

Calvin, W. M., R. N. Clark, R. H. Brown, and J. R. Spencer, Spectra of the icy Galilean satellites from 0.2 to 5 microns: A compilation, new observations, and a recent summary, *J. Geophys. Res.* **100**, 19 041–19 048, 1995.

Cameron, A. G. W., Formation of the outer planets and satellites, in *Planetary Satellites*, J. A. Burns (ed), University of Arizona Press, pp. 463–471, 1977.

Canup, R. M. and W. R. Ward, Formation of the Galilean satellites: Conditions of accretion, *AJ* **124**, 3404–3423, 2002.

Carlson, R. W., A tenuous carbon dioxide atmosphere on Jupiter's moon Callisto, *Science* **283**, 820, 1999.

Carlson, R. W., W. Smythe, K. Baines, E. Barbinis, K. Becker, R. Burns, S. Calcutt, W. Calvin, R. Clark, G. Danielson, A. Davies, P. Drossart, T. Encrenaz, F. Fanale, J. Granahan, G. Hansen, P. Herrera, C. Hibbitts, J. Hui, P. Irwin, T. Johnson, L. Kamp, H. Kieffer, F. Leader, E. Lellouch, R. Lopes-Gautier, D. Matson, T. McCord, R. Mehlman, A. Ocampo, G. Orton, M. Roos-Serote, M. Segura, J. Shirley, L. Soderblom, A. Stevenson, F. Taylor, J. Torson, A. Weir, and P. Weissman, Near-infrared spectroscopy and spectral mapping of Jupiter and the Galilean satellites: Results from *Galileo*'s initial orbit, *Science* **274**, 385–388, 1996.

Carlson, R. W., M. S. Anderson, R. E. Johnson, W. D. Smythe, A. R. Hendrix, C. A. Barth, L. A. Soderblom, G. B. Hansen, J. B. McCord, J. B. Dalton, J. H. Clark, J. H. Shirley, A. C. Ocampo, and D. L. Matson, Hydrogen peroxide on the surface of Europa, *Science* **283**, 2062–2064, 1999a.

Carlson, R. W., R. E. Johnson, and M. S. Anderson, Sulfuric acid on Europa and the radiolytic sulfur cycle, *Science* **286**, 97–99, 1999b.

Carr, M. H., M. J. S. Belton, K. Bender, H. Breneman, R. Greeley, J. W. Head, K. P. Klaasen, A. S. McEwen, J. M. Moore, S. Murchie, R. T. Pappalardo, J. Plutchak, R. Sullivan, G. Thornhill, and J. Veverka, The *Galileo* Imaging Team plan for observing the satellites of Jupiter, *J. Geophys. Res.* **100**, 18 935–18 956, 1995.

Carr, M. H., M. J. S. Belton, C. R. Chapman, M. E. Davies, P. Geissler, R. Greenberg, A. S. McEwen, B. R. Tufts, R. Greeley, and R. Sullivan, Evidence for a subsurface ocean on Europa, *Nature* **391**, 363, 1998.

Cassen, P., R. T. Reynolds, and S. J. Peale, Is there liquid water on Europa?, *Geophys. Res. Lett.* **6**, 731–734, 1979.

Cassen, P. M., S. Peale, and R. T. Reynolds, Structure and thermal evolution of the Galilean satellites, in *Satellites of Jupiter*, D. Morrison (ed), University of Arizona Press, pp. 93–128, 1982.

Chapman, C. R., W. J. Merline, B. Bierhaus, S. Brooks, and *Galileo* Imaging Team, Cratering in the jovian system: Intersatellite comparisons, in *Lunar and Planetary Science Conference Abstracts*, p. 1927, 1998.

Chyba, C. F., Life on other moons, *Nature* **385**, 201, 1997.

Chyba, C. F., ed., *Europa Orbiter Science Definition Team Report*, NASA, 1998.

Chyba, C. F., Energy for microbial life on Europa, *Nature* **403**, 381–382, 2000a.

Chyba, C. F., Energy for microbial life on Europa (Correction), *Nature* **406**, 368, 2000b.

Chyba, C. F. and K. P. Hand, Life without photosynthesis, *Science* **292**, 2026–2027, 2001.

Chyba, C. F. and G. D. McDonald, The origin of life in the solar system: Current issues, *Ann. Rev. Earth Planet. Sci.* **23**, 215–250, 1995.

Chyba, C. F. and C. B. Phillips, Possible ecosystems and the search for life on Europa, *Proc. Natl. Acad. Sci.* **98**, 801–804, 2001.

Chyba, C. F., S. J. Ostro, and B. C. Edwards, Radar detectability of a subsurface ocean on Europa, *Icarus* **134**, 292–302, 1998.

Chyba, C. F., D. P. Whitmire, and R. Reynolds, Planetary habitability and the origins of life, in *Protostars and Planets IV*, V. Mannings, A. P. Boss, and S. S. Russell (eds), University of Arizona Press, pp. 1365–1393, 2000.

Clark, B. E., P. Helfenstein, J. Veverka, M. Ockert-Bell, R. J. Sullivan, P. E. Geissler, C. B. Phillips, A. S. McEwen, R. Greeley, G. Neukum, T. Denk, and K. Klaasen, Multispectral terrain analysis of Europa from *Galileo* images, *Icarus* **135**, 95–106, 1998.

Clark, R. N., Ganymede, Europa, Callisto, and Saturn's rings: Compositional analysis from reflectance spectroscopy, *Icarus* **44**, 388–409, 1980.

Cody, G. D., N. Z. Boctor, T. R. Filley, R. M. Hazen, J. H. Scott, A. Sharma, and H. S. Yoder, Primordial carbonylated iron–sulfur compounds and the synthesis of pyruvate, *Science* **289**, 1337–1340, 2000.

Collins, G. C., J. W. Head, R. T. Pappalardo, and N. A. Spaun, Evaluation of models for the formation of chaotic terrain on Europa, *J. Geophys. Res.* **105**, 1709–1716, 2000.

Consolmagno, G. J. and J. S. Lewis, Structural and thermal models of icy Galilean satellites, in *Jupiter*, T. Gehrels (ed), University of Arizona Press, pp. 1035–1051, 1976.

Consolmagno, G. J. and J. S. Lewis, Preliminary thermal history models of icy satellites, in *Planetary Satellites*, J. A. Burns (ed), University of Arizona Press, pp. 492–500, 1977.

Consolmagno, G. J., D. T. Britt, and C. P. Stoll, The porosities of ordinary chondrites: Models and interpretation, *Meteoritics Plan. Sci.* **33**, 1221–1229, 1998.

Cooper, J. F., R. E. Johnson, B. H. Mauk, H. B. Garrett, and N. Gehrels, Energetic ion and electron irradiation of the icy Galilean satellites, *Icarus* **149**, 133–159, 2001.

Coyne, G. V., Galileo's telescopic observations: The marvel and meaning of discovery, in *The Three Galileos: The Man, The Spacecraft, The Telescope*, C. Barbieri, J. Rahe, T. V. Johnson, and A. M. Sohus, eds, pp. 1–3, Kluwer, 1997.

Crawford, G. D. and D. J. Stevenson, Gas-driven water volcanism in the resurfacing of Europa, *Icarus* **73**, 66–79, 1988.

Cronin, J. F., Acid-labile amino acid precursors in the Murhison meteorite: II. A search for peptides and amino acyl amides, *Origins Life* **7**, 343–348, 1976.

Davies, M. E., T. R. Colvin, J. Oberst, W. Zeitler, P. Schuster, G. Neukum, A. S. McEwen, C. B. Phillips, P. C. Thomas, J. Veverka, M. J. S. Belton, and G. Schubert, The control networks of the Galilean satellites and implications for global shape, *Icarus* **135**, 372–376, 1998.

De La Chapelle, S., H. Milsch, O. Castelnau, and P. Duval, Compressive creep of ice containing a liquid intergranular phase: Rate-controlling processes in the dislocation creep regime, *Geophys. Res. Lett.* **26**, 251, 1999.

Delitsky, M. L. and A. L. Lane, Chemical schemes for surface modification of icy satellites: A road map, *J. Geophys. Res.* **102**, 16 385–16 390, 1997.

Delitsky, M. L. and A. L. Lane, Ice chemistry on the Galilean satellites, *J. Geophys. Res.* **103**, 31 391–31 404, 1998.

Dole, S. H., *Habitable Planets for Man*, Blaisdell, 1964.

Durham, W. B. and L. A. Stern, Rheological properties of water ice-applications to satellites of the outer planets, *Ann. Rev. Earth Planet. Sci.* **29**, 295–330, 2001.

Durham, W. B., L. A. Stern, and S. H. Kirby, Rheology of ice I at low stress and elevated confining pressure, *J. Geophys. Res.* **106**, 11 031–11 042, 2001.

Fagents, S. A., R. Greeley, R. J. Sullivan, R. T. Pappalardo, L. M. Prockter, and T. *Galileo* SSI Team, Cryomagmatic mechanisms for the formation of Rhadamanthys Linea, triple band margins, and other low-albedo features on Europa, *Icarus* **144**, 54–88, 2000.

Fanale, F. P., T. V. Johnson, and D. L. Matson, Io's surface and the histories of the Galilean satellites, in *Planetary Satellites*, J. A. Burns (ed), University of Arizona Press, pp. 379–405, 1977.

Fanale, F. P., Y. H. Li, E. Decarlo, N. Domergue-Schmidt, S. K. Sharma, K. Horton, J. C. Granahan, and *Galileo* NIMS Team, Laboratory simulations of the chemical evolution of Europa's aqueous phase, in *Lunar and Planetary Science Conference Abstracts*, p. 1248, 1998.

Fanale, F. P., J. C. Granahan, R. Greeley, R. T. Pappalardo, J. I. Head, J. Shirley, R. Carlson, A. Hendrix, J. Moore, T. B. McCord, and M. Belton, Tyre and Pwyll: *Galileo* orbital remote sensing of mineralogy versus morphology at two selected sites on Europa, *J. Geophys. Res.* **105**, 22 647–22 657, 2000.

Fanale, F. P., Y.-H. Li, E. de Carlo, C. Farley, S. K. Sharma, K. Horton, and J. C. Granahan, An experimental estimate of Europa's "ocean" composition independent of *Galileo* orbital remote sensing, *J. Geophys. Res.* **106**, 14 595–14 600, 2001.

Fei, Y., C. M. Bertka, and L. W. Finger, High-pressure iron–sulfur compound, $Fe_3S_2$, and melting relations in the Fe–FeS system, *Science* **275**, 1621–1523, 1997.

Figueredo, P. H. and R. Greeley, Geologic mapping of the northern leading hemisphere of Europa from *Galileo* solid-state imaging data, *J. Geophys. Res.* **105**, 22 629–22 646, 2000.

Figueredo, P. H. and R. Greeley, Resurfacing history of Europa from pole-to-pole geological mapping, *Icarus*, **167**, 287–312, 2004.

Figueredo, P. H., F. C. Chuang, J. Rathbun, R. L. Kirk, and R. Greeley, Geology and origin of Europa's mitten feature (Murias Chaos), *J. Geophys. Res.* **107**, 2–1, 2002.

Fimmel, R. O., W. Swindell, and E. Burgess, *Pioneer Odyssey: Encounter with a Giant*, NASA, SP-349, 1974.

Folkner, W. M., C. F. Yoder, D. N. Yuan, E. M. Standish, and R. A. Preston, Interior structure and seasonal mass redistribution of Mars from radio tracking of *Mars Pathfinder*, *Science* **278**, 1749–1752, 1997.

Friedson, A. J. and D. J. Stevenson, Viscosity of rock–ice mixtures and applications to the evolution of icy satellites, *Icarus* **56**, 1–14, 1983.

Gaidos, E. J. and F. Nimmo, Tectonics and water on Europa, *Nature* **405**, 637, 2000.

Gaidos, E. J., K. H. Nealson, and J. L. Kirschvink, Life in ice-covered oceans, *Science* **284**, 1631–1633, 1999.

Gammon, E. J., H. Klefte, and M. J. Clouter, Elastic constants of ice samples by brillouin spectroscopy, *J. Phys. Chem.* **87**, 4025–4029, 1983.

Geissler, P., R. Greenberg, G. Hoppa, A. McEwen, R. Tufts, C. Phillips, B. Clark, M. Ockert-Bell, P. Helfenstein, J. Burns, J. Veverka, R. Sullivan, R. Greeley, R. T. Pappalardo, J. W. Head, M. J. S. Belton, and T. Denk, Evolution of lineaments on Europa: Clues from *Galileo* multispectral imaging observations, *Icarus* **135**, 107–126, 1998a.

Geissler, P., R. Greenberg, G. Hoppa, P. Helfenstein, A. McEwen, R. Pappalardo, R. Tufts, M. Ockert-Bell, R. Sullivan, and R. Greeley, Evidence for non-synchronous rotation of Europa, *Nature* **391**, 368, 1998b.

Geissler, P., R. Greenberg, G. Hoppa, A. McEwen, R. Tufts, C. Phillips, B. Clark, M. Ockert-Bell, P. Helfenstein, J. Burns, J. Veverka, R. Sullivan, R. Greeley, R. T. Pappalardo, J. W. Head, M. J. S. Belton, T. Denk, and *Galileo* Imaging Team, A recently active lineament on Europa?, in *Lunar and Planetary Science Conference Abstracts*, p. 1904, 1998c.

Geissler, P., R. Greenberg, G. V. Hoppa, B. R. Tufts, M. Milazzo, and the *Galileo* Imaging Team, Rotation of lineaments in Europa's southern hemisphere, in *Lunar and Planetary Science Conference Abstracts*, p. 1743, 1999.

Giese, B., R. Wagner, and G. Neukum, The local topography of Europa: Stereo analysis of *Galileo* SSI images and implications for geology, *Geophys. Res. Abstr.* **1**, 742, 1999.

Gold, T., The deep, hot biosphere, *Proc. Natl. Acad. Sci.* **89**, 6045–6049, 1992.

Goldreich, P., Final spin states of planets and satellites, *AJ* **71**, 1, 1966.

Goldsby, D. L. and D. L. Kohlstedt, Grain boundary sliding in fine-grained ice I, *Scripta Mat.* **37**, 1399–1406, 1997.

Goldsby, D. L. and D. L. Kohlstedt, Superplastic deformation of ice: Experimental observations, *J. Geophys. Res.* **106**, 11 017–11 030, 2001.

Golombek, M. P. and W. B. Banerdt, Constraints on the subsurface structure of Europa, *Icarus* **83**, 441–452, 1990.

Grant, F. S. and G. F. West, *Interpretation Theory in Applied Geophysics*, McGraw-Hill Book Co., 1965.

Greeley, R., Geology of Europa: *Galileo* update, in *The Three Galileos: The Man, The Spacecraft, the Telescope*, C. Barbieri, J. Rahe, T. V. Johnson, and A. M. Sohus, eds, pp. 191–200, Kluwer, 1997.

Greeley, R., R. Sullivan, K. C. Bender, K. S. Homan, S. A. Fagents, R. T. Pappalardo, and J. W. Head, Europa triple bands: *Galileo* images, in *Lunar and Planetary Science Conference Abstracts*, pp. 455–456, 1997.

Greeley, R., R. Sullivan, M. D. Coon, P. E. Geissler, B. R. Tufts, J. W. Head, R. T. Pappalardo, and J. M. Moore, Terrestrial sea ice morphology: Considerations for Europa, *Icarus* **135**, 25–40, 1998a.

Greeley, R., R. Sullivan, J. Klemaszewski, K. Homan, J. W. Head, R. T. Pappalardo, J. Veverka, B. E. Clark, T. V. Johnson, K. P. Klaasen, M. Belton, J. Moore, E. Asphaug, M. H. Carr, G. Neukum, T. Denk, C. R. Chapman, C. B. Pilcher, P. E. Geissler, R. Greenberg, and R. Tufts, Europa: Initial *Galileo* geological observations, *Icarus* **135**, 4–24, 1998b.

Greeley, R., P. H. Figueredo, D. A. Williams, F. C. Chuang, J. E. Klemaszewski, S. D. Kadel, L. M. Prockter, R. T. Pappalardo, J. W. Head, G. C. Collins, N. A. Spaun, R. J. Sullivan, J. M. Moore, D. A. Senske, B. R. Tufts, *et al.*, Geologic mapping of Europa, *J. Geophys. Res.* **105**, 22 559–22 578, 2000.

Greenberg, R., Orbital evolution of the Galilean satellites, in *Satellites of Jupiter*, D. Morrison (ed), University of Arizona Press, pp. 65–92, 1982.

Greenberg, R., Galilean satellites: Evolutionary paths in deep resonance, *Icarus* **70**, 334–347, 1987.

Greenberg, R. and S. J. Weidenschilling, How fast do Galilean satellites spin?, *Icarus* **58**, 186–196, 1984.

Greenberg, R., P. Geissler, G. Hoppa, B. R. Tufts, D. D. Durda, R. Pappalardo, J. W. Head, R. Greeley, R. Sullivan, and M. H. Carr, Tectonic processes on Europa: Tidal stresses, mechanical response, and visible features, *Icarus* **135**, 64–78, 1998.

Greenberg, R., G. V. Hoppa, B. R. Tufts, P. Geissler, J. Riley, and S. Kadel, Chaos on Europa, *Icarus* **141**, 263–286, 1999.

Greenberg, R., P. Geissler, B. R. Tufts, and G. V. Hoppa, Habitability of Europa's crust: The role of tidal-tectonic processes, *J. Geophys. Res.* **105**, 17 551–17 562, 2000.

Greenberg, R., P. Geissler, G. Hoppa, and B. R. Tufts, Tidal-tectonic processes and their implications for the character of Europa's icy crust, *Rev. Geophys.* **40**, 1–33, 2002a.

Greenberg, R., A. R. Sarid, T. A. Hurford, G. V. Hoppa, B. R. Tufts, and P. Geissler, Europa's surface-area budget: Identification of convergence features by strike-slip reconstructions, in *Lunar and Planetary Science Conference Abstracts*, p. 1903, 2002b.

Hansen, G. B. and T. B. McCord, Amorphous and crystalline ice on the Galilean satellites: A balance between thermal and radiolytic processes, in *Lunar and Planetary Science Conference Abstracts*, p. 1630, 2000.

Hansen, G. B., T. B. McCord, W. M. Smythe, and R. W. Carlson, The state of water ice on the icy Galilean satellites from the *Galileo* NIMS investigation, in *Nantes 98 International Symposium on The Jovian System after Galileo, the Saturnian System Before Cassini-Huygens*, 1998.

Harris, D. L., Photometry and colorimetry of planets and satellites, in *Planets and Satellites*, G. P. Kuiper and B. M. Middlehurst (eds), University of Chicago Press, p. 305, 1961.

Head, J. W. and R. T. Pappalardo, Brine mobilization during lithospheric heating on Europa: Implications for formation of chaos terrain, lenticula texture, and color variations, *J. Geophys. Res.* **104**, 27 143, 1999.

Head, J. W., R. T. Pappalardo, and R. Sullivan, Europa: Morphological characteristics of ridges and triple bands from *Galileo* data (E4 and E6) and assessment of a linear diapirism model, *J. Geophys. Res.* **104**, 24 223–24 236, 1999.

Helfenstein, P. and E. M. Parmentier, Fractures on Europa: Possible response of an ice crust to tidal deformation, in *Lunar and Planetary Science Conference Abstracts*, pp. 1987–1998, 1980.

Helfenstein, P. and E. M. Parmentier, Patterns of fracture and tidal stresses on Europa, *Icarus* **53**, 415–430, 1983.

Helfenstein, P. and E. M. Parmentier, Patterns of fracture and tidal stresses due to nonsynchronous rotation: Implications for fracturing on Europa, *Icarus* **61**, 175–184, 1985.

Hendrix, A. R., C. A. Barth, C. W. Hord, and A. L. Lane, Europa: Disk-resolved ultraviolet measurements using the *Galileo* Ultraviolet Spectrometer, *Icarus* **135**, 79–94, 1998.

Hendrix, A. R., C. A. Barth, A. I. F. Stewart, C. W. Hord, and A. L. Lane, Hydrogen peroxide on the icy Galilean satellites, in *Lunar and Planetary Science Conference Abstracts*, p. 2043, 1999.

Hermance, J. F., Electrical conductivity models of the crust and mantle, in *Global Earth Physics: A Handbook of Physical Constants*, T. J. Ahrens (ed), pp. 190–205, AGU, 1995.

Hibbitts, C. A., T. B. McCord, and G. B. Hansen, Distributions of $CO_2$ and $SO_2$ on the surface of Callisto, *J. Geophys. Res.* **105**, 22 541–22 558, 2000.

Hoppa, G. V., B. R. Tufts, R. Greenberg, and P. Geissler, Strike-slip faults on Europa: Global shear patterns driven by tidal stress, *Icarus* **141**, 287–298, 1999a.

Hoppa, G. V., B. R. Tufts, R. Greenberg, and P. E. Geissler, Formation of cycloidal features on Europa, *Science* **285**, 1899–1902, 1999b.

Hoppa, G. V., R. Greenberg, P. Geissler, B. R. Tufts, J. Plassmann, and D. D. Durda, Rotation of Europa: Constraints from terminator and limb positions, *Icarus* **137**, 341–347, 1999c.

Hoppa, G. V., B. R. Tufts, R. Greenberg, and P. E. Geissler, Europa's sub-jovian hemisphere from *Galileo* I25: Tectonic and chaotic surface features, in *Lunar and Planetary Science Conference Abstracts*, p. 1380, 2000.

Hoppa, G. V., B. Randall Tufts, R. Greenberg, T. A. Hurford, D. P. O'Brien, and P. E. Geissler, Europa's rate of rotation derived from the tectonic sequence in the Astypalaea region, *Icarus* **153**, 208–213, 2001.

Hussmann, H., T. Spohn, and K. Wieczerkowski, Thermal equilibrium states of Europa's ice shell: Implications for internal ocean thickness and surface heat flow, *Icarus* **156**, 143–151, 2002.

Jenyon, M. K., *Salt Tectonics*, Elsevier Applied Science, 1986.

Johnson, R. E., Sodium at Europa, *Icarus* **143**, 429–433, 2000.

Johnson, R. E., M. L. Nelson, T. B. McCord, and J. C. Gradie, Analysis of *Voyager* images of Europa: Plasma bombardment, *Icarus* **75**, 423–436, 1988.

Johnson, R. E., R. M. Killen, J. H. Waite, and W. S. Lewis, Europa's surface composition and sputter-produced ionosphere, *Geophys. Res. Lett.* **25**, 3257, 1998.

Johnson, T. V. and T. B. McCord, Spectral geometric albedo of the Galilean satellites, 0.3 to 2.5 microns, *ApJ* **169**, 589, 1971.

Johnson, T. V., L. A. Soderblom, J. A. Mosher, G. E. Danielson, A. F. Cook, and P. Kupperman, Global multispectral mosaics of the icy Galilean satellites, *J. Geophys. Res.* **88**, 5789–5805, 1983.

Kadel, S. D., S. A. Fagents, R. Greeley, and the *Galileo* SSI Team, Trough-bounding ridge pairs on Europa: Considerations for an endogenic model of formation, in *Lunar and Planetary Science Conference Abstracts*, p. 1078, 1998.

Kadel, S. D., F. C. Chuang, R. Greeley, and J. M. Moore, Geological history of the Tyre region of Europa: A regional perspective on Europan surface features and ice thickness, *J. Geophys. Res.* **105**, 22 656–22 669, 2000.

Kargel, J. S., Brine volcanism and the interior structures of asteroids and icy satellites, *Icarus* **94**, 368–390, 1991.

Kargel, J. S., Aqueous chemical evolution and hydration state of Europa's salts, in *Lunar and Planetary Science Conference Abstracts*, p. 1851, 1999.

Kargel, J. S. and G. J. Consolmagno, Magnetic fields and the detectability of brine oceans in Jupiter's icy satellites, in *Lunar and Planetary Science Conference Abstracts*, p. 643, 1996.

Kargel, J. S., J. Z. Kaye, J. W. Head, G. M. Marion, R. Sassen, J. K. Crowley, O. P. Ballesteros, S. A. Grant, and D. L. Hogenboom, Europa's crust and ocean: Origin, composition, and the prospects for life, *Icarus* **148**, 226–265, 2000.

Kasting, J. F., D. P. Whitmire, and R. T. Reynolds, Habitable zones around main sequence stars, *Icarus* **101**, 108–128, 1993.

Kattenhorn, S. A., Nonsynchronous rotation evidence and fracture history in the bright plains region, Europa, *Icarus* **157**, 490–506, 2002.

Khurana, K. K., M. G. Kivelson, D. J. Stevenson, G. Schubert, C. T. Russell, R. J. Walker, and C. Polanskey, Induced magnetic fields as evidence for subsurface oceans on Europa and Callisto, *Nature* **395**, 777–780, 1998.

Kivelson, M. G., K. K. Khurana, D. J. Stevenson, L. Bennett, S. Joy, C. T. Russell, R. J. Walker, C. Zimmer, and C. Polanskey, Europa and Callisto: Induced or intrinsic fields in a periodically varying plasma environment, *J. Geophys. Res.* **104**, 4609–4626, 1999.

Kivelson, M. G., K. K. Khurana, C. T. Russell, M. Volwerk, R. J. Walker, and C. Zimmer, *Galileo* magnetometer measurements: A stronger case for a subsurface ocean at Europa, *Science* **289**, 1340–1343, 2000.

Kuiper, G. P., Infrared observations of planets and satellites, *AJ* **62**, 245, 1957.

Leith, A. C. and W. B. McKinnon, Is there evidence for polar wander on Europa?, *Icarus* **120**, 387–398, 1996.

Lucchitta, B. K. and L. A. Soderblom, The geology of Europa, in *Satellites of Jupiter*, D. Morrison (ed), University of Arizona Press, pp. 521–555, 1982.

Lucchitta, B. K., L. A. Soderblom, and H. M. Ferguson, Structures on Europa, *Lunar and Planetary Science Conference Abstracts* **12**, 1981.

Lunine, J. I. and D. J. Stevenson, Formation of the Galilean satellites in a gaseous nebula, *Icarus* **52**, 14–39, 1982.

Malhotra, R., Tidal origin of the Laplace resonance and the resurfacing of Ganymede, *Icarus* **94**, 399–412, 1991.

Malin, M. C. and D. C. Pieri, Europa, in *Satellites*, J. A. Burns and M. S. Matthews (eds), University of Arizona Press, pp. 689–717, 1986.

Matson, D. L. and R. H. Brown, Solid-state greenhouses and their implications for icy satellites, *Icarus* **77**, 67–81, 1989.

McCollom, T. M., Methanogenesis as a potential source of chemical energy for primary biomass production by autotrophic organisms in hydrothermal systems on Europa, *J. Geophys. Res.* **104**, 30 729, 1999.

McCord, T., Surface composition reveals icy Galilean satellites' past, *Eos* **81**, 209, 2000.

McCord, T. B., R. Carlson, W. Smythe, G. Hansen, R. Clark, C. Hibbitts, F. Fanale, J. Granahan, M. Segura, D. Matson, T. Johnson, and P. Martin, Organics and other molecules in the surfaces of Callisto and Ganymede, *Science* **278**, 271–275, 1997.

McCord, T. B., G. B. Hansen, R. N. Clark, P. D. Martin, C. A. Hibbitts, F. P. Fanale, J. C. Granahan, M. Segura, D. L. Matson, T. V. Johnson, R. W. Carlson, W. D. Smythe, and G. E. Danielson, Non-water-ice constituents in the surface material of the icy Galilean satellites from the *Galileo* Near Infrared Mapping Spectrometer investigation, *J. Geophys. Res.* **103**, 8603–8626, 1998a.

McCord, T. B., G. B. Hansen, F. P. Fanale, R. W. Carlson, D. L. Matson, T. V. Johnson, W. D. Smythe, J. K. Crowley, P. D. Martin, A. Ocampo, C. A. Hibbitts, and J. C. Granahan,

Salts on Europa's surface detected by *Galileo*'s Near Infrared Mapping Spectrometer, *Science* **280**, 1242, 1998b.

McCord, T. B., G. B. Hansen, D. L. Matson, T. V. Jonhson, J. K. Crowley, F. P. Fanale, R. W. Carlson, W. D. Smythe, P. D. Martin, C. A. Hibbitts, J. C. Granahan, and A. Ocampo, Hydrated salt minerals on Europa's surface from the *Galileo* Near Infrared Mapping Spectrometer (NIMS) investigation, *J. Geophys. Res.* **104**, 11 827–11 852, 1999.

McCord, T. B., G. B. Hansen, and C. A. Hibbitts, Hydrated salt minerals on Ganymede's surface: Evidence of an ocean below, *Science* **292**, 1523–1525, 2001a.

McCord, T. B., T. M. Orlando, G. Teeter, G. B. Hansen, M. T. Sieger, N. G. Petrik, and L. Van Keulen, Thermal and radiation stability of the hydrated salt minerals epsomite, mirabilite, and natron under Europa environmental conditions, *J. Geophys. Res.* **106**, 3311–3320, 2001b.

McCord, T. B., G. Teeter, G. B. Hansen, M. T. Sieger, and T. M. Orlando, Brines exposed to Europa surface conditions, *J. Geophys. Res.* **107**, 4–1, 2002.

McEwen, A. S., Exogenic and endogenic albedo and color patterns on Europa, *J. Geophys. Res.* **91**, 8077–8097, 1986a.

McEwen, A. S., Tidal reorientation and the fracturing of Jupiter's moon Europa, *Nature* **321**, 49–51, 1986b.

McKinnon, W. B., Evolution of the interior of Europa, and the plausibility of active, present-day hydrothermal systems, in *Europa Ocean Conference*, pp. 50–51, 1996.

McKinnon, W. B., Convective instability in Europa's floating ice shell, *Geophys. Res. Lett.* **26**, 951, 1999.

McKinnon, W. B., Sulphate content of Europa's ocean and shell: Geological and astrobiological implications, *BAAS* **34**, 914–915, 2002.

McKinnon, W. B. and E. L. Shock, Ocean karma: What goes around comes around on Europa (or does it?), in *Lunar and Planetary Science Conference Abstracts*, p. 2181, 2001.

McMahon, S. K., Overview of the Planetary Data System, *Planet. Space Sci.* **44**, 3–12, 1996.

Melosh, H. J., Global tectonics of a despun planet, *Icarus* **31**, 221–243, 1977.

Mileikowsky, C., F. A. Cucinotta, J. W. Wilson, B. Gladman, G. Horneck, L. Lindegren, J. Melosh, H. Rickman, M. Valtonen, and J. Q. Zheng, Natural transfer of viable microbes in space: 1. From Mars to Earth and Earth to Mars, *Icarus* **145**, 391–427, 2000.

Montgomery, R. B., Oceanographic data, in *American Institute of Physics Handbook*, D. E. Gray (ed), pp. 123–132, McGraw-Hill, 1963.

Moore, J. M., E. Asphaug, R. J. Sullivan, J. E. Klemaszewski, K. C. Bender, R. Greeley, P. E. Geissler, A. S. McEwen, E. P. Turtle, C. B. Phillips, B. R. Tufts, J. W. Head, R. T. Pappalardo, K. B. Jones, C. R. Chapman, M. J. S. Belton, R. L. Kirk, and D. Morrison, Large impact features on Europa: Results of the *Galileo* nominal mission, *Icarus* **135**, 127–145, 1998.

Moore, J. M., E. Asphaug, M. J. S. Belton, B. Bierhaus, H. H. Breneman, S. M. Brooks, C. R. Chapman, F. C. Chuang, G. C. Collins, B. Giese, R. Greeley, J. W. Head, S. Kadel, K. P. Klaasen, J. E. Klemaszewski, K. P. Magee, J. Moreau, D. Morrison, G. Neukum, R. T. Pappalardo, C. B. Phillips, P. M. Schenk, D. A. Senske, R. J. Sullivan, E. P. Turtle, and K. K. Williams, Impact features on Europa: Results of the *Galileo* Europa Mission (GEM), *Icarus* **151**, 93–111, 2001.

Moore, M. H. and R. L. Hudson, IR detection of $H_2O_2$ at 80 K in ion-irradiated laboratory ices relevant to Europa, *Icarus* **145**, 282–288, 2000.

Moore, W. B., Coupling tidal dissipation and convection, *BAAS* **33**, 1106, 2001.

Moore, W. B. and G. Schubert, The tidal response of Europa, *Icarus* **147**, 317–319, 2000.

Moroz, V. I., Infrared spectrophotometry of the Moon and the Galilean satellites of Jupiter, *AZh* **42**, 1287, 1965.

Morrison, D., Radiometry of satellites and of the rings of Saturn, in *Planetary Satellites*, J. A. Burns (ed), University of Arizona Press, pp. 269–301, 1977.

Morrison, D. and M. S. Matthews, *Satellites of Jupiter*, University of Arizona Press, 1982.

Morrison, D. and N. D. Morrison, Photometry of the Galilean satellites, in *Planetary Satellites*, J. A. Burns (ed), University of Arizona Press, pp. 363–378, 1977.

Mosqueira, I. and P. R. Estrada, Formation of the regular satellites of giant planets in an extended gaseous nebula: I. Subnebula model and accretion of satellites, *Icarus* **163**, 198–231, 2003a.

Mosqueira, I. and P. R. Estrada, Formation of the regular satellites of giant planets in an extended gaseous nebula: II. Satellite migration and survival, *Icarus* **163**, 232–255, 2003b.

Mueller, S. and W. B. McKinnon, Three-layered models of Ganymede and Callisto: Compositions, structures, and aspects of evolution, *Icarus* **76**, 437–464, 1988.

Nelson, M. L., T. B. McCord, R. N. Clark, T. V. Johnson, D. L. Matson, J. A. Mosher, and L. A. Soderblom, Europa: Characterization and interpretation of global spectral surface units, *Icarus* **65**, 129–151, 1986.

Neukum, G., Bombardment history of the jovian system, in *The Three Galileos: The Man, The Spacecraft, The Telescope*, C. Barbieri, J. Rahe, T. V. Johnson, and A. M. Sohus, eds, pp. 201–212, Kluwer, 1997.

Nimmo, F. and E. Gaidos, Strike-slip motion and double ridge formation on Europa, *J. Geophys. Res.* **107**, 5–1, 2002.

O'Brien, D. P., P. Geissler, and R. Greenberg, A melt-through model for chaos formation on Europa, *Icarus* **156**, 152–161, 2002.

Ojakangas, G. W. and D. J. Stevenson, Episodic volcanism of tidally heated satellites with application to Io, *Icarus* **66**, 341–358, 1986.

Ojakangas, G. W. and D. J. Stevenson, Polar wander of an ice shell on Europa, *Icarus* **81**, 242–270, 1989a.

Ojakangas, G. W. and D. J. Stevenson, Thermal state of an ice shell on Europa, *Icarus* **81**, 220–241, 1989b.

Pappalardo, R., Upwarped domes on Europa: Constraints on mottled terrain formation, in *Lunar and Planetary Science Conference Abstracts*, p. 1719, 2000.

Pappalardo, R. and M. D. Coon, A sea ice analog for the surface of Europa, in *Lunar and Planetary Science Conference Abstracts*, p. 997, 1996.

Pappalardo, R. and R. J. Sullivan, Evidence for separation across a gray band on Europa, *Icarus* **123**, 557–567, 1996.

Pappalardo, R., J. W. Head, R. Greeley, R. J. Sullivan, C. Pilcher, G. Schubert, W. B. Moore, M. H. Carr, J. M. Moore, and M. J. S. Belton, Geological evidence for solid-state convection in Europa's ice shell, *Nature* **391**, 365, 1998a.

Pappalardo, R., J. W. Head, N. D. Sherman, R. Greeley, R. J. Sullivan, and *Galileo* Imaging Team, Classification of Europan ridges and troughs and a possible genetic sequence, in *Lunar and Planetary Science Conference Abstracts*, p. 1859, 1998b.

Pappalardo, R., J. W. Head, and R. Greeley, The hidden ocean of Europa, *Sci. Amer.* pp. 34–43, 1999a.

Pappalardo, R. T., M. J. S. Belton, H. H. Breneman, M. H. Carr, C. R. Chapman, G. C. Collins, T. Denk, S. Fagents, P. E. Geissler, B. Giese, R. Greeley, R. Greenberg, J. W. Head, P. Helfenstein, G. Hoppa, S. D. Kadel, K. P. Klaasen, J. E. Klemaszewski, K. Magee, A. S. McEwen, J. M. Moore, W. B. Moore, G. Neukum, C. B. Phillips, L. M. Prockter, G. Schubert, D. A. Senske, R. J. Sullivan, B. R. Tufts, E. P. Turtle, R. Wagner, and K. K. Williams, Does Europa have a subsurface ocean? Evaluation of the geological evidence, *J. Geophys. Res.* **104**, 24 015–24 056, 1999b.

Patterson, G. W. and R. T. Pappalardo, Compression across ridges on Europa, in *Lunar and Planetary Science Conference Abstracts*, p. 1681, 2002.

Peale, S. J., Rotation histories of the natural satellites, in *Planetary Satellites*, J. A. Burns (ed), University of Arizona Press, pp. 87–111, 1977.

Peale, S. J., Orbital resonances, unusual configurations and exotic rotation states among planetary satellites, in *Satellites*, J. A. Burns and M. S. Matthews (eds), University of Arizona Press, pp. 159–223, 1986.

Peale, S. J., Origin and evolution of the natural satellites, *ARA&A* **37**, 533–602, 1999.

Peale, S. J. and M. H. Lee, A primordial origin of the Laplace relation among the Galilean satellites, *Science* **298**, 593–597, 2002.

Pierazzo, E. and C. F. Chyba, Cometary delivery of biogenic elements to Europa, *Icarus* **157**, 120–127, 2002.

Pieri, D. C., Lineament and polygon patterns on Europa, *Nature* **289**, 17–21, 1981.

Pilcher, C. B., S. T. Ridgeway, and T. B. McCord, Galilean satellites: Identification of water frost, *Science* **178**, 1087–1089, 1972.

Pollack, J. B. and F. Fanale, Origin and evolution of the Jupiter satellite system, in *Satellites of Jupiter*, D. Morrison (ed), University of Arizona Press, pp. 872–910, 1982.

Prinn, R. G. and B. Fegley, Kinetic inhibition of CO and $N_2$ reduction in circumplanetary nebulae: Implications for satellite composition, *ApJ* **249**, 308–317, 1981.

Prockter, L. M. and R. T. Pappalardo, Folds on Europa: Implications for crustal cycling and accommodation of extension, *Science* **289**, 941–944, 2000.

Prockter, L. M., A. M. Antman, R. T. Pappalardo, J. W. Head, and G. C. Collins, Europa: Stratigraphy and geological history of the anti-jovian region from *Galileo* E14 Solid State Imaging data, *J. Geophys. Res.* **104**, 16 531–16 540, 1999.

Prockter, L. M., R. T. Pappalardo, and J. W. Head, Strike-slip duplexing on Jupiter's icy moon Europa, *J. Geophys. Res.* **105**, 9483–9488, 2000.

Prockter, L. M., J. W. Head, R. T. Pappalardo, R. J. Sullivan, A. E. Clifton, B. Giese, R. Wagner, and G. Neukum, Morphology of Europan bands at high resolution: A mid-ocean ridge-type rift mechanism, *J. Geophys. Res.* **107**, 4–1, 2002.

Ransford, G. A., A. A. Finnerty, and K. D. Collerson, Europa's petrological thermal history, *Nature* **289**, 21–24, 1981.

Rathbun, J. A., G. S. Musser, and S. W. Squyres, Ice diapirs on Europa: Implications for liquid water, *Geophys. Res. Lett.* **25**, 4157, 1998.

Reynolds, R. T. and P. M. Cassen, On the internal structure of the major satellites of the outer planets, *Geophys. Res. Lett.* **6**, 121–124, 1979.

Reynolds, R. T., S. W. Squyres, D. S. Colburn, and C. P. McKay, On the habitability of Europa, *Icarus* **56**, 246–254, 1983.

Riley, J., G. V. Hoppa, R. Greenberg, B. R. Tufts, and P. Geissler, Distribution of chaotic terrain on Europa, *J. Geophys. Res.* **105**, 22 599–22 616, 2000.

Ross, M. N. and G. Schubert, Tidal heating in an internal ocean model of Europa, *Nature* **325**, 133, 1987.

Sagan, C., Circumstellar habitable zones: An introduction, in *Circumstellar Habitable Zones, Proceedings of The First International Conference*, L. R. Doyle (ed), Travis House Publications, pp. 3–14, 1996.

Sarid, A. R., R. Greenberg, G. V. Hoppa, T. A. Hurford, B. R. Tufts, and P. Geissler, Polar wander and surface convergence of Europa's ice shell: Evidence from a survey of strike-slip displacement, *Icarus* **158**, 24–41, 2002.

Schenk, P. M., Thickness constraints on the icy shells of the Galilean satellites from a comparison of crater shapes, *Nature* **417**, 419–421, 2002.

Schenk, P. M. and W. B. McKinnon, Fault offsets and lateral crustal movement on Europa: Evidence for a mobile ice shell, *Icarus* **79**, 75–100, 1989.

Schenk, P. M. and R. T. Pappalardo, A pre-*Galileo* view of tectonism on Europa, *Eos* **77**, S173, 1996.

Schenk, P. M. and R. T. Pappalardo, Stereo and photoclinometric topography of chaos and anarchy on Europa: Evidence for diapiric origins, in *Lunar and Planetary Science Conference Abstracts*, p. 2035, 2002.

Schubert, G., T. Spohn, and R. T. Reynolds, Thermal histories, compositions and internal structures of the moons of the solar system, in *Satellites*, J. A. Burns and M. S. Matthews (eds), University of Arizona Press, pp. 224–292, 1986.

Shimoyama, A. and R. Ogasawara, Dipeptides and diketopiperazines in the Yamato-791198 and Murchison carbonaceous chondrites, *Origins Life Evol. Biosph.* **32**, 165–179, 2002.

Shirley, J. H. and R. Carlson, Water ice grain size variations on Europa, *Eos* **81**, F793, 2000.

Showman, A. P. and R. Malhotra, Tidal evolution into the Laplace resonance and the resurfacing of Ganymede, *Icarus* **127**, 93–111, 1997.

Smith, B. A., L. A. Soderblom, R. Beebe, J. Boyce, G. Briggs, M. Carr, S. A. Collins, A. F. Cook II, G. E. Danielson, M. E. Davies, G. E. Hunt, A. P. Ingersoll, T. V. Johnson, H. Masursky, J. F. McCauley, D. Morrison, T. Owen, C. Sagan, E. M. Shoemaker, R. G. Strom, V. E. Suomi, and J. Veverka, The Galilean satellites and Jupiter: *Voyager 2* imaging science results, *Science* **206**, 927–950, 1979a.

Smith, B. A., L. A. Soderblom, T. V. Johnson, A. P. Ingersoll, S. A. Collins, E. M. Shoemaker, G. E. Hunt, H. Masursky, M. H. Carr, M. E. Davies, A. F. Cook, J. M. Boyce, T. Owen, G. E. Danielson, C. Sagan, R. F. Beebe, J. Veverka, J. F. McCauley, R. G. Strom, D. Morrison, G. A. Briggs, and V. E. Suomi, The Jupiter system through the eyes of *Voyager 1*, *Science* **204**, 951–957, 1979b.

Smythe, W. D., R. W. Carlson, A. Ocampo, G. B. Hansen, T. B. McCord, D. L. Matson, and the *Galileo* NIMS team, Absorption bands at 3.5, 4.03, and 4.25 μm in the spectrum of Europa, *Eos* **79**, F534, 1998.

Solomon, S. C., On the early thermal state of the moon, in *Origin of the Moon*, R. M. Canup and K. Righter (eds), University of Arizona Press, pp. 435–452, 1986.

Sotin, C., J. W. Head, and G. Tobie, Europa: Tidal heating of upwelling thermal plumes and the origin of lenticulae and chaos melting, *Geophys. Res. Lett.* **29**, 74–1, 2002.

Space Studies Board, N. R. C., *A Science Strategy for the Exploration of Europa*, National Academy Press, 1999.

Space Studies Board, N. R. C., *New Frontiers in the Solar System: An Integrated Exploration Strategy*, National Academy Press, 2003.

Spaun, N. A., J. W. Head, G. C. Collins, L. M. Prockter, and R. T. Pappalardo, Conamara Chaos region, Europa: Reconstruction of mobile polygonal ice blocks, *Geophys. Res. Lett.* **25**, 4277, 1998.

Spaun, N. A., J. W. Head, R. T. Pappalardo, and T. The *Galileo* SSI Team, Chaos and lenticulae on Europa: Structure, morphology and comparative analysis, in *Lunar and Planetary Science Conference Abstracts*, p. 1276, 1999a.

Spaun, N. A., L. M. Prockter, R. T. Pappalardo, J. W. Head, G. C. Collins, A. Antman, R. Greeley, and the *Galileo* SSI Team, Spatial distribution of lenticulae and chaos on Europa, in *Lunar and Planetary Science Conference Abstracts*, p. 1847, 1999b.

Spaun, N. A., R. T. Pappalardo, and J. W. Head, Equatorial distribution of chaos and lenticulae on Europa, in *Lunar and Planetary Science Conference Abstracts*, p. 2132, 2001.

Spaun, N. A., R. T. Pappalardo, and J. W. Head, Evidence for shear failure in forming near-equatorial lineae on Europa, *J. Geophys. Res.* **108**, 14–1, 2003.

Spencer, J. R., *The Surfaces of Europa, Ganymede, and Callisto: An Investigation Using Voyager IRIS Thermal Infrared Spectra*, Ph.D. thesis, University of Arizona, 1987a.

Spencer, J. R., Thermal segregation of water ice on the Galilean satellites, *Icarus* **69**, 297–313, 1987b.

Spencer, J. R., L. K. Tamppari, T. Z. Martin, and L. D. Travis, Temperatures on Europa from *Galileo* PPR: Nighttime thermal anomalies, *Science* **284**, 1514–1516, 1999.

Squyres, S. W. and S. K. Croft, The tectonics of icy satellites, in *Satellites*, J. A. Burns and M. S. Matthews (eds), University of Arizona Press, pp. 293–341, 1986.

Squyres, S. W., R. T. Reynolds, and P. M. Cassen, Liquid water and active resurfacing on Europa, *Nature* **301**, 225, 1983.

Stempel, M. M. and R. T. Pappalardo, Lineament orientations through time near Europa's leading point: Implications for stress mechanisms and rotation of the icy shell, in *Lunar and Planetary Science Conference Abstracts*, p. 1661, 2002.

Stevenson, D. J., Heterogeneous tidal deformation and geysers on Europa, in *Europa Ocean Conference*, pp. 69–70, 1996.

Stevenson, D. J., Europa's ocean: The case strengthens, *Science* **289**, 1305–1307, 2000a.

Stevenson, D. J., Limits on the variation of thickness of Europa's ice shell, in *Lunar and Planetary Science Conference Abstracts*, p. 1506, 2000b.

Stevenson, D. J., T. Spohn, and G. Schubert, Magnetism and thermal evolution of the terrestrial planets, *Icarus* **54**, 466–489, 1983.

Stevenson, D. J., A. W. Harris, and J. I. Lunine, Origins of satellites, in *Satellites*, J. A. Burns and M. S. Matthews (eds), University of Arizona Press, pp. 39–88, 1986.

Sullivan, R., R. Greeley, K. Homan, J. Klemaszewski, M. J. S. Belton, M. H. Carr, C. R. Chapman, R. Tufts, J. W. Head, and R. Pappalardo, Episodic plate separation and fracture infill on the surface of Europa, *Nature* **391**, 371,372, 1998.

Sullivan, R., J. Moore, and R. Pappalardo, Mass-wasting and slope evolution on Europa, in *Lunar and Planetary Science Conference Abstracts*, p. 1747, 1999.

Tamppari, L. K., J. R. Spencer, and T. Z. Martin, Observing the icy jovian satellites with the *Galileo* Photopolarimeter Radiometer instrument, *J. Geophys. Res.* **100**, 18 973–18 984, 1995.

Thomson, R. E. and J. R. Delaney, Evidence for a weakly stratified Europan ocean sustained by seafloor heat flux, *J. Geophys. Res.* **106**, 12 355–12 366, 2001.

Tufts, B. R., R. Greenberg, G. Hoppa, and P. Geissler, Astypalaea Linea: A large-scale strike-slip fault on Europa, *Icarus* **141**, 53–64, 1999.

Tufts, B. R., R. Greenberg, G. Hoppa, and P. Geissler, Lithospheric dilation on Europa, *Icarus* **146**, 75–97, 2000.

Turtle, E. P. and E. Pierazzo, Thickness of a europan ice shell from impact crater simulations, *Science* **294**, 1326–1328, 2002.

Turtle, E. P., H. J. Melosh, and C. B. Phillips, Tectonic modeling of the formation of europan ridges, *Eos* **79**, F541, 1998.

Turtle, E. P., C. B. Phillips, H. J. Melosh, and A. S. McEwen, Constraints on the thickness of the europan lithosphere from numerical models of crater collapse, *BAAS* **31**, 1177, 1999.

Van Keulen, L. M., T. B. McCord, G. B. Hansen, C. A. Hibbitts, and J. K. Crowley, The effect of grain size on the near-infrared reflectance spectra of some hydrated salt minerals, in *Lunar and Planetary Science Conference Abstracts*, p. 1539, 2000.

Wächtershäuser, G., Pyrite formation; the first energy source for life: A hypothesis, *Syst. Appl. Microbiol.* **10**, 207–210, 1988.

Wang, H. and D. J. Stevenson, Convection and internal melting of Europa's ice shell, in *Lunar and Planetary Science Conference Abstracts*, p. 1293, 2000.

Weber, A. L., Sugars as the optimal biosynthetic carbon substrate of aqueous life throughout the universe, *Origins Life Evol. Biosph.* **30**, 33–43, 2000.

Weertman, J., Theory of water-filled crevasses in glaciers applied to vertical magma transport beneath oceanic ridges, *J. Geophys. Res.* **76**, 1171–1183, 1971.

Whitman, W. B., D. C. Coleman, and W. J. Wiebe, Prokaryotes: The unseen majority, *Proc. Natl. Acad. Sci. USA* **95**, 6578–6583, 1998.

Williams, J. G., D. H. Boggs, C. F. Yoder, J. T. Ratcliff, and J. O. Dickey, Lunar rotational dissipation in solid body and molten core, *J. Geophys. Res.* **106**, 27 933–27 968, 2001.

Williams, K. K. and R. Greeley, Estimates of ice thickness in the Conamara Chaos region of Europa, *Geophys. Res. Lett.* **25**, 4273, 1998.

Yoder, C. F., How tidal heating in Io drives the Galilean orbital resonance locks, *Nature* **279**, 767–770, 1979.

Yoder, C. F., Astrometric and geodetic properties of the earth and the solar system, in *Global Earth Physics: A Handbook of Physical Constants*, T. J. Ahrens (ed), pp. 1–31, AGU, 1995.

Yoder, C. F. and S. J. Peale, The tides of Io, *Icarus* **47**, 1–35, 1981.

Yoder, C. F. and W. L. Sjogren, Tides on Europa, in *Europa Ocean Conference*, pp. 89–90, 1996.

Zahnle, K., L. Dones, and H. F. Levison, Cratering rates on the Galilean satellites, *Icarus* **136**, 202–222, 1998.

Zimmer, C., K. K. Khurana, and M. G. Kivelson, Subsurface oceans on Europa and Callisto: Constraints from *Galileo* magnetometer observations, *Icarus* **147**, 329–347, 2000.

Zolotov, M. Y. and E. L. Shock, Composition and stability of salts on the surface of Europa and their oceanic origin, *J. Geophys. Res.* **106**, 32 815–32 828, 2001.